THE PIEZOMAGNETIC EFFECT IN SEISMICALLY ACTIVE AREAS

A DISSERTATION

SUBMITTED TO THE DEPARTMENT OF GEOPHYSICS

AND THE COMMITTEE ON THE GRADUATE DIVISION

OF STANFORD UNIVERSITY

IN PARTIAL FULFILLMENT OF THE REQUIREMENTS

FOR THE DEGREE OF

DOCTOR OF PHILOSOPHY

by

Sheldon Breiner

August, 1967

ACKNOWLEDGMENTS

I am grateful to the late Professor J. L. Soske who encouraged me and provided the initial faculty support for this investigation of the piezomagnetic effect. Dr. C. P. Sonett of Ames Research Center of the National Aeronautics and Space Administration, Dr. Carl Menneken of the U. S. Naval Postgraduate School, and Professor S. H. Ward of the University of California each graciously provided a rubidium magnetometer for the duration of the project. Varian Associates loaned four rubidium vapor magnetometers and much of the electronic test equipment used in this investigation.

Marvin Harris ably assisted me in the field work in California, Nevada and Idaho. I thank Mr. Howard Harris for providing me with a semi-permanent base in the Hollister area.

Dr. T. Rikitake of the Earthquake Research Institute of the University of Tokyo provided unpublished data concerning a possible piezomagnetic event at Matsushiro. Information concerning fault creep at Hollister was always kindly provided by Dr. Don Tocher.

With the untimely death of Professor Soske in October 1966, Professor Robert L. Kovach accepted the responsibilities of the project and guided me to a satisfactory completion of my research project.

TABLE OF CONTENTS

ABSTRACT

The piezomagnetic properties or magnetostrictive effects of rock under stress have been widely discussed and experimentally observed in the laboratory. The results of these investigations indicate that a change in the subsurface stress should manifest itself as a change in the susceptibility and remanent magnetization of rock and therefore in the local geomagnetic field. Observations of the geomagnetic field on the surface of the earth might thus represent a means for the remote observation of changes in tectonic stress.

The observed change in field intensity that would result is a function of the stress change, the unstressed susceptibility of the underlying rock, the magnetic stress sensitivity, the volume of rock under stress, and the distance to the center of the volume. The estimates of field change on the surface vary from a few thousandths to a few tens of gammas. The time signature of the stress changes in seismically active areas, however, is unknown. Furthermore, small changes in the local field must be resolved in the presence of geomagnetic micropulsations much larger than the expected piezomagnetic effects. By measuring the difference between two stations, the ionospherically-induced micropulsations are largely removed permitting one to observe local disturbances in the field.

Such an array of magnetometers was set up on the San

Andreas fault first as a five station network from San Bruno to Hollister, California, a distance of 120 km. Following identification of events, the array was reorganized as a high density net near Hollister. The signals from each magnetometer are telemetered on leased telephone lines to one location where the differences are recorded along with the total field intensity from the common reference station.

During two years operation local changes in the magnetic field were observed in December, 1965, February, June, July, and October 1966, on the Hollister differential record. In every case and at no other times abrupt creep displacement of the San Andreas fault, ranging from 0.5 to 4 mm has occurred in the vicinity of Hollister some tens of hours after the magnetic event. Following the establishment of the higher density net, another local magnetic event was observed on the four local magnetometers but not on stations 40 kilometers to the northwest. The event appeared simultaneously at each station with amplitudes from 0.8 to 2.5 gammas and with a duration of 60 to 90 minutes. Creep displacement of about 4 mm followed 16 hours later and local earthquakes 4 days later.

If indeed the magnetic events are manifestations of subsurface stress changes, then this will have been the first reported observation of the nature of the time signature of the stress change in a seismically active area. With this evidence, the source of the stress change is believed to be

deep, perhaps 10 to 20 km. The signature of the observed piezomagnetic effects appears to follow the logarithmic variation of creep behavior of rocks, lending support to a mechanism of creep or plastic deformation. The local earthquakes could therefore be interpreted as brittle readjustments to the new strain environment and as such are aftershocks of a zero frequency earthquake, i.e., creep displacement.

1. INTRODUCTION

The piezomagnetic properties or magnetostrictive effects of rock under stress have been widely discussed and experimentally observed in the laboratory (Wilson, 1922; Kalashnikov and Kapitsa, 1952; Grabovsky and Parkhomenko, 1953; and Kapitsa, 1955). The results of these investigations indicate that a change in the subsurface stress should manifest itself as a change in the susceptibility and remanent magnetization of rock and therefore in the local geomagnetic field. Observations of the geomagnetic field on the earth's surface might consequently represent a means for the remote observation of changes in tectonic stress.

Seismic events reflect changes in stress and may thus exhibit geomagnetic variations of local origin. Such variations have, to some extent, been observed at the time of local earthquakes, as reported by Kato (1938), Kato, et al., (1950), Kato, et al., (1953a), Miyakoshi (1953), Breiner (1964), and Rikitake (1966).

In spite of the interest in the possible correlation of earthquakes and geomagnetic events as once expressed by Wilson (1922) it was not until recently that both sufficient laboratory evidence and sensitive instrumentation for field measurements were made available. The resulting renewed interest in this subject is evidenced by the recent appearance of numerous reviews of magnetic investigations as they might

be applied to seismic events. A principal objective is the possibility that through continuous observations of the geomagnetic field, one might be able to predict the time and location of earthquakes (Lapina, 1953; Kalashnikov, 1954; Stacey, 1962; and Shapiro, 1966).

A complete investigation of the piezomagnetic effect requires expertise in at least four somewhat unrelated fields: geomagnetism, seismology, rock magnetism, and tectonophysics. Moreover, the key knowledge from each of these fields which is most relevant to this investigation does not, in fact, yet appear in the literature. The principal unanswered questions from each of these fields are:

What is the nature of the geomagnetic noise that would obscure subtle local changes in the field?

What is the mechanism of earthquakes?

Exactly how do the stress-dependent magnetic properties of rock depend upon temperature, pressure, and rock type?

What is the time signature and spatial distribution of the stresses associated with earthquakes and crustal deformation?

The immediate goals of this work were first, to observe the nature of any changes in the geomagnetic field that are local, i.e., whose origin directly or induced is not in the ionosphere; and secondly, to investigate the existence or

extent of any correlation between these events and local seismic or strain events. Possible causes of observed local changes in the geomagnetic field were examined qualitatively and quantitatively to determine their origin particularly in light of piezomagnetic theory. The indirect objective was to demonstrate a possible means for the remote observation of stress changes.

2. THEORETICAL BASIS OF THE PIEZOMAGNETIC EFFECT

A. Piezomagnetism in Stressed Rock

The magnetic properties of rocks are almost entirely the properties of the spinel minerals, especially magnetite, which the rock contains. Of particular concern in this work are the magnetic susceptibility and remanent magnetization as a function of the external stress on the rock.

Magnetite has cubic symmetry for its magnetocrystalline parameters in the absence of stress. Application of a compressive stress creates magnetocrystalline anisotropy so that the easy directions of magnetization, along which the domains are oriented, are deflected away from the axis of compression. This phenomenon, investigated both theoretically and experimentally in the laboratory, is described as piezomagnetism, or inverse or converse magnetostriction. Some investigators prefer to define this phenomenon as the magnetoelastic, seismomagnetic, or magnetoseismic effect.

The magnetic susceptibility of rock is usually directly proportional to its fraction of magnetite (or other ferrimagnetic minerals), which may vary from 10^{-1} in basic igneous rocks to 10^{-5} for certain sedimentary rocks. The corresponding susceptibility would be 2×10^{-2} to 2×10^{-6} cgs emu, respectively. The magnetite occurs as grains whose size varies from 1 to 10^{-6} mm in diameter. Within each grain there exist domains, or regions of uniform magneti-

zation, whose size, direction, and mobility largely determine the actual magnetic susceptibility. The latter two properties are, in turn, a function of the applied stress transmitted from the external stress on the rock sample as a whole.

Susceptibility

The dependence of magnetization upon stress may be described in terms of the energies associated with stress and with the magnetization of the domains. The strain energy of a domain in terms of the stress, σ, following Bozorth (1951) can be expressed as

$$E_\sigma = \frac{3}{2}\lambda_s \sigma \sin^2\theta$$

where λ_s is the magnetostriction constant at saturation and $\theta = 0$, the original position where $E = 0$. The magnetization energy, on the other hand, is

$$E_H = -HI = -HI_s\cos\theta$$

where I is the magnetization, and I_s, the spontaneous or saturation (maximum) magnetization of the domain material, and H is the applied field.

The sum of the energies is a minimum when

$$\frac{d\ [E_\sigma + E_H]}{d\theta} = 0$$

Thus

$$3\lambda_s \sigma \sin\theta \cos\theta + HI_s \sin\theta = 0$$

Substituting, $\cos = \frac{I}{I_s}$, gives, $\frac{I}{H} = \frac{I_s^2}{3\lambda_s \sigma}$

But from the definition of susceptibility,

$$k = \frac{I}{H}$$

where k is the susceptibility or proportionality constant between the intensity of magnetization and the applied field. Define

$$s = \frac{3\lambda_s k}{I_s^2}$$

s has units of σ^{-1} and is the piezomagnetic fraction of the susceptibility produced by a stress, σ. This term relates the susceptibility to stress and is known as the stress sensitivity. s is solely a function of the magneto-crystalline parameters, λ_s, I_s, and k for each of the grains of magnetite present in the rock. Inserting the appropriate constants for magnetite where λ_s varies from 20 to 40 x 10^{-6} and I_s varies from 300 to 400 cgs/cm^3, (Grabovsky and Parkhomenko, 1953) and k from 0.3 to 0.6, we have

$$-1.1 \times 10^{-10} < s < -7.5 \times 10^{-10} \frac{cm^2}{dynes}$$

Most of the experimental work is expressed in bars or kg/cm^2 so that

$$s = -1.1 \times 10^{-4} \text{ to } -7.5 \times 10^{-4} \frac{cm^2}{kg} \ (\approx \text{bars})^{-1}$$

The above values are the approximate range of values obtained by Grabovsky and Parkhomenko from their experiments on magnetite.

The stress dependence s, is the proportionality constant relating the change of stress to the change in magnetic susceptibility. This may be expressed as

$$s = \frac{1}{k_0} \frac{dk}{d\sigma} \frac{cm^2}{kg}$$

where k and k_0 are the susceptibility and initial susceptibility and $d\sigma$ the applied stress in the direction of the measured susceptibility. In physical terms, s describes the ease by which the susceptibility will vary with a given increment of stress and in this sense represents a stress susceptibility in an applied stress field analogous to the magnetic susceptibility in an applied magnetic field. Using the theoretical limits of s derived above, a plot of the approximate fractional change in susceptibility versus stress is shown in Figure 1a, the different slopes representing the limits of s.

The relationship expressed in Figure 1a represents only a linear approximation of the actual behavior, for the slope

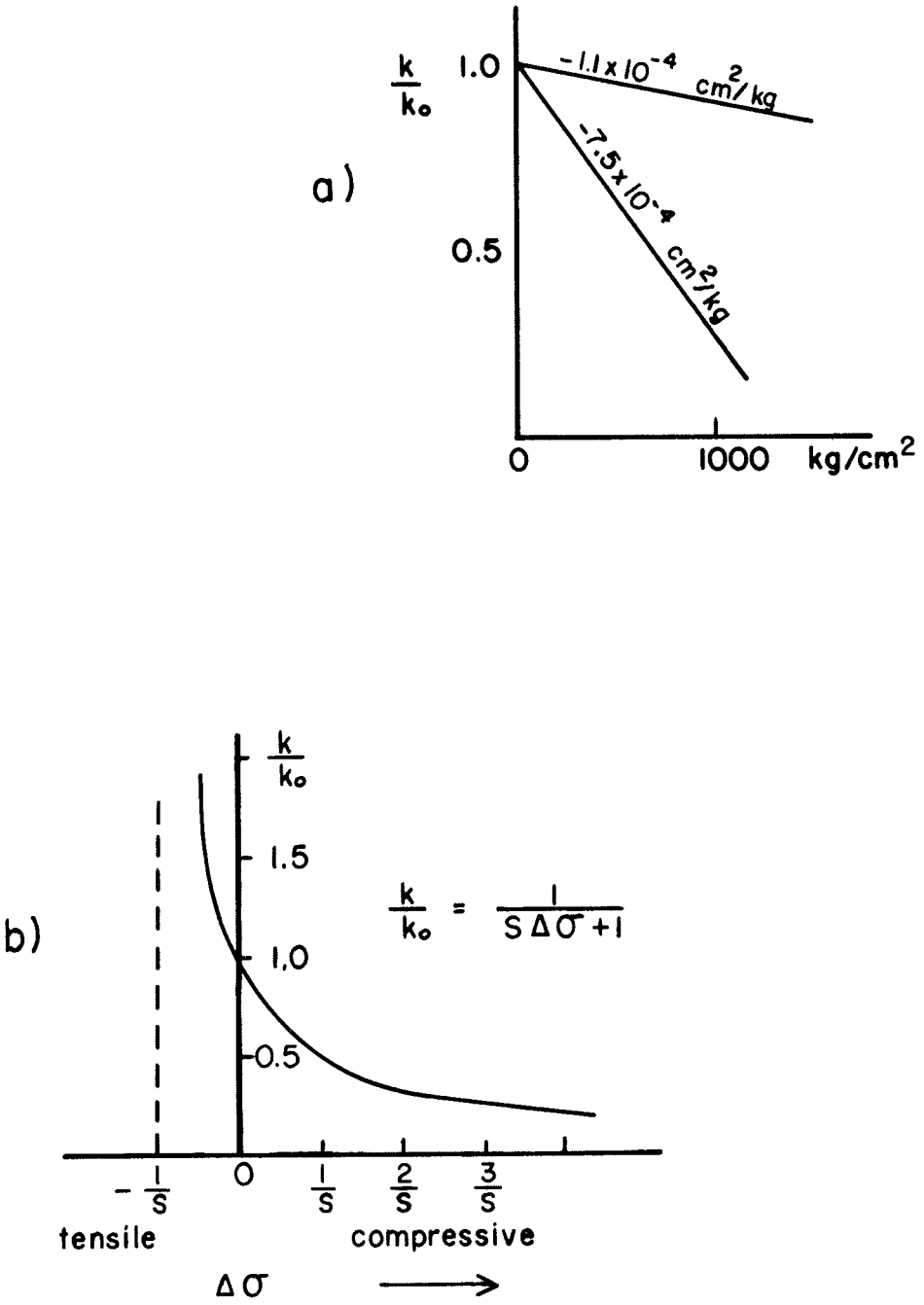

Fig. 1. Theoretical variation of stress sensitivity:
a) Limits derived from a linear approximation,
b) Following Kern (1961)

s, is itself, a function of the susceptibility, k. From the expression for the stress sensitivity, s, we have

$$s = \frac{1}{k_0} \frac{dk}{d\sigma}$$

$$\approx \frac{1}{k} \frac{\Delta k}{\Delta \sigma} = \frac{1}{k} \frac{k_0 - k}{\Delta \sigma} = -\frac{1}{k} \frac{k - k_0}{\Delta \sigma}$$

where $k \approx k_0$ and the derivatives are expressed as simple differentials. Then

$$(s\ \Delta\sigma + 1) = \frac{k_0}{k}$$

after inverting both sides we have,

$$\frac{k}{k_0} = \frac{1}{s\ \Delta\sigma + 1}$$

This expression for $\frac{k}{k_0}$, is identical to that derived by Kern (1961) from other considerations and is shown in Figure 1b as a function of positive and negative values of $\Delta\sigma$, i.e., both compressive and tensile stresses. Empirical results confirm this general form of stress dependence for the susceptibility. Perhaps the most significant feature is the higher stress dependence for tensile stress. However, tensile stress in an incompressible medium will result from a compressive stress at right angles to it. Therefore, the tensile stress dependence can also be described as the stress

dependence of the susceptibility perpendicular to the applied compressive stress and the experimental results are usually presented as the latter.

Remanence

Using thermodynamic considerations, Kern has developed a theory in which the stress sensitivity for both susceptibility and remanent magnetization are equal and expressed as

$$\frac{k}{k_0} = \frac{I}{I_0} = \frac{a}{\sigma + a}$$

where I = remanent magnetization and

$$a = \frac{1}{s} = \text{'virtual initial stress'}$$

Kern's equivalence between the stress sensitivities of the remanent and induced magnetization (susceptibility) can therefore be used to consider the effects of remanence. The behavior of the remanence vector is analogous to that of the easy direction of magnetization, i.e., it is deflected away from the axis of compression. Néel (1959), in fact, predicts theoretically that the remanent vector will be deflected so as to represent a stress sensitivity of $-2.5 \times 10^{-4} \frac{cm^2}{kg}$. The remanent vector should be in the general direction of the present induced field - discounting reversals, structural anomalies, etc. and represents a more complicated

situation with regard to random stress than does the susceptibility. Stacey (1964) suggests that because of the results demonstrated by Graham (1957), the stress dependence of the remanent magnetization be treated merely as an enhanced stress-dependent susceptibility.

Hydrostatic Stress

The applied stress considered in the above analysis is a linear compression or the deviatoric stress if hydrostatic stress about the sample is considered. Since it is the magnetoelastic anisotropy that is affected by the external stress, it follows that a stress system with perfect symmetry, such as hydrostatic stress, will have no effect on the susceptibility (Kapitsa, 1955). On the other hand, Kern (1961) demonstrates theoretically that susceptibility of an assemblage of magnetite grains decreases with hydrostatic compression. It might follow, therefore, that hydrostatic stresses causing a change in volume also create changes in magnetization, a particularly important consideration when applied to stresses at great depth.

Laboratory Investigations of Piezomagnetism

The earliest experiments to investigate the effect of stress on the magnetic properties or rock were those of Wilson (1922). In these investigations he subjected specimens of magnetite, dolerite, and granite to compressive stresses up to 1,000 kg/cm^2. The induced moment was observed using a

suspended magnet near the specimen which was contained in a nonmagnetic frame. The susceptibility change decreased in the direction of the applied stress from zero to 10% of the original susceptibility at the maximum stress of 1000 kg/cm^2 for the rocks examined. The lower values of change were partially due to the limited sensitivity of the magnetometer used. The susceptibility changes measured at right angles to the compressive stress increased by a factor of three greater than the susceptibility changes parallel to the applied stress at low stresses. Although many of the theories of rock magnetism had not yet been developed, Wilson concluded that it would be interesting to use this phenomena for the remote monitoring of tectonic stress.

The effect of stress on magnetization was not further studied in the laboratory for the next twenty-five years. Recently, however, fairly comprehensive investigations were performed on magnetite, and igneous and volcanic rocks by Kapitsa (1955), Kalashnikov and Kapitsa (1952), Grabovsky (1949), Grabovsky and Parkhomenko (1953), Graham (1957), Nagata and Kinoshita (1965), Nagata (1966), and Hodych (personal communication). Variations of these experiments usually involved applications of confined or unconfined compressive stress and different methods and directions of measuring the susceptibility.

Some specific points must first be covered by the results of the experiments in order to evaluate the theoreti-

cal basis of the piezomagnetic effects. In order of their importance these questions are:

1. Variation of magnetic susceptibility versus stress.
   a. As a function of initial susceptibility, k_0
   b. As a function of rock type
   c. As a function of direction of stress
2. Variation of remanence as a function of stress.
3. Effects of hydrostatic stress on magnetic properties.
4. The effects of stress on susceptibility and remanence at particularly low levels of stress, i.e., hyperbolic curve versus linear approximation.
5. Time dependence of the effects with regard to the decay of effects and any mechanical hysteresis.
6. Reversibility.

Beginning with studies on magnetite, the main carrier of rock magnetic properties, Grabovsky (1949) and Grabovsky and Parkhomenko (1953) investigated the effects of stress on the susceptibility and remanent magnetization. Well ordered results were obtained unlike those obtained with the normal inhomogeneous, random assortment of magnetite grains. The results showed a stress dependence of approximately -1.5×10^{-4} cm^2/kg for susceptibility and approximately the same value for remanent magnetization.

The stress dependence of susceptibilities for various

rocks is summarized in Figure 2. One may deduce a linear behavior for stresses above 400 kg/cm^2 with a slope of -1 to $-3\times10^{-4}\ \frac{cm^2}{kg}$ which is a 1% to 3% change in susceptibility per 100 kg/cm^2 stress. For small stresses, on the order of 100 kg/cm^2, however, the slopes are somewhat lower except for the positive dependence specimens which exhibit the highest slope of any curves, up to 6% change in susceptibility for 100 kg/cm^2 stress.

The stress dependence of the susceptibility, since it is a magnetostrictive anistropy phenomena, is at the same time a function of the direction in which the susceptibility is measured with regard to the applied stress. Two of the samples, andesite and basalt in Figure 2, which exhibit the largest negative stress sensitivity in the stress direction also showed a positive dependence, in fact the largest dependence, when measured normal to the stress.

Inasmuch as this study relates to stresses incurred in seismically active areas, the stresses of interest are those in the lower stress regions. Figure 3 summarizes experimental data in the zero to 200 kg/cm^2 increment of applied stress.

The effect of a change in hydrostatic stress on the magnetic susceptibility is a subject which is neither well understood nor are investigations in agreement. Kapitsa (1955) states "Induced magnetization of rocks should depend essentially on external stresses or more precisely, on the

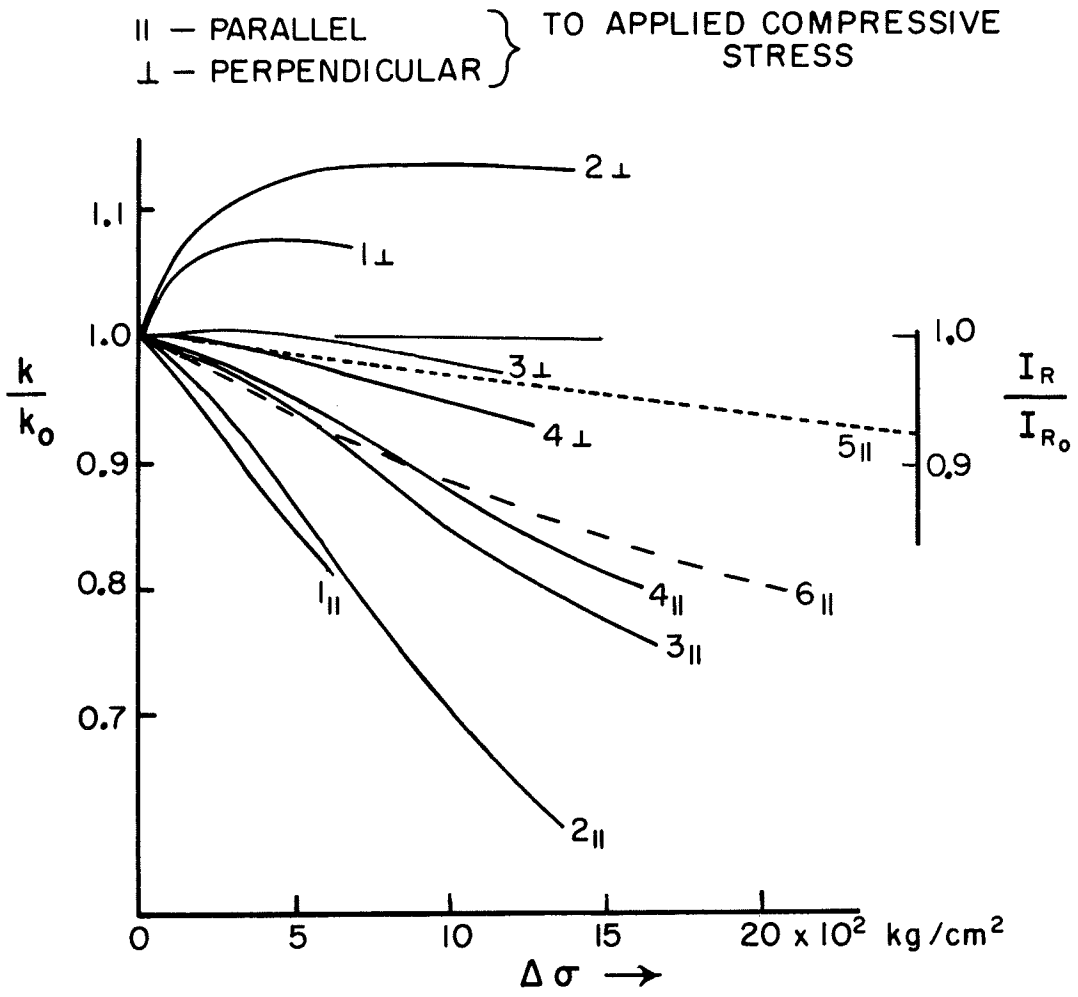

1. andesite — Kalashnikov and Kapitsa (1952)
2. basalt — Kapitsa (1955)
3. diabase — Kapitsa (1955)
4. basalt — Kalashnikov and Kapitsa (1952)
5. magnetite — Grabovsky and Parkhomenko (1953)
6. magnetite — Nagata (1966)

Figure 2. Piezomagnetic stress sensitivities obtained from a number of laboratory investigations.

magnetoelastic anistropy caused by external stresses. Consequently it may be supposed that uniform compression from all sides would have little effect on magnetic properties and only differences in principal stresses will affect magnetic properties of rock." On the other hand, Nagata and Kinoshita (1965) state "The effect of hydrostatic compression on the magnetic susceptibility of an assemblage of magnetite grains has been theoretically studied by Kern (1961) to prove that the susceptibility decreases hyperbolically with increasing compression."

The effect of rapidly changing stresses, particularly the release of stress has been shown by Kapitsa (1955) to have a delayed effect on the magnetic susceptibility with a relaxation time on the order of minutes for the examples of rock studied. This observation could have important consequences in the actual observation of such phenomena. It follows that the magnetic susceptibility analog of a rapidly changing stress will have a much lower rate of change especially if the stress is released by seismic events. Moreover, the magnetic field will therefore not change so fast as to generate a corresponding electric field by a rapid rate of change in flux density and there should be no electric potential generated from the piezomagnetic effect, even with seismic release of stress.

Certain irreversible effects were described in the various laboratory investigations. These effects occurred

at low stresses only and generally, if not always, disappeared either by repeated stress cycling or by annealing. The effects must therefore be due to such causes as internal stresses not completely relieved, anomalous mechanical treatment of the specimens, etc. Nagata (1965) states that no effect would be observed during the accumulation of stresses but only upon the release of such stresses. If this were true, the irreversible effect would create large anomalies in seismic regions during geologic time by the repeated cycling of tectonic stresses. On the other hand, such cycling has been shown by others to reduce or remove the irreversible effects.

B. Prior Reports of Possible Piezomagnetic Observations and Related Effects

The piezomagnetic effects as they are herein discussed and analyzed are those field changes which arise as a direct result of subsurface stress changes. Specifically, piezomagnetic changes are not the following:

1. Field changes which arise directly from thermal effects.
2. Apparent field changes due to mechanical vibrations of the moving parts of a magnetometer.
3. Magnetic field changes resulting from changes in an associated electric current.
4. Changes in absolute field intensity as a consequence of the secular variation of the field.

One of the objectives of this work is to present evidence on the existence of the piezomagnetic effect and to make clear the evidence against the attributing the observations in this investigation to the other phenomena enumerated above.

Subtle facts are involved in the reported observations of apparent local magnetic field effects that are associated with seismic activity. Any or all of the above five phenomena may be contributory to the reported observations of the magnetic field disturbances associated with earthquakes. Before

proceeding to the analysis of the piezomagnetic effect, it is therefore necessary to critically examine the prior reports.

The association between earthquakes and other natural phenomena has always intrigued man. The earliest reports of the coincidence of geomagnetic phenomena and earthquakes were usually not supported by sufficient objective evidence to permit valid criticism of the observations or their interpretation. Nevertheless, the number of reports and early dates of many of these observations is by itself evidence that many persons have applied themselves to the task of recording this phenomena. For example, changes in the geomagnetic field have been reported in 1755, 1799, 1822, 1842, 1844, 1846, 1851, and 1861 by Sart, Humboldt, Arage, Pilla, Palmieri, Lamont, and others (Milne, 1890). Reports by Humboldt, for example, in 1799 stated that the dip of the field diminished by 48' while the declination and horizontal intensity remained unchanged during an earthquake in South America. A large change in the inclination of the vector without a change in the components is not self consistent. An interpretation of this event as a field change is therefore invalid. In 1887 many years after self recording magnetic variometers had been in use, especially throughout Europe, a very large earthquake occurred on the Italian coast (Liguria) which caused large oscillations on most of variometers throughout Europe especially in Italy, Spain,

France, Switzerland, and Russia (Orlov, 1887). The disturbances did not all occur at the same time, however, but were observed at progressively later times as the distances from the epicenter to the variometer increased. This earthquake and its manifestations on the magnetograms, more than any other incident, gave rise to much speculation on the relation of seismic and magnetic disturbances.

Clearly, the obvious suggestion as to the cause of these reported disturbances is that the suspended magnet in the variometer responds mechanically to the seismic waves and thus behaves as a seismograph. Moreaux (Hazard, 1914) suspended a copper bar identical to a magnet in a variometer and noted that the copper bar did not respond to earthquakes as did the variometer claiming that this was indeed a magnetic phenomenon. Reid (1914) demonstrated, however, that the forces and moment of inertia on a magnet are different than those of a copper bar and their response to accelerations on their pivots will be quite different.

Milne (1894) drawing from a statement by Stukely in 1756 attributed the cause of the magnetic disturbances to electrical discharges between the earth and sky. Milne stated that the decrease in earthquakes in San Francisco from 136 between 1850 and 1865 to 88 between 1866 and 1881 was the result of the equalization of potentials by the installation of railroad tracks across the country.

Burbank (1905) conducted a systematic comparison of

the magnetograms and seismograms of the U.S. Coast and Geodetic Survey. Only a qualitative comparison of the signatures was obtained with no specific conclusions as to their relationship except that the magnetographs do indeed appear to respond to seismic surface waves. Bauer (1906) examined the magnetograms throughout the United States for the San Francisco earthquake of 1906 and concluded that the magnetic disturbances occurred at the time of the arrival of the surface waves.

Remarkably few reports have appeared since 1910 regarding the sudden disturbances on suspended-magnet variometers at the time of earthquakes. A few reports by Gouin, (1965) and Kato and Utashiro, (1949) are identical to the earlier ones cited above. Gouin's observations held the same inconsistencies as did Humboldt's in 1799. Kalashnikov (1954) reported on the disturbances recorded by induction coil magnetometers at the time of earthquakes. Such a device responds to $\frac{dB}{dt}$, the time rate of change of flux, and is thus particularly sensitive even to small motion of the coils. The transient effect reported by Moore (1964) at Kodiac island before the Alaskan earthquake of 1964 were disturbances that would certainly be disregarded on any electronic device if they had occurred at that particular time. The sensing element, a fluxgate component sensor, again was not only sensitive to seismic motions but was operating in the automobile lot of a motel only 40 feet

from the main highway (Moore, personal communication, 1964).

Differential proton magnetometers operating in the seismically active area of Matsushiro, Japan showed a steadily changing intensity difference over a 70-day period as reported by Rikitake (1966). Other long term single sensor observations show local differences in the field in a completely random sequence due to the large effects of a nearby (4 km.) direct current railway. Measurement of the effects of the changing direct currents at the proton magnetometer station were found to be ± 4 gammas throughout the day and night.

Kato (1938, 1940) was the first to report slow changes in the local geomagnetic field that might be associated with local earthquakes. Reports by Kato (1938, 1940) Kato and Tahazi (1953b) and by Rikitake (1951), involve, in their words, a rising Curie isotherm moving upward in an active volcano. The volume of rock which loses its ferrimagnetic properties produces a decrease in the local inducing field and thus a decrease in the field intensity.

Other reports, such as those by Rothé (1950), claimed to have observed a locally anomalous secular variation that was associated with local seismic activity. Omer (1945) compared the seismicity maps with the maps of nonlinear secular variation to conclude that these phenomena may be related.

Thus, it appears that of all the reported observations

only two observers reported on non-volcanic sources, and non-secular change magnetic events apparently related to earthquakes.

The more recent reports describe changes in dip apparently associated with large local earthquakes. There is insufficient information, however, to evaluate even the most basic requisites to determine the validity of these subtle events. The earliest of these related the results of comparing magnetic inclination measurements made in 1895 and then 18 years later. From the observed differences, Kato (1953a) concluded that the changes were definitely related to earthquakes in 1896 and 1897. A two-minutes-of-arc change in dip of a mechanical inclinometer which may have occurred instantaneously with a large local earthquake was reported by Kato and Utashiro (1949) without qualification even though it was exactly as those reported in the last century and whose validity is certainly in question. The changes in dip over many months or years was interpreted by Kato et.al., (1953b) as a significant event but Miyakoshi (1953) shows the same rate of secular change at many other observatories in Japan without association to seismic events. The calculated dipole moments of the observations of Kato (1953a) are approximately 10^{17} cgs and if real, and the result of piezomagnetic effects, are unjustifiably large. This will be shown in a following section of this work. Moreover, the depth to some of the dipole centers was reported as 35 kilo-

meters, deeper than the estimated Curie isotherm (particularly in Japan) and therefore not even in the ferrimagnetic regime. Also, movement of the Curie isotherm at these depths is not possible at the observed rates. Therefore, large volumes of material losing or acquiring ferrimagnetic properties cannot be included as a cause of the magnetic variation. In spite of the inconsistencies of the reported observations, there nevertheless appears to be some evidence that real changes in the local magnetic field were observed and which perhaps require a more careful correlation and re-evaluation.

Miyakoshi (1953) presented magnetograms of anomalous declination which span a period of 18 months. The variations of interest are first the anomalous rate of change from a normal of 3' to 9' of arc per year to a total change of 6' of arc over an 8 month period. A magnitude 7 earthquake occurred during this 8 month period at a distance of 40 kilometers from the magnetic declinometer and at a depth of 20 kilometers. Superimposed upon this anomalous change was a markedly steeper change of slope during a two week span one week before the seismic event. A similar set of observations are reported for another event with similar behavior except that the earthquake was 60 kilometers distant at a depth of 70 kilometers. The observations are well documented with records of other declinometers showing the normal secular change and daily activity at this time. There is, in this report, however, a minor inconsistency in that the

other declinometers show no similarity in any behavior to the anomalous variations at the other two stations. That is to say, the anomalous variations at the other two stations do not even appear to show the normal ionospheric variations present on the other magnetographs in Japan which of course raises the question of validity on the observations themselves. The author suggested without any substantiation that the direction of the declination was, in each case, towards the epicenter. Magnetic forces by virtue of their complex dipole fields, would not necessarily cause such a directional change in flux. Such an observation, therefore, is irrelevant with regard to the location of the epicenter.

In summary, the observational evidence collected since organized magnetic measurements began suggests that there are changes in the local field that have some association in time with large local earthquakes. As the mechanical stability of suspended magnetic variometers are always in question in the presence of large siesmic surface waves, their evidence is much in question. There have been at least four reports by Kato et.al., (1950, 1953b), Miyakoshi (1953), Breiner (1964), and Rikitake (1966) that demonstrate local changes in the field with a time scale too long to be attributed to seismic vibrations. These changes were all very small and all were presented with independent records to show that they were indeed local events. Perhaps most important, each of these reports involved rather long term events with

questionable, if any discrete changes that directly accompanied the earthquake. In other words, these reports indicate that the span of time of the magnetic events was considerably longer than a few seconds of duration of the earthquake with which they might be associated.

C. The Time Signature of the Piezomagnetic Effect

Introduction

Recognition of a piezomagnetic effect on the continuous records of the geomagnetic field depends, in part, upon the knowledge of its time signature. The piezomagnetic effect is an analog representation of the changes in stress and as such is a means for the remote measurement of stress, possibly even in the focal regions of earthquakes and creep centers. There is almost a complete lack of any observational evidence on the changes in stress in seismic regions. This lack of direct evidence places the prediction of stress changes in the realm of pure speculation but in the realistic bounds guided by laboratory and field strain observations. It is this very lack of stress data which places strong emphasis on the desirability for some means of measuring the stress changes in such regions.

Hypotheses for at least a qualitative time signature of the stress changes and their piezomagnetic effects can be approached through an evaluation of the observed strain changes in seismically active areas. In fact, the observational evidence, at least in some cases, indicates that the earthquake itself is not the principal stress/strain event but perhaps only a consequence or local readjustment towards equilibrium of the local stress field. Orowan (1960) con-

tends, that the earthquake source cannot be regarded as a consequence but rather a cause of fault displacement and that neither radiated seismic energy nor geodetic strain data is an accurate measure of the source energy or associated stress. The total energy and therefore the stress released during the processes connected with an earthquake might therefore be considerably larger than deduced from radiated seismic energy.

Field Evidence for the Time Signature of Stress Changes

The variations in stress have never been observed directly in seismically active areas though in situ point measurements of stress are made in certain mining investigations (Judd, 1964). Observations of other phenomena such as tilt, strain, or energy release can be related to stress but there are many unknowns in their functional relationships. Moreover, all of these measurements involve displacements of the surface of the ground and may not represent the true variations of stress or even the same phenomena as it occurs at depth.

Seismic waves, at least in part, derive their energy from the strain energy stored in the focal region. The stresses necessary to maintain these strains must therefore be released suddenly at the moment of the generation of the earthquake. As the elastic strain propogates the stresses decrease, along a fault, or radially, if a volume strain is

involved. The strain changes observed in connection with many local and distant earthquakes tend to confirm such a form for the stress variation.

Laboratory investigations (Watanabe, 1963) on the brittle fracture of rock have shown that as the applied stress is increased the strains and therefore the internal stresses accumulate in stepwise fashion, analogous to the Barkhausen effect of magnetic domain orientation. Not only are the stresses stepwise but the stress actually decreases in each step as the rock is strained, this behavior being known as stick-slip faulting (Brace and Byerlee, 1966). Such behavior of the stress as it manifests itself in seismic events has been observed on numerous foreshock sequences (Watanabe, 1964). However, small strains are not truly representative of the total stress picture when the rock is strained through creep or plastic deformation. The sudden release of stress when the rock specimen fractures is also not representative behavior when the specimen, its confining pressure, and constraints are scaled up to the dimensions of a real fault.

The strain variations from a large magnitude earthquake in Peru, (Benioff, 1964) exhibited a complex variation in time, including an appreciable remaining stress which Benioff interprets as the source of the aftershock energy. The strain signature shows excellent agreement with a mathematical model proposed by Pekeris (1955). This strain evidence with its theoretical justification might provide a reasonable expecta-

tion of the stress variations for large magnitude seismic events.

The cumulative energy release of an aftershock sequence also indicates the existence of large strain and therefore stresses following large earthquakes. Benioff (1951) expresses this energy release as a function of time to demonstrate its analog to the creep functions of rock in the laboratory when stressed for a long period of time.

The object of this investigation of the piezomagnetic effect is not limited to the changes in stress directly associated with earthquakes but also those changes which might occur before earthquakes or even during a seismic period. Tilt observations, particularly in Japan, have provided considerable evidence that there are indeed stress changes which do not occur simultaneously with earthquakes. Many of these anomalous tilt changes have begun before and continued well after large local earthquakes indicating that the stress changes have a much longer duration than the few seconds of the seismic event (Sassa and Nishimura 1963). A common feature of most of these tilt events was that most of them have followed not seconds or days but 2 to 10 hours later by large magnitude local earthquakes (Kitamura, 1964; Hagiwara, 1964; Tsuboi, 1962). A few anomalous secular tilt observations have also been reported to be associated with earthquakes (Hasoyama, 1952).

Deformations of the earth's surface have been reported,

however, which were not followed or associated directly with earthquakes. Aseismic displacements of the San Andreas and associated fault systems described as rupture creep have been reported by Koch (1933), Tocher (1960), and Bolt (1966). The creep events reported by Tocher (examined in detail in other sections in this work) occur spasmodically in discrete jumps during a few hours every few months and are usually not accompanied by local earthquakes. The other cited reports of creep and reports of geodetic triangulation (Whitten, 1966) indicate that fault displacement and perhaps the associated stress changes are continuous, at least within the resolution afforded by several years of annual readings. Appreciable (1.5 cm) surface strain, associated with a magnitude 3.6 earthquake on the San Andreas fault 600 kilometers from the Hollister creep zone have been reported by Brune and Allen (1967). The strain changes span a finite length of time, on the order of a few days to tens of days, during which the stress would also vary.

Conclusions drawn from the above evidence, particularly with regard to the San Andreas fault, supports the idea that the stress variations are much more complex and span a longer period of time than the seismic energy by itself indicates. The strain changes, on the other hand, must be related to the stress variation but not necessarily in the elastic region. The surface expression of the strain with its limitations is the best field evidence available for the

time signature of the stress changes.

Theoretical Model of the Time Signature

Reid (1910) analyzed the geodetic triangulation data across the San Andreas fault before and after the San Francisco earthquake of 1906. From this study he concluded that before the earthquake the areas away from the immediate fault trace were displaced in a right lateral sense from a line normal to the trace. The greater the distance from the fault, the greater was the displacement, with no displacement at the trace itself. From repeated surveys, Reid determined that the strain was increasing in time linearly over the time scale of his observations. The fault displacement accompanying the earthquake caused points to move inversely with respect to their displacement before the earthquake. More specifically, points near the fault were caused to "rebound" and move in a right lateral sense from its former continuation across the fault.

If one assumes that the surface strain did vary directly with time, that the surface strain reflected the subsurface strain at least to the focal depth, and the strain was within the elastic limit, then by Hooke's law

$$\text{strain} \propto \text{stress}$$

and

$$\text{strain} \propto \text{time}$$

therefore

$$\text{stress} \propto \text{time}$$

From a large scale long term viewpoint, then, a linear increase

in stress with respect to time is perhaps the most likely basis for the accumulation of strain energy. For lack of strong evidence to the contrary, a linear signature for the stress increase will be adopted as the primary stress or tectonic stress field about the fault. No theory presently exists to draw upon that would explain a regional non-linear accumulation of stress.

The above assumption of a linear change is restricted to the accumulation of stress only and not the release. Furthermore, the linear change is suggested as the normal rate of increase for the fault. The change may not be linear for short periods of time preceeding strain events nor linear for local stress accumulation such as might occur following a local transfer of strain on the fault.

An objection to a constant low rate stress is the lack of any evidence for tidal triggering of earthquakes. If the total stress that is relieved in an earthquake requires tens of years to accumulate, then the cyclic tidal forces generate pulses of stress whose peak values are always somewhat greater than the instantaneous value of stress. No direct measurements of stress have ever been made on active faults, direct measurements at depth have never been possible and linear strain variations over long periods of time such as from tilt or strainmeters have never been reported. Lack of evidence for linear variations, however, does not weaken the argument as this type of instrumental observation

represents a most difficult task.

Practically all theories of rock deformation particularly under high hydrostatic stresses involve non-linear anelastic behavior, or effects which are time dependent. The nature of the non-linear strain (and stress) behavior of rock is, at best, imperfectly understood. The best source of information from which to establish a hypothesis on the stress/time signature for this study must come from empirical evidence. The tilt, strain, and magnetic information cited above serves only to guide the overall balance of whether to expect linear or non-linear variations. Laboratory investigations on the stress behavior of rocks, however, provide usable empirical relationships of stress and strain versus time under a variety of conditions.

Numerous laboratory experiments have been conducted to reproduce as nearly as possible the conditions expected at depth. The rocks at any depth are subjected to a hydrostatic stress. Consider, for example, a column of rock of mean density 2.5 gm/cc^3. The stress exerted at a depth of 1 kilometer (10^5 cm) in this column is 2.5×10^8 $dynes/cm^2$ or 250 kg/cm^2. Because of the low rate of accumulation of tectonic stress, the deviatoric stress ($\Delta\sigma$) is likely to be acting upon the rocks for a considerable length of time. Furthermore, through geologic time, this stress is also undergoing cyclic behavior each time the stress is relieved by strain release in rupture or other means of deformation.

Deformation of rock specimens when subjected to such behavior in the laboratory principally exhibit the phenomenon of creep behavior in which the strain rate is non-linear with respect to time (Griggs, 1939; Lomnitz, 1956). All crystalline rocks and in fact most sedimentary rocks can therefore exhibit creep deformation under the typical subsurface conditions. This phenomenon will be used as the basis for determining the time variations of the stress field.

Griggs (1939), Robertson (1960), and Lomnitz (1956) investigated creep phenomena and found that the relationship

$$\frac{d\varepsilon}{dt} = kt^{-n}$$

where ε = strain

originally suggested by Andrade (1910) represents most rocks studied in the low hydrostatic stress condition. Lomnitz determined that n = 1 especially for intrusive rocks such as granodiorite and gabbro. In our model we will assume the values also held for granite. Letting n = 1 and integrating both sides with respect to t, we have

$$\varepsilon = -k_1 \log t + k_2$$

where k_1 and k_2 are constants which describe respectively the rate of strain and the elastic strain independent of time.

The development of the non-linear stress variation is based upon the premise that those changes are local effects and the result of relaxation of the primary regional stresses described above in the treatment of the stress accumulation. "Local" in this respect might refer to lengths of the fault a few tens of kilometers but probably not hundreds of kilometers. Following the approach of Benioff (1951) we shall assume that the strains arising from these relaxation effects whether they accompany creep, shear, or a seismic event, act as a constraint in the local stress field. In other words, the local stress variations simply follow the large scale strain variations and are proportional to them. Then the local stress for small strains can be expressed by Hooke's law as

$$\Delta\sigma = \mu\varepsilon$$

where μ is the effective modulus of rigidity. Using strain as the common variable relating local stress and time, we have

$$\Delta\sigma = -\mu k_1 \log t + \mu k_2$$

The constant k_2 determines the long term extremely low rate stress accumulation whereas the constant k_1 partially determines the rate of stress release through creep deformation. This expression will be used to predict the time signature of stress.

Application of Theory to Observed Events

From the field investigation of the piezomagnetic effect described subsequently in Part 3, we have the most frequently observed signatures as shown in Figure 4. The magnetic intensity is, of course, represented here as a function of time. However, by simply replotting the data we see in Figure 5 that the observed variation is directly proportional to log t and, in fact, follows the same general expression given above in the rheological development for $\Delta\sigma$. We have

$$\Delta F\ (\sigma,t) = -k_1 \log t + k_2$$

Where k_2 is a linear term not shown in the Figures. Thus, the magnetic field intensity variation is shown here as the analog of the stress variation. This result follows, of course, from the theory of the piezomagnetic effect given in the previous section. The similarity of the time dependence of the postulated and observed results do not, of course, prove that these observations represent the piezomagnetic effect. Reasonable assumptions were used in the development of the theory so that the agreement between the signatures does lend support for the validity of these piezomagnetic observations.

The signatures in Figure 6a occurred just before measured aseismic shear displacement of the fault which was later

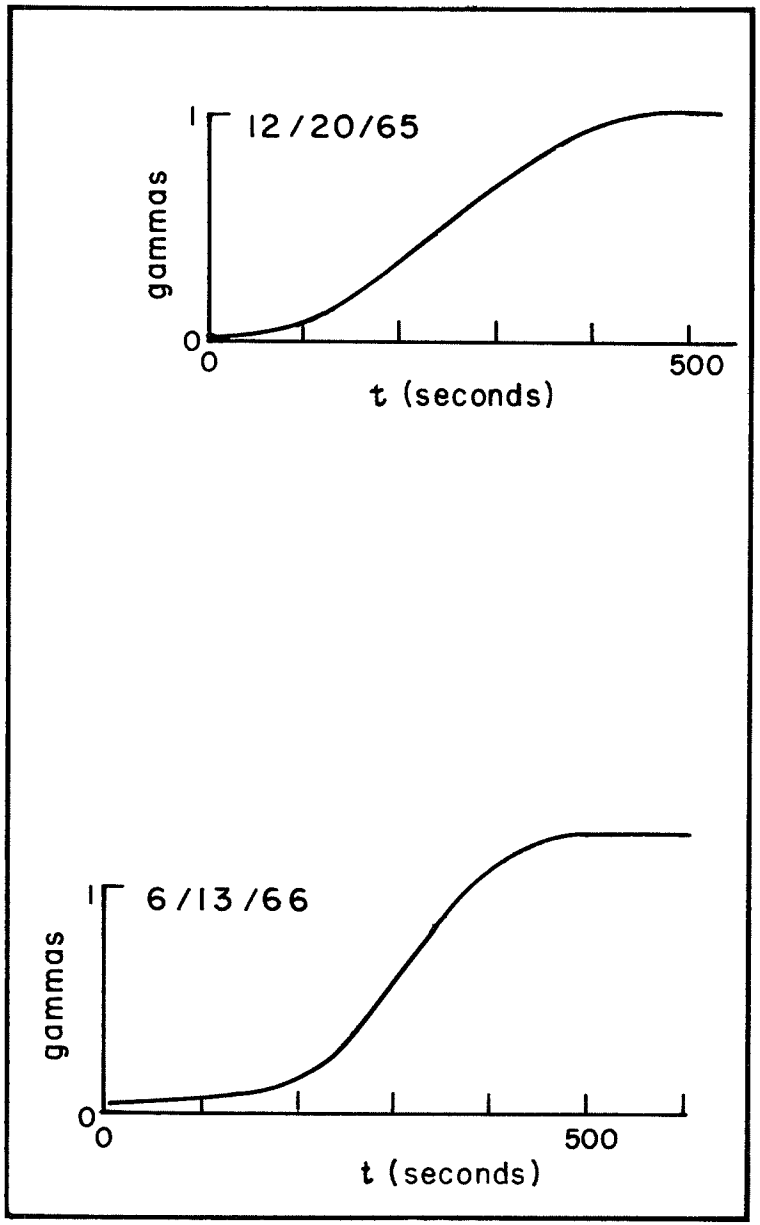

Fig. 4. Typical signatures of local magnetic events which precede fault creep displacement.

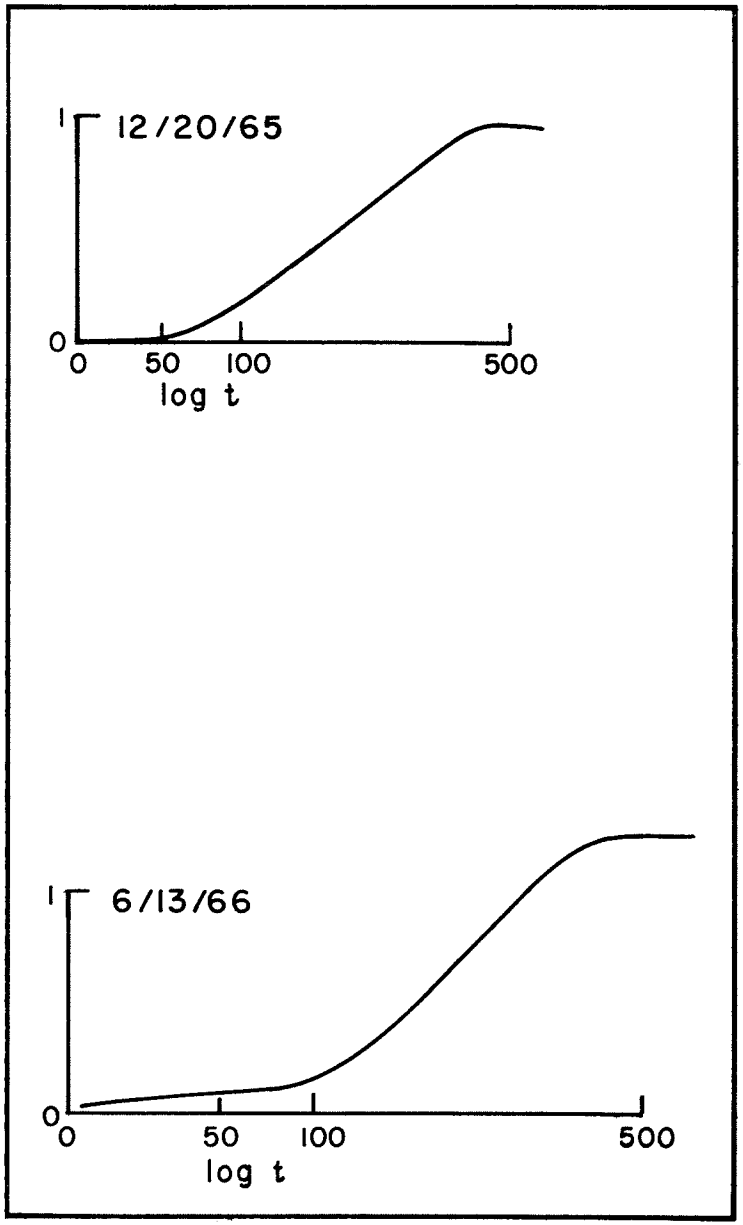

Fig. 5. Local magnetic events as a function of log of time.

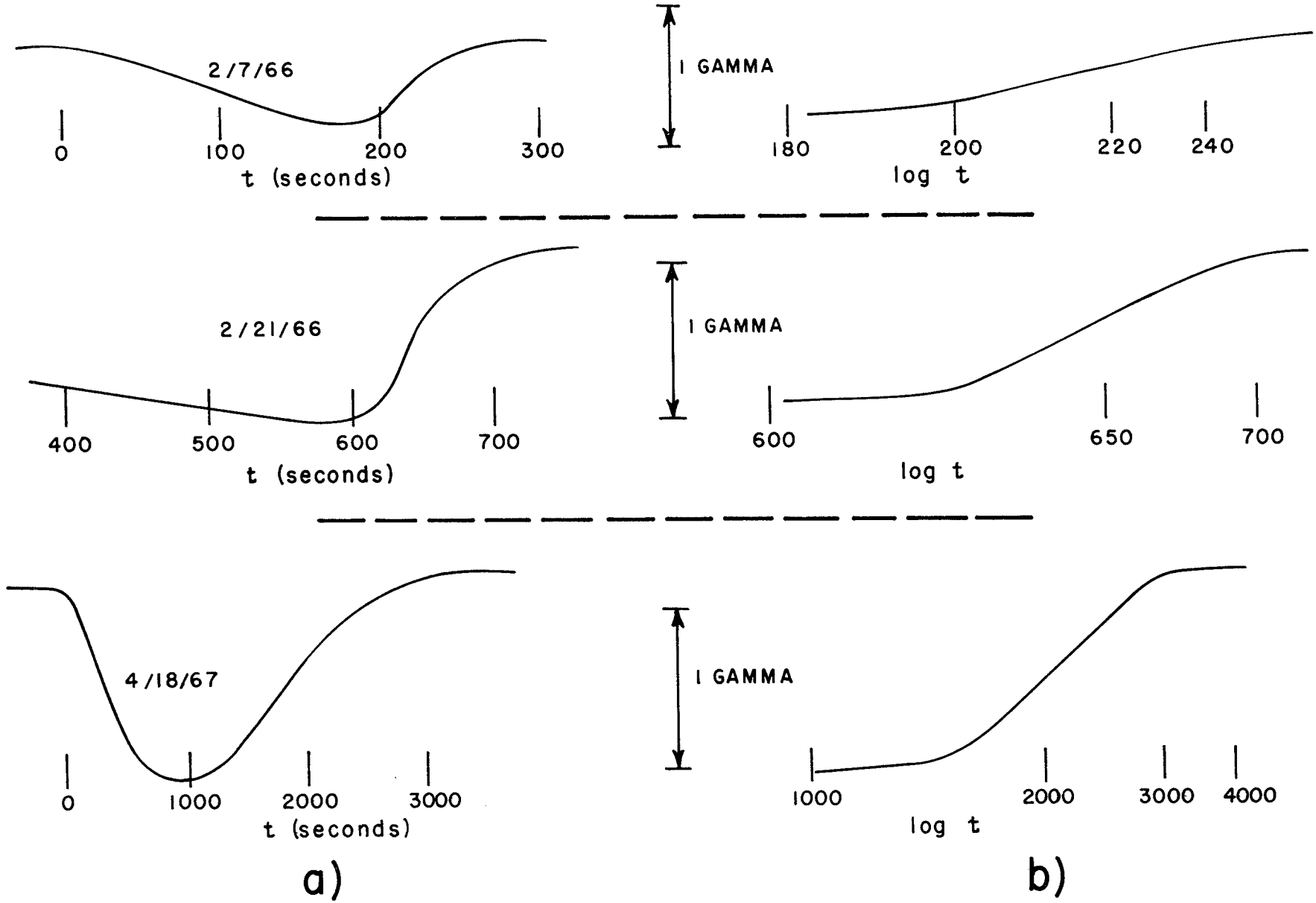

Fig. 6. Local magnetic events of the type which precede large creep displacement and occasional small earthquakes, a) as a function of time, b) the non-linear portions as a function of log of time.

followed by a local earthquake. In these cases the magnetic intensity and presumably the stress, did not remain offset but returned as part of the same phenomena. This time variation fits a somewhat different function than the more often observed signatures of Figure 4, above. The intensity decreases directly with time reaching a peak value and then follows the logarithmic expression in the same sense as the events in Figure 4. An interpretation of the stress variation of this signature in light of the above model would be

$$\Delta\sigma = \mu\varepsilon \qquad t_0 > t > t_1$$

$$\Delta\sigma = k_1 \log t + k_2 \qquad t_1 > t > t_2$$

The stress increased linearly to a time t and then returned by transient creep to its initial value. The signatures are replotted as a function of log t in Figure 6b.

Robertson (1960) suggested that fracturing is an important mechanism of transient creep, that is, the creep which follows the logarithmic variation. He noted that the process of transient creep decreased sharply with an increase in hydrostatic stress. He interpreted this fact by suggesting fracturing as an important mechanism of creep. The presence of fractures decreases with hydrostatic stress. If the observed piezomagnetic effects do indeed reflect stress as a function of transient creep phenomena, then the effect

should originate in relatively shallow regions.

On a local scale, there is a similar problem of why there may be a change in stress either without or before an observed rupture creep or seismic event. Griggs (1954), Orowan (1960), and Griggs and Handin (1960) have pointed out that rocks under high hydrostatic stress and long term deviatoric stress can deform by viscous creep where the rate of deformation is very small below a value of stress equal to a value called the creep strength. The rate of strain increases exceedingly fast for small values of stress above this level and the deformation becomes almost self accelerating. The mechanism by which this might take place might be shear melting initiated by creep instability (Orowan, 1960) a self-accelerating phenomena of deformation which concentrates itself in narrow regions. The rise in temperature from the release of strain energy would further accelerate the deformation particularly in the regions where the deformation began. Although this suggestion was presented to explain the apparent faulting that occurs at the depths of intermediate and deep focus earthquakes, the phenomena of creep instability and consequential propagation of strains and stresses at less than the speed of elastic waves might also apply to the piezomagnetic observations presented here. The transfer of strains which result from slow creep or plastic deformation would also impart additional stresses on adjacent portions of the stressed region. Stress

changes would accompany these effects and could conceivably propagate at a velocity orders of magnitude lower than a corresponding elastic wave.

D. Quantitative Considerations of the Piezomagnetic Effect

Introduction

Determination of the possible amplitude of the piezomagnetic effect is perhaps the most important result of the laboratory studies as they apply to piezomagnetic observations in the field. Estimates of these effects together with analytically derived signatures permit us to assess the requirements for observing this phenomenon.

Expressed as a change in field intensity, ΔF, from a unit dipole source of small dimensions, the piezomagnetic effect is a function of the change in stress, $\Delta\sigma$; stress sensitivity, s; magnetic susceptibility, k_0; ambient field intensity, F; volume of rock, V; distance to the source, r; and orientation of the dipole, θ.

$$\Delta F = \frac{\Delta\sigma \; s \; k_0 \; FV}{r^3} \; f(\theta)$$

The volume, distance to the source, susceptibility, and stress change may each vary two or three orders of magnitude from one field condition to another. The limits of s, F, and $f(\theta)$ are considerably smaller. Estimates of the magnitude of the piezomagnetic effect, then, require an understanding of each factor in this expression. From this, we may then determine the possible values for a component

magnetic field intensity anomaly as would be observed with a magnetometer on the surface.

Stress Dependence

The magnetic susceptibility anisotropy introduced by the application of deviatric stresses was discussed earlier with references to the theoretical work of Kern (1961) and Stacey (1962b) and particularly the laboratory investigations of Grabovsky and Parkhomenko (1953), Kalashnikov and Kapitsa (1952), and Kapitsa (1955). For convenience in computing the piezomagnetic anomalies, we may express the magnetic susceptibility dependence in terms of its components, S_c and S_t, parallel and perpendicular, respectively, to the applied compressive stress. Since rocks are largely incompressible, S_t is, in fact, the stress dependence of the resulting tensile stress. The stress sensitivities determined for a number of volcanic and igneous rocks (Kapitsa, 1955) appears in Figure 2, as a function of stress. The dependence in the low values of stress, namely the region of 200 kg/cm^2 or less, are shown because this region is more applicable to the real case than is the region of several thousand kg/cm^2 used in the laboratory investigations. The tensile stress dependence is similarly plotted and is considered important because of the high tensile stress dpendence in the low stress regions.

The piezomagnetic properties of a given rock type

depend not only upon its stress sensitivity but also upon the susceptibility and remanent magnetization. The latter is so highly variable within a rock type, dependent upon its local mechanical and thermal history, and so dependent upon the orientation of its remanence vector with respect to the applied stresses that a quantitative description of the stress dependence is not meaningful. The susceptibility does, however, lend itself to a quantitative study in connection with the stress sensitivity because it is more predictable and is also an isotropic quantity with respect to the stress application. The product of the susceptibility and stress sensitivity is the magnetic susceptibility change per unit stress change per unit volume and thus represents the principal rock-determined properties for the amplitude of piezomagnetic effect. This expression is listed in Table 1 for various rock types, together with compressive and tensile stress sensitivities assuming total magnetization in a field of 50,000 gammas.

Piezomagnetic Dipole Anomaly

The change in magnetization created by stress produces a piezomagnetic anomaly that varies in time and space. In order to examine the relative importance of the magnetic, geometric and stress environment considerations, we can create a simple piezomagnetic model and vary the critical parameters one at a time. However, we need only to treat

Table 1. Specific Piezomagnetic Parameters for Selected Rock Samples

Ref.	Rock Type	Susceptibility, k_0 (cgs)	Stress Sensitivity, S @100 kg/cm^2 (cm^2/kg) S_c	S_t	$S=(S_c^2+S_t^2)^{1/2}$	Piezomagnetization/stress, (gauss/cm^3/kg/cm^2)
1	basalt	3.5×10^{-3}	-2.7×10^{-4}	4.6×10^{-4}	5.3×10^{-4}	9.2×10^{-2}
1	basalt	3.7×10^{-3}	-0.8×10^{-4}	-0.4×10^{-4}	0.9×10^{-4}	1.7×10^{-2}
2	basalt	3.8×10^{-3}	-1.2×10^{-4}	4.8×10^{-4}	4.9×10^{-4}	9.3×10^{-2}
1	andesite	1.8×10^{-3}	-3.2×10^{-4}	2.7×10^{-4}	4.2×10^{-4}	3.8×10^{-2}
1	diabase	4.6×10^{-3}	-1.0×10^{-4}	0.6×10^{-4}	1.2×10^{-4}	2.8×10^{-2}
2	diabase	7.1×10^{-3}	-0.8×10^{-4}	1.0×10^{-4}	1.3×10^{-4}	4.6×10^{-2}
1	syenite	1.3×10^{-3}	-0.6×10^{-4}	2.7×10^{-4}	2.8×10^{-4}	3.6×10^{-2}
2	syenite	1.7×10^{-3}	-0.3×10^{-4}	0.8×10^{-4}	0.9×10^{-4}	0.8×10^{-2}
1	hornblendite	3×10^{-2}	-1.1×10^{-4}	1.5×10^{-4}	1.9×10^{-4}	2.9×10^{-2}
1	diorite porphyry	8×10^{-5}	-0.4×10^{-4}	- - - - -	0.4×10^{-4}	0.02×10^{-2}
1	basalt	5×10^{-4}	-0.3×10^{-4}	- - - - -	0.3×10^{-4}	0.08×10^{-2}
1	gabbro	10^{-4}	-0.3×10^{-4}	- - - - -	0.5×10^{-4}	0.03×10^{-2}
1	diorite	5.3×10^{-3}	-0.2×10^{-4}	- - - - -	0.2×10^{-4}	0.53×10^{-2}
2	diorite	7.1×10^{-3}	$+0.3 \times 10^{-4}$	0.6×10^{-4}	0.3×10^{-4}	1.1×10^{-2}

F = 50,000 gammas
1 Kalashnikov and Kapitsa (1952)
2 Kapitsa (1955)

the anomaly in the spatial domain at a point in time when it is at its maximum value.

The simplest model is one in which the piezomagnetic effects are determined for a unit volume and then integrated over the entire source. The magnetic intensity from an infinitesimal volume, dV, at a distance, r, from the point of observation is

$$\Delta F = \int_V \frac{\vec{M}(\sigma)\,dV}{r^3} \quad f(\theta) = \int_{z_0}\int_{y_0}\int_{x_0} \frac{\vec{M}[\sigma(x_0, y_0, z_0)]\,dx_0\,dy_0\,dz_0}{(x^2 + y^2 + z^2)^{3/2}} (1+3\cos^2\theta)^{1/2}$$

where M is the dipole moment per unit volume and θ is the angle between the direction of the moment and the radial line to the point of observation. The dipole moment per unit volume is

$$\vec{M} = \Delta k \vec{F}$$

The susceptibility change, Δk, is of course, a product of the stress sensitivity, S, initial susceptibility, k_0, and stress change $\Delta\sigma$. Because we are calculating the maximum value of the piezomagnetic anomaly, the maximum magnetization is the resultant of the othogonal components of stress and stress sensitivities, each of which are

$$\Delta k_c = S_c \, \Delta\sigma_c \, k_0$$

$$\Delta k_t = S_t \, \Delta\sigma_t \, k_0$$

and $$\Delta k = k_0 [(S_c \, \Delta\sigma_c)^2 + (S_t \, \Delta\sigma_t)^2]^{1/2}$$

Substituting

$$\Delta \vec{F} = \int_{z_0} \int_{y_0} \int_{x_0} \frac{k_0 [(S_c \, \Delta\sigma_c)^2 + (S_t \, \Delta\sigma_t)^2]^{1/2} (1+3\cos^2\theta)^{1/2}}{(x^2 + y^2 + z^2)^{3/2}} \, dx_0 \, dy_0 \, dz_0$$

Assuming that the stress distribution, stress sensitivities, and susceptibility are all constant within the volume, these variables can be removed from the integration process. Furthermore, if the volume under consideration is spherical, the magnetic dipole effects are identical to the intensity from an infinitesimal dipole of equal dipole moment located at the center of the volume. Further, if the radius of the sphere and the radius to the source are equal, we have

$$\Delta \vec{F} = k_0 \vec{F} \, [(S_c \, \Delta\sigma_c)^2 + (S_t \, \Delta\sigma_t)^2]^{1/2} (1 + 3 \cos^2\theta)^{1/2} \frac{\frac{4}{3}\pi R^3}{R^3}$$

The term involving θ simply describes the maximum intensity of a dipole source as a function of the angle from its axis. Assuming that the point of observation is on the dipole axis (high magnetic latitude), $\theta = 0$ so that

$$(1 + 3 \cos^2\theta)^{1/2} = 2$$

The stress changes $\Delta\sigma_c$ and $\Delta\sigma_t$ can be related by considering the rock to be under pure shear

$$\Delta\sigma_c = \Delta\sigma_t = \Delta\sigma$$

Then substituting we get,

$$\Delta F_{max} = \frac{4}{3}\pi\ k_0\ \vec{F} \cdot \Delta\sigma\,(S_c^2 + S_t^2)^{1/2} \cdot 2$$

Possible values of k_0, $\Delta\sigma$, S_c and S_t, have been given in Table 1. Throughout this analysis, the field intensity, $\vec{F}$, is considered constant in amplitude and direction and equal to 50,000 gammas. The variations in the observed anomaly for different susceptibility values and various values of stress and stress sensitivities are shown in Figure 7.

The relative values of S_c and S_t are important with regard to component measurements of the field since they determine the direction of the piezomagnetic dipole direction. The amplitude of the anomaly varies linearly with susceptibility and stress change. However, since these quantities are probably unknown within one or two orders of magnitude at depth in the earth this estimate of the piezomagnetic anomaly could be in error by several orders of magnitude. Assuming the minimum values for k_0 and $\Delta\sigma_t$ to be 10^{-4} cgs units and 10 kg/cm^2 and S_c and S_t to be 2×10^{-4} and

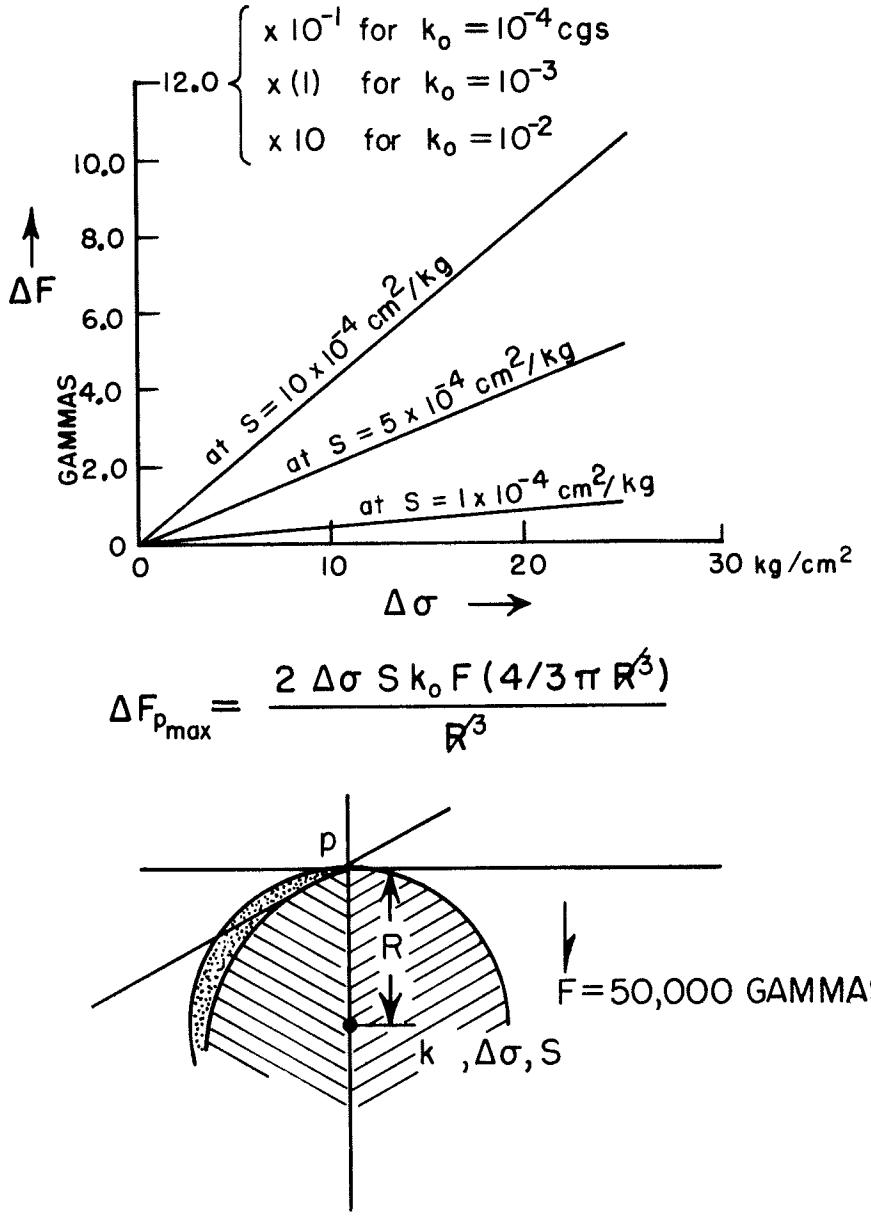

Fig. 7. The maximum amplitude of a piezomagnetic anomaly as a function of the expressed geometry, susceptibility, stress change and stress sensitivity.

6×10^{-4} cm^2/kg respectively, we get

$$\Delta F = \frac{4}{3}\pi \times 10^{-4} \times 5 \times 10^{4} \times 10 \ (4 + 36)^{1/2} \times 10^{-4}$$

$$= 0.12 \text{ gammas}$$

Inserting maximum estimates for k_0 and $\Delta\sigma_t$ of 10^{-3} cgs and 10^2 kg/cm^2 respectively,

$$\Delta F = \frac{4}{3}\pi \times 10^{-3} \times 5 \times 10^{4} \times 10^{2} \ (40)^{1/2} \times 10^{-4}$$

$$= 12.0 \text{ gammas}$$

The susceptibility of the area under study is unlikely to differ by much more than the assumed limits so that a reasonable value of the susceptibility might be an average value of the limiting estimates. The corresponding limits of the maximum expected piezomagnetic anomaly for stress changes between 10 and 100 kg/cm^2 would then be 0.60 and 6.0 gammas.

Piezomagnetic Anomaly Over Strike Slip Fault Model

Stress Distribution on Strike Slip Fault of Infinite Horizontal Extent

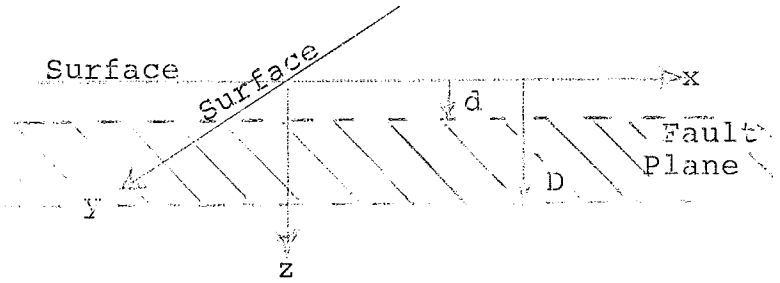

Figure 8. Strike-slip fault geometry.

From dislocation theory of Steketee (1958), Chinnery (1963) derived the expression for the shear stresses on a strike slip fault of infinite horizontal extent (Figure 8). These expressions are

$$\tau_{yx} = \frac{U\mu}{2\pi}\left[\frac{d+z}{y^2+(d+z)^2} - \frac{D+z}{y^2+(D+z)^2} + \frac{d-z}{y^2+(d-z)^2} - \frac{D-z}{y^2+(D-z)^2}\right]$$

and

$$\tau_{zx} = \frac{U\mu y}{2\pi}\left[\frac{1}{y^2+(D+z)^2} - \frac{1}{y^2+(d-z)^2} - \frac{1}{y^2+(d+z)^2} + \frac{1}{y^2+(d-z)^2}\right]$$

where U is the displacement, μ, the modulus of rigidity, and d and D, the depths to the top and bottom of the fault respectively. These expressions were evaluated for a fault of 5 kilometers depth assuming a displacement of 1 centimeter (Figure 9).

The shear stress τ_{yx} and τ_{zx} can each be resolved into their corresponding compressive and tensile stresses and these stresses, in turn, expressed as a piezomagnetic component of the change in susceptibility. The compressive and tensile stresses can be treated in terms of their coordinate components so that the stress sensitivities, S_c and S_t may be applied separately. The vector sum of the piezomagnetic components for each value of τ_{yx} and τ_{zx} can be determined, integrated over the subsurface body of a

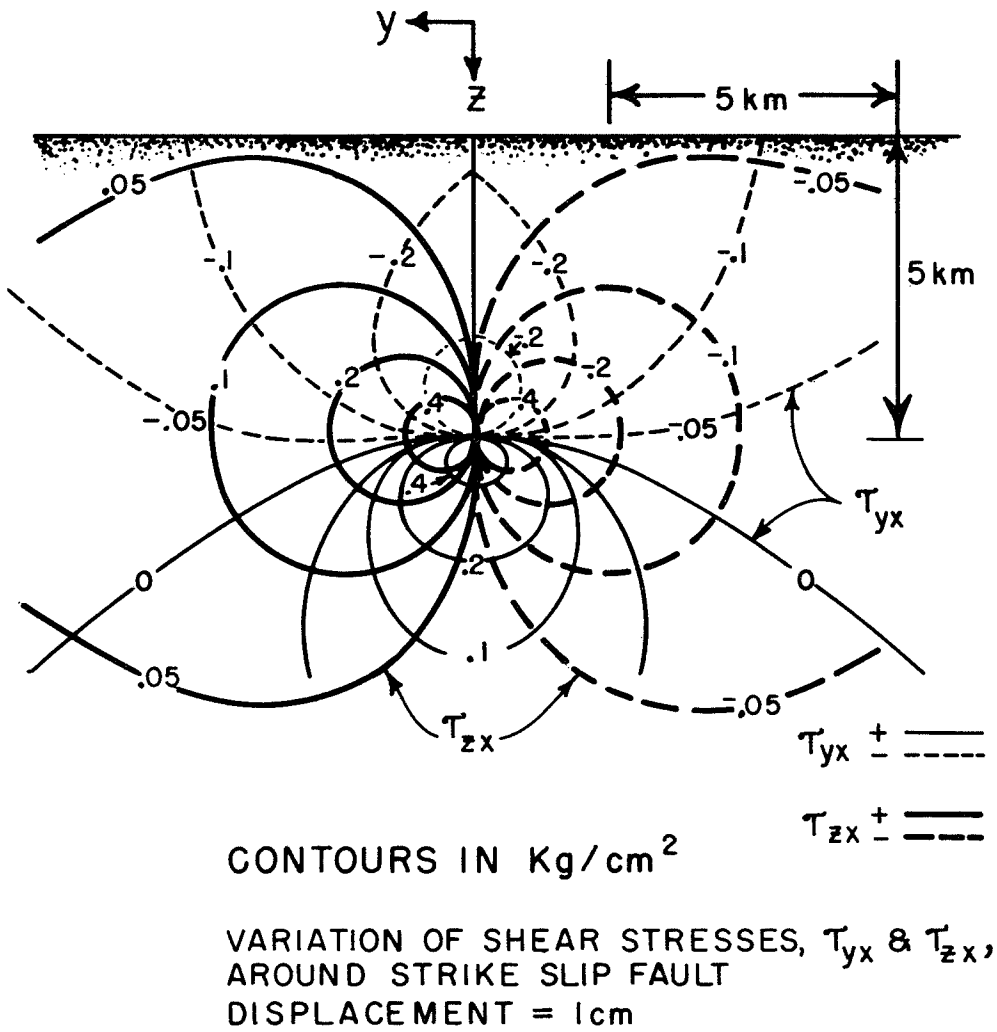

Figure 9. The variation of shear stress about a strike-slip fault of infinite extent.

given susceptibility and expressed as a component of total field intensity.

This strike slip fault model involves pure shear. Therefore, the compressive stress, σ_c, and tensile stress, σ_t, are equal in magnitude to each other and to the applied shear stress (Figure 10).

$$\tau_{yx} = \sigma_{c_z} = \sigma_{t_z}$$

$$\tau_{zx} = \sigma_{c_y} = \sigma_{t_y}$$

$2\theta = \alpha = 90°$

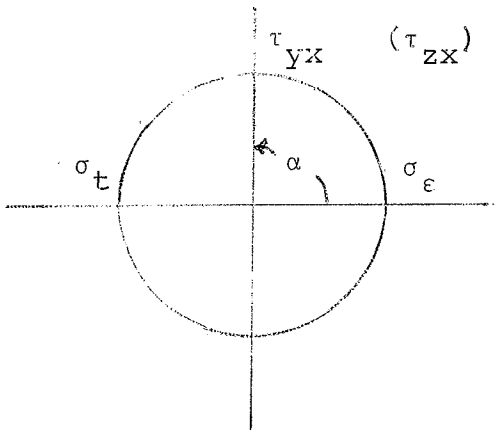

Figure 10. Mohr's stress circle diagram.

where the subscript z and y of σ denotes the normal of the plane containing the stress. Also from Mohr's diagram of Figure 10, σ_c and σ_t are each 45 degrees from the direction of their respective shear stress, i.e., $\theta = 45°$.

Stresses in Horizontal Plane

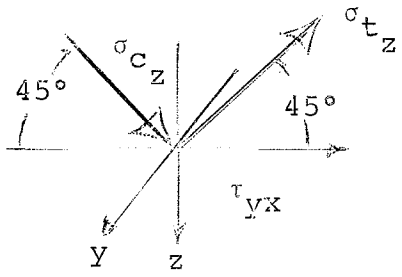

Figure 11.

Stresses in Vertical Plane

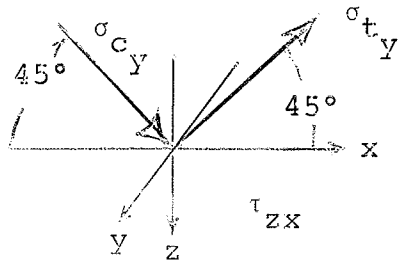

Figure 12.

(Compressive and tensile representation of shear stress.)

The product of a stress and its appropriate stress sensitivity is a component of susceptibility anistropy and can be treated as a vector unlike stress itself which, of course, is a tensor. The compressive and tensile stress representation of the shear stresses, τ_{yx} and τ_{yz} are shown in Figure 11 and 12. The magnitude of the vector sum of the susceptibility anistropy vectors which correspond to these stresses for the shear stress τ_{yx} is

$$\left|\overrightarrow{S\sigma}_{\tau_{yx}}\right| = \left[\left|\overrightarrow{S_c\sigma_{c_z}}\right|^2 + \left|\overrightarrow{S_t\sigma_{t_z}}\right|^2\right]^{\frac{1}{2}} = \sqrt{2}\,\tau_{yx}(S_c^2+S_t^2)^{\frac{1}{2}}$$

As shown in Figure 13. The vector $\overrightarrow{S\sigma}_{yx}$ determines the direction of the infinitesimal piezomagnetic dipole and lies in the horizontal plane with direction cosines

$$\alpha = \frac{\sqrt{\frac{2}{2}}\,\tau_{yx}\,(S_c + S_t)}{\sqrt{2}\,\tau_{yx}\,(S_c^2 + S_t^2)^{1/2}}$$

$$= \frac{S_c + S_t}{2(S_c^2+S_t^2)^{1/2}}$$

and $$\beta = \frac{S_c - S_t}{2\ (S_c^{\,2}+S_t^{\,2})^{1/2}}$$

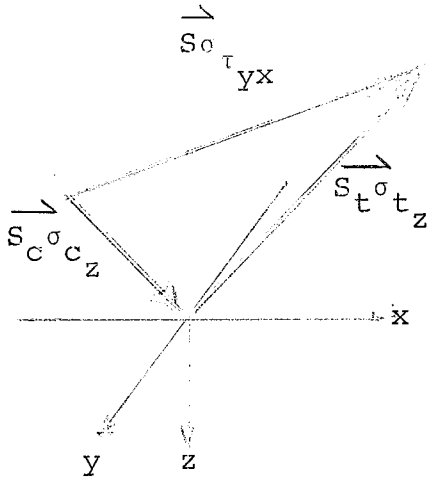

Figure 13. Susceptibility anisotropy components of τ_{yx}.

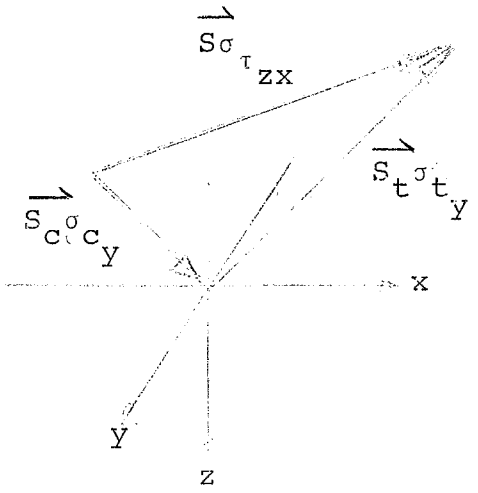

Figure 14. Susceptibility anisotropy components of τ_{yz}.

In a similar manner, we may derive the piezomagnetic component for the remaining shear stress. From Figure 14, we have

$$\left|\overrightarrow{S\sigma}_{\tau_{zx}}\right| = \sqrt{2}\ \tau_{zx}\ (S_c^{\,2} + S_t^{\,2})^{1/2}$$

The vector $\overrightarrow{S\sigma}_{zx}$ which again, determines the direction of the induced magnetic dipole at such point in the subsurface, lies in the vertical x-z plane or plane of the fault and has direction cosines,

$$\alpha = \frac{S_c + S_t}{2(S_c^2 + S_t^2)}^{1/2}$$

$$\beta = \frac{S_c - S_t}{2(S_c^2 + S_t^2)}^{1/2}$$

The derived formulation for the magnitude of $S\sigma_{\tau_{yx}}$ and $S\sigma_{\tau_{zx}}$ represent the coefficients of the magnetic susceptibility, k_0. The direction cosines of these vectors give the direction of the magnetization created by the piezomagnetic anisotropy. The expression for the anomaly in the earth's field created by a unit dipole source is then,

$$\Delta F = \frac{M\ (S,\sigma,\ k_0,F)}{r^3}\ V\ f(\theta,\phi)$$

$$\text{where } M = (S\sigma_{\tau_{yx}} + S\sigma_{\tau_{zx}})\ k_0\ F$$

and $f(\theta,\phi)$ is the function which determines the total field component at the surface from the dipole sources. This function is integrated over the entire volume under stress to determine the effect observed on the total magnetic intensity on the surface.

The model considered here is a strike-slip fault of infinite length and constant displacement of 1 cm. The depth and magnetic environment are varied for the following models:

A) Susceptibility of 5×10^{-3} cgs units to lower edge of fault at depths of 5, 10 and 20 km; stress sensitivities of $S_c = -2 \times 10^{-4}$ cm^2/kg and $S_t = 4 \times 10^{-4}$ cm^2/kg.

B) Susceptibility of 5×10^{-2} to lower edge of fault at depths of 5, 10, and 20 km; stress sensitivities of $S_c = -3 \times 10^{-4}$ cm^2/kg and $S_t = 6 \times 10^{-4}$ cm^2/kg.

The magnetic potential of a piezomagnetic anomaly is developed (Breiner, 1967) from the dislocation theory of Chinnery (1963). The total magnetic intensity profiles computed from the potential gradients are shown in Figure 15a and Figure 15b for models A and B, respectively. The conditions of model A do not represent an exprapolation to depth of the known rock type around the Hollister area of the San Andreas fault but rather to susceptibility of serpentinized rock which may exist above the base of the crust. The profiles of model B represent the effect of stress and high stress sensitivities on rocks of high remanent magnetization at depth. The amplitude of the larger anomalies of model B are of the same order of magnitude as the local magnetic events observed on the San Andreas fault.

The magnitude of the stresses about the strike slip fault model can also be estimated from strain energy considerations. Certain assumptions must first be made on the extent of the

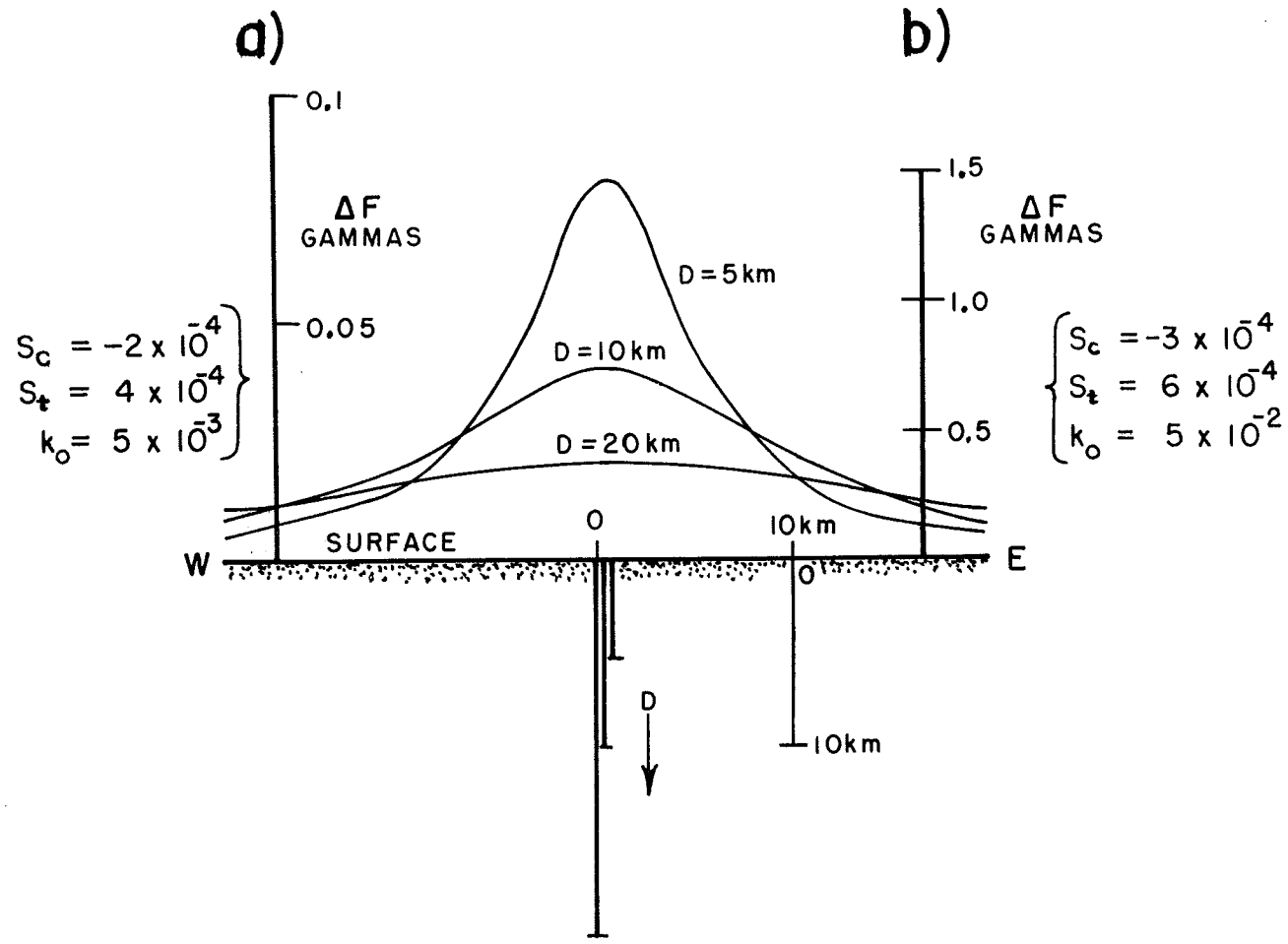

Figure 15. Piezomagnetic anomaly on a line normal to a strike-slip fault of infinite extent.

strain away from the fault. In addition, the shear stress and its compressive and tensile components are assumed to be constant over the fault plane and its immediate environment. Geodetic observations show an annual displacement of approximately 2 cm over an area 10 kilometers either side of the San Andreas fault (Burford, 1967). Therefore, the strain for large discrete creep events averaging two per year, is 1 cm over 10 kilometers, or 10^{-6}, which will be adopted as a reasonable estimate of a strain. Within the elastic limits before permanent deformation we have for the shear stress

$$\tau = \mu\varepsilon$$

$$= 6 \times 10^{11} \times 10^{-6}$$

$$= 6 \times 10^{5} \text{ dynes/cm}^2$$

$$= 0.6 \text{ kg/cm}^2$$

The value of the shear stress from ordinary strain observations thus agrees reasonably well with that suggested by dislocation theory as shown in Figure 9. Since the stresses are transmitted from the deep crustal rock, the elastic strain may be greater at depth. The stresses necessary to produce these strains are proportionately greater just as

in the dislocation theory.

Considering the stressed sources as a volume of magnetic rock of susceptibility $k_0 = 5 \times 10^{-3}$ cgs units on one side of the San Andreas fault, we may estimate the maximum piezomagnetic effect as that from a semi-infinite half-space of susceptibility, Δk, where

$$\Delta k = k_0 \, \Delta\sigma \, S$$

$$= 5 \times 10^{-3} \times 0.6 \times 6 \times 10^{-4}$$

$$= 1.8 \times 10^{-6}$$

Then the observed anomaly would be

$$\Delta F = 2\pi \, \Delta k \, F$$

$$= 2\pi \times 1.8 \times 10^{-6} \times 5 \times 10^{4}$$

$$= 0.56 \text{ gammas}$$

To produce an anomaly of 1 to 2 gammas by this mechanism, one or more of the assumed parameters must be increased by a factor of 2 to 4. The susceptibility may be greater at depth, the stress sensitivity may involve considerable remanence or the actual stresses may be higher by virtue of a higher modulus of rigidity at depth.

E. Telluric Phenomena Related to the Piezomagnetic Effect

Effect of Telluric Currents or Micropulsations

The observed geomagnetic micropulsations on the surface of the earth are, for the most part, the direct magnetic effects of ionospheric currents. The remaining portion of the micropulsation effects represent the magnetic field from circulating currents within the earth which are induced by the same ionospheric current system. Variations in the subsurface telluric currents must be examined in any consideration of local magnetic events because they are so intimately associated with the micropulsation phenomena. Stress associated factors which affect the local amplitude or direction of these currents are or particular importance as they apply to the interpretation of local magnetic effects. Such phenomena as the effects of stress on resistivity and the change of telluric potential associated with a changing piezomagnetic field have been examined for their contribution to the reported observations of the piezomagnetic effect.

Telluric Currents

Telluric currents are described and measured by their potentials on the surface. The conduction paths of the telluric currents are generally three dimensional, however the bulk of the flow occurs at depths of hundreds of kilometers (Chapman and Bartels, 1951). The direction of the

current on the surface is approximately constant at most sites. The amplitude, as measured in terms of the potential difference between two electrodes, varies by a few millivolts per kilometer during the day.

There is considerable difficulty in measuring long period or low amplitude quasi d-c levels of the telluric currents because of the chemical and electrode potentials and the variable contact resistance of the electrodes. No absolute potential has ever been observed as large as 1 millivolt per kilometer (Chapman and Bartels, 1951). Inasmuch as the current system is a result of induction no absolute level is to be expected. It has been observed that the daily mean during a disturbed day does differ from the quiet mean by 0.1 millivolt per kilometer so that apparently there are detectable long period, low amplitude telluric currents.

The best known fact of telluric currents is that their behavior is very similar to that of the geomagnetic micropulsations. The association of the two as a function of frequency comprises the magnetotelluric method of exploration. The telluric currents and micropulsations originate for the most part from ionospheric phenomena. The micropulsations, as observed on the surface of the earth, may owe one quarter of their amplitude to the magnetic field of the telluric currents and the remainder may be due to the magnetic field of the overhead current system.

To evaluate the magnetic contribution of the telluric currents, consider a homogeneous current in an infinite horizontal plane of intensity i amp/cm^2 extending to a depth d. The magnetic field intensity from such a current would be,

$$\Delta F = 2\pi \, i \, d/10 \quad \text{Gauss}$$

For an assumed current, i, of 10^{-11} amperes and d of 200 kilometers (Chapman and Bartels, 1951), therefore,

$$\Delta F = 2\pi \times 10^{-11} \times 2 \times 10^{7} \times 10^{-1} \quad \text{Gauss}$$

$$= 12 \text{ gammas}$$

which may represent a portion of the total geomagnetic diurnal variation.

Stress Induced Resistivity Effects

The telluric currents have been introduced primarily to evaluate them as a possible source of the observed magnetic phenomena described herein as piezomagnetic effects. The effects of stress on resistivity have shown that for igneous rocks such as granite or granodiorite under confining stresses equivalent to a depth of several kilometers an increase of stress on the order of 100 kg/cm^2 will increase the resistivity by approximately 1% (Brace, 1966).

If the resistivity in the telluric current paths varies in a time short compared with the period of the d-c or very low frequency component of the telluric variation, then the associated currents (and perhaps also the potential) will also vary. The length of the period of the telluric current was introduced here as a necessary consideration for there must be a non-zero level of current to be effected by the resistivity change. The fact that the driving ionospheric current is not constant makes the recognition of a small local change very difficult as it is in the case of the piezomagnetic effect in the presence of magnetic micropulsations.

From Ohm's law, we have

$$E = i R$$

where E is the potential between two telluric electrodes, i the effective current, and R, the effective resistance of the telluric current paths. If E remains constant then the change in i is inversely proportional to the change of resistance, R, which in turn is proportional to the change in resistivity, ρ. Surface strain observations indicate that the maximum depth at which the resistivity change is relevant to this problem is probably not greater than a few tens of kilometers.

The bulk of the current flow which contributes to the

diurnal variation is the result of current at depths greater than hundreds of kilometers (Chapman and Bartels, 1951). Therefore if, say, only 10% of the current which contributes to the proposed maximum 12 gamma portion of the observed surface field is affected by stress-resistivity effects and the increase in resistivity itself causes only a 1% decrease in this portion of the current, then the magnetic effect is

$$10^{-1} \times 10^{-2} \times 12 \text{ gammas} = 1.2 \times 10^{-2} \text{ gammas}$$

Moreover, the 12 gamma contribution considered above represents the largest possible component of the quasi d-c current which, in fact, does not even exist most of the time. If the potential also varies with the change in resistivity, then the current effects and the resultant magnetic changes are even smaller than estimated above. The magnetic changes computed on the basis of the piezomagnetic effects are directly proportional to the variations in stress as are the magnetic changes derived from telluric considerations. If the other parameters chosen for these models are reasonable, then regardless of the actual variations of the stress, the piezomagnetic effects are probably one or more orders of magnitude larger than any magnetic effect of stress-dependent telluric currents.

Telluric Response of the Piezomagnetic Effect

Whether or not there exists a measurable telluric response to the direct effects of a changing subsurface stress, there should be a potential developed by the time-varying piezomagnetic effect itself. From Maxwell's equations we have

$$\frac{dF}{dt} = \frac{10^3}{xz}$$

where x is the horizontal length and z the vertical depth of a fault face over which the piezomagnetic change, dF, is changing at a rate of $\frac{dF}{dt}$. This potential corresponds to a gradient of

$$10^{-3} \left[\frac{xz}{2(x+z)}\right] \frac{dF}{dt} \text{ volts/km}$$

Let x = 30 kilometers, z = 20 kilometers, and from the piezomagnetic events shown in Figure 4, the maximum rate of change, $\frac{dF}{dt} = 2 \times 10^{-3}$ gammas/second. Then the potential gradient is given by

$$10^{-3} \frac{30 \times 20}{2(30+20)} \left(2 \times 10^{-3}\right) = 1.2 \times 10^{-3} \text{ mv/km}$$

Such a change in the potential is at least an order of magnitude smaller than it is possible to resolve on a telluric record. Therefore, if a telluric event is observed

associated with a piezomagnetic effect of a type observed, it should not be the result of a change in flux and probably is not observable as a result of a stress-induced change in resistivity.

F. Local Magnetic Field Changes from Fault Displacement of Structural Blocks

Spatial magnetic anomalies are usually present around major strike slip faults such as the San Andreas fault as a consequence of the widely different rock types brought into juxtaposition. The right lateral displacement of one side of a fault from another will cause the local geomagnetic anomalies associated with the masses on one side of the fault to move with respect to observation points on the opposite side. The entire distribution of anomalies as they appear on the surface are of course the effect of all disturbing masses and only a portion of the equi-intensity contours would be distorted as a result of displacement. Local magnetic changes should therefore certainly result from fault displacement.

The magnitude of this change is determined by the spatial gradient in the direction of the fault movement of the local anomalies. The anomaly can be considered stationary and the point of observation on the other side can be displaced horizontally on the residual magnetic field contours which express only the contributions from the stationary anomalies. In most cases along the San Andreas fault, the anomalies are the result of geologic structures whose long dimensions are parallel to the fault and the gradient in this direction is small. This is not always the case, however, especially

at the contact of rocks exhibiting the susceptibility contrasts. Unfortunately a contour map of the entire area of interest about the San Andreas fault is not yet available.

As an estimate of the magnitude of this change, consider, for example, an anomaly of 200 gammas from a source 1 kilometer distant. The anomaly width for most of the anomaly amplitude will generally be approximately 1 1/2 times the depth. To the first approximation, therefore, on one side of the anomaly where the horizontal gradient is largest, we have

$$(200)/[(\tfrac{3}{2})(\tfrac{1}{2})(1\ \text{km})] = \frac{2 \times 10^2}{0.75} =$$

$$2.7 \times 10^2\ \gamma/\text{km} = 2.7 \times 10^{-3}\ \gamma/\text{cm}$$

If the same anomaly were observed from a point $\frac{1}{3}$ of a kilometer away, the anomaly would be approximately $(3)^2(200)\gamma$ (most anomalies whose dimensions are large compared to the distance to the point of observation, vary inversely with the square of the distance). The 'half-width' distance would be $(\frac{3}{2})(\frac{1}{2})\ \frac{1}{3}$ km and the gradient,

$$3^2(200/[(\tfrac{3}{2})(\tfrac{1}{2})(\tfrac{1}{3})] =$$

$$\frac{1.8 \times 10^3}{(0.25)} = 7.2 \times 10^3\ \gamma/\text{km} = 7.2 \times 10^{-2}\ \gamma/\text{cm}$$

For displacements of 0.5 cm which are observed during creep rupture on the surface or 1 cm which may be the overall actual displacement of one side of the fault with respect to the other, we can expect changes on the order of a few thousandths to a few tenths of a gamma. Moreover, if the magnetometer observations are on both sides of the fault as in the case in this study, we might expect a maximum greater than this amount depending of course upon the direction, and magnitude of the gradients and on which side of the fault the anomalies are located. The time signature of the change should reflect the actual displacement.

3. MAGNETOMETER ARRAYS FOR OBSERVATIONS OF THE PIEZOMAGNETIC EFFECT

A. Experimental Factors

The experimental considerations for observation of the piezomagnetic effect can be described in terms of environmental or instrumental criteria. The results of the laboratory investigations of the magnetic properties of rocks and the factors which constitute the expression for the piezomagnetic effect determine the relative importance of the various parameters which must be considered. Logistic consideration and the reduction of undesirable noise in the observations are equally important.

Environment

Tectonic Stress Variations

Piezomagnetic effects are directly proportional to changes in stress so that an area must first be selected which is undergoing rapid or frequent changes in subsurface stress. High seismicity is certainly one indication of such changes in tectonic stress although we may not know specifically where or when such changes are taking place or even whether or not the rate of the stress change is constant. Tidal forces also create changes in subsurface stress but are probably so uniform over a large area of observation and the magnetic effects so identical to certain tidal ionospheric magnetic effects that this cause of subsurface stress change

is not useful for piezomagnetic observations. Therefore, seismically active areas appear to present the best natural environment for the stress aspects of piezomagnetic observations.

Susceptibility of Underlying Rock Types

The laboratory investigations of the magnetostrictive properties show that the amplitude of the piezomagnetic effect is directly proportional to the susceptibility and remanent magnetization of the rocks under stress. Selection of a site should therefore be guided by the presence of high magnetic susceptibility rocks with high remanence, if possible. What is known about specific rock types and their magnetic properties is usually derived from surface outcrops but it is the rocks at depth which undergo the stress changes and are therefore, the significant rock types. Surface magnetic surveys would aid in this selection, the large low gradient anomalies indicative of high susceptibility rocks at depth. Such ultrabasic or mafic rock types as peridotite, dunite, serpentine, gabbro, or basalt are preferable to granitic rocks or sedimentary rocks. If the focal depth of earthquakes in the studied area is indicative of the depth to the source of stress changes, then the depths of interest are several to tens of kilometers. As a generalization, the magnetic susceptibility of the rocks increases with depth. The limiting depth in all of these piezomagnetic

analyses is the depth to the Curie isotherm for magnetite which is 560°C reached at an average depth of 28 kilometers for a continental geothermal gradient of approximately 20°C/km. Below this depth the rocks possess no ferrimagnetic properties and cannot contribute to the piezomagnetic effect.

Logistics

Practical limitations also govern the environmental selection for piezomagnetic observations. Since magnetometers must be used, the area must be free of man-made interferences of the local magnetic field which would present itself as noise or false events in the data. The area must, of course, be free of vehicles, direct current power lines, and man-carried ferromagnetic objects. Power must also be available for magnetometers and depending upon the telemetering or recording methods, a telephone line must also be available. For subtle reasons, remote observations near the continental coastline should also be avoided.

The piezomagnetic events may be very local phenomena associated with the stress region at the focus of an earthquake or similar event. As a practical consideration, we cannot hope that an earthquake of significant magnitude would occur sufficiently close to a given magnetometer to observe the piezomagnetic effects. Therefore a multiple sensor array is required to widen the effective monitoring of local magnetic effects.

Instrumental Considerations

Sensitivity

Measurement of the piezomagnetic effect naturally involves magnetometers. The change in susceptibility results in a change in the induced magnetization which together with the stress-affected remanent magnetization manifests itself as dipole perturbations of the earth's field intensity. From the expression for the field intensity of the piezomagnetic anomaly, the changes indicated are small and may range from zero to a few tens of gammas. The magnetometer must therefore be capable of resolving extremely small changes in field intensity.

Stability

The time signature of the piezomagnetic effect discussed earlier is such that the small anomaly expected may occur slowly over days, weeks, or perhaps years. Putting aside the question of whether or not it is possible to recognize small changes over long periods of time, it is at least desirable to be able to resolve these changes instrumentally. The magnetometer used therefore requires a high degree of stability, i.e., very low drift so that any changes that are observed can at least be attributed to the magnetic field intensity whatever its origin.

Microphonics

Inasmuch as the area to be selected for the observations

is seismically active, there shall be ground motion and vibration of the magnetometer. Mechanical shock of the component parts of a magnetometer might produce false magnetic events during passage of a seismic wave or even apparent permanent changes of the field after a large seismic wave or even apparent permanent changes of the field after a large seismic shock. The magnetometer should therefore be substantially free of microphonic effects.

Differential Reduction of Time Variations

Almost all of the variations of the geomagnetic field at the surface of the earth are the result of solar-related phenomena known as micropulsations, diurnal variations, or magnetic storms. These changes are often several orders of magnitude larger than the expected piezomagnetic effects and may even have similar time signatures. The latter must therefore be resolved in the presence of these normal ionospheric time variations. The micropulsations originate primarily in the ionosphere at a distance of several hundred kilometers. The dimensions of the current system is of the same order of magnitude. At points only a few tens of kilometers apart on the earth's surface, the time variations are essentially identical and the difference in the variations is therefore constant. A piezomagnetic source originating within the earth much nearer to one observation point than another will be expressed almost wholly on the difference record. An array of stations properly arranged can thus

effectively reduce the 'noise' of the time variations and allow observations of a local piezomagnetic anomaly.

Correlation Instruments

Recognition of a piezomagnetic effect is greatly facilitated as a result of the correlation of local magnetic events with other events indicative of local changes in stress. Meaningful measurement of stress at the earth's surface is not yet practical and at present stress cannot be measured at great depth. Seismic events are indicative of stress changes but quantitative relationships between changes in tectonic stress and earthquakes are not well understood. Nevertheless, the general level of seismicity and individual medium-to-large earthquakes are manifestations of stress changes so that seismic information represents a usable variable for correlation with piezomagnetic observations.

Strain is more easily related to stress changes within the elastic limit than are seismic events and in a somewhat more complex way when permanent deformation is involved. Moreover, strain measurements are being made in several seismically active areas. Quantitative strain observations are obtained through geodetic surveys, strain seismographs, creep instrumentation, extensometers, visual field observations, and tiltmeters.

Sites Selected

Several sites were selected for the investigation of

piezomagnetic effect. The basis for selection for each site varied: for some it was the existence of correlation instruments, for others it was the seismicity, and for some the logistic criteria were conveniently established. The geologic/magnetic environment, seismicity, and complete instrumental setup of each site are described in sections 3B through 3F. The 5 sites actually occupied were:

1. San Andreas fault from 36° 40' to 37° 40' North latitude
2. Fairview, Nevada
3. Whitecloud Mountains, Idaho
4. Mercury, Nevada
5. Matsushiro, Japan

Magnetometer Instrumentation

The experimental considerations outlined above dictate the general magnetometer sensitivity and stability requirements, the need for a plurality of instruments, and the necessity of operating in some kind of noise-cancelling mode. Beginning with sensitivity, the magnetometers available today with a sensitivity better than 0.1 gamma are the fluxgate, induction coil, proton, and optically pumped magnetometers. The high stability requirements rule out the use of the first two instruments. Moreover the fluxgate and induction coil magnetometers are sensitive to seismic vibrations and both will record the effects of a slight misalignment of

the sensor, say, accompanying the surface waves of a local earthquake, as an apparent change in field intensity much the same as the magnetographs have done for the past 100 years. The alignment would have to be maintained to 1" of arc for 0.1 gamma stability. The induction coil also cannot measure slowly varying fields because its signal is proportional to the time rate of change of flux only and it will thus not respond to changes with periods much longer than 100 seconds. Of the remaining two magnetometers, the proton magnetometer is somewhat more stable but the optically pumped magnetometer is more sensitive and more important, was made available for this investigation.

Rubidium vapor optically pumped and monitored magnetometers were used throughout this investigation. Seven instruments, Varian Associates Model V-4936 Rubidium Vapor Station Magnetometer (Figure 16) were loaned for a period of three years by the organizations listed in the acknowledgments. The manufacturer specified 0.01 gamma sensitivity but the magnetometers were each modified to provide higher sensitivity (0.003 gamma), better long term stability, and improved signal demodulator performance.

The process of optical pumping as used in a rubidium magnetometer involves the interaction of the magnetic moment and angular momentum of the valence electron of rubidium with the ambient magnetic field (de Zafra, 1960). This atomic phenomena is accomplished by four principal items in

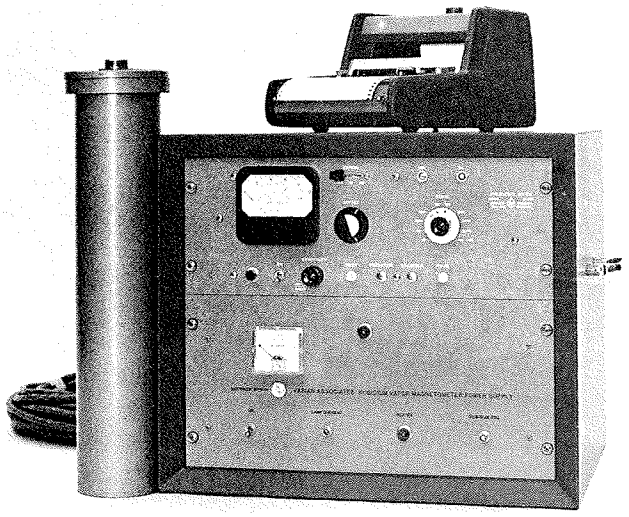

Figure 16. V-4936 rubidium vapor station magnetometer.

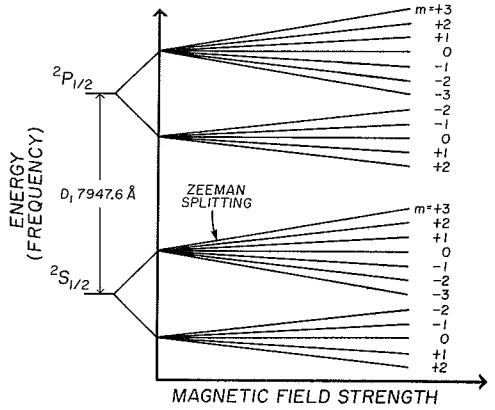

Figure 17. Energy level diagram for rubidium^{85}.

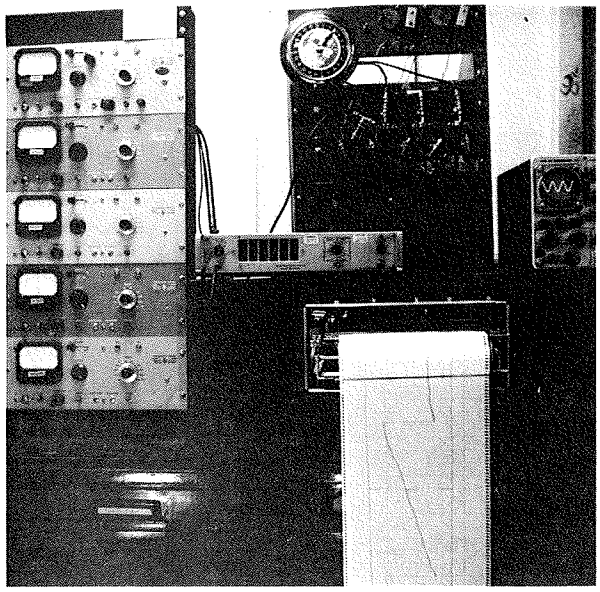

Figure 18. Receiving console of 5-station San Andreas fault differential magnetometer array.

the magnetometer sensor: a rubidium light source, a rubidium vapor absorption coil, a photodetector, and a servo-loop amplifier. The rubidium 85 light source is used as an energy source of photons (wavelength 7948 angstroms), which are focused through a glass cell containing rubidium 85 vapor. The transparency of this cell is decreased when the rubidium photons are absorbed by the valence electrons of rubidium: this absorption raised the electron's energy, causing the electron to rise from $^2S_{1/2}$ ground state to the $^2P_{1/2}$ excited state (Figure 17). The rise of the electron to the $^2P_{1/2}$ state must, by quantum mechanical rules, be accompanied by an increase of +1 in the corresponding sublevel. The absorbed photon energy is soon reradiated, and the electron drops back with equal probability to any one of the sublevels of the ground state, ready to absorb another photon. However, since there are the same number of sublevels in the ground state and the excited state, the electrons in the highest sublevel of the ground state cannot rise to the excited state nor absorb additional photons. A large number of electrons are thus "pumped" into this highest sublevel of the ground state, and because the photons pass freely through the vapor coil, the cell becomes transparent.

Sweeping the vapor cell with a weak alternating magnetic field disrupts this state and allows pumping to begin again. If one varies the frequency of the applied field and observes the light transmitted through the vapor cell, a sharp absorp-

tion is seen to occur when the applied field has a frequency

$$f = 4.667\ F$$

where f = frequency (in Hz) and F is the total magnetic field intensity, in gammas. The electrons undergoing the transition between energy sublevels actually precess about the ambient magnetic field vector (earth's field) at a Larmor frequency determined by the Zeeman splitting of the levels (Figure 17).

In the instrument itself, the modulation of the transmitted light is detected by the photocell. The current from the photocell is amplified, changed in phase, and used as a feedback signal to drive the alternating magnetic field about the vapor cell. This arrangement thus constitutes an oscillator whose frequency is proportional to the total magnetic field intensity at a rate fixed by an atomic constant, 4.667 Hz/gamma. From the equation above, this frequency is 233,000 Hz in a field of 50,000 gammas

The signal from this magnetic field-dependent oscillator is then mixed with that from a stable reference oscillator to obtain an audio frequency difference also proportional to the field intensity at the same rate. This audio frequency is then either transmitted through telephone lines or passed directly to a frequency discriminator which transforms this frequency to a voltage for display on a strip chart recorder. Transmission through telephone lines, because it is frequency-modulated information, does not involve any signal loss or

distortion through very long transmission paths.

At sites 4 and 5 differential recordings were obtained directly by replacing the stable reference oscillator by the signal from another oscillator, the resulting audio frequency automatically representing the differential variations. The magnetometers were operated separately at sites 2 and 3, the difference obtained by overlaying one chart record over another and plotting the differences. There is always sufficient activity on the records, never repetitious, to align the records of two near magnetometers even without time notations on the record.

The most complete observations were obtained on the San Andreas fault where an array of 5 stations was set up. The audio frequency signals from each magnetometer were telemetered to a base station. Each signal was still based upon the same atomic constant so that any variation in time between their signals is a local magnetic event and not any type of miscalibration, etc. The audio frequency signals were each mixed with one signal which served as a common reference signal and the difference frequency was demodulated and recorded as a voltage on a strip chart (Figure 18).

The drift of the station magnetometer with respect to one reference station was found to be less than ± 1 gamma per month. In order to make certain that they were not varying, say, with temperature, in the same manner which might not ordinarily be detected, one instrument (the

Stanford magnetometer) was compared to a proton station magnetometer. The rubidium magnetometer varied less than 0.4 gamma for an ambient change of 14°C.

B. San Andreas Fault Array

Setting

Geology

The central portion of the San Andreas fault in which the study was involved is in the central Coast ranges in a region of late Mesozoic and Cenezoic highly folded and faulted eugeosynclinal sediments, altered submarine volcanics, and large exposures of crystalline basement rocks.

The prominent structures of geologic contacts trend NW-SE. The most significant structural feature is the San Andreas and nearby Hayward and Calaveras strike-slip faults. Smaller en échelon strike slip faults are common throughout the area. The Pilarcitos fault is closely parallel to the San Andreas in the northern half of the area and is the fault over which the major displacement occurred up to Miocene time. Scattered inactive thrust faults usually marking the contact of altered serpentine masses are common. No single anticlinal or synclinal fold dominates the immediate area.

The crustal structure of this portion of the San Andreas fault has been examined by geophysical means. On the basis of seismic refraction profiles, Eaton (1963) and Healy (1963) report a crustal thickness of approximately 20 to 23 km with a possible intermediate layer from 12 to 22 km in depth.

Velocities determined from the profiles for the shallow and intermediate crustal and upper mantle layers are 6.0, 6.8 and 8.0 km/sec respectively. Press (1957) determined the crustal thickness to be approximately 30 km. using the phase velocity of Rayleigh waves and did not resolve an intermediate layer. The intermediate layer attains particular significance in the interpretation of the results of this work. The phase velocity evidence was reinterpreted by Thompson and Talwani (1964) to produce a possible crustal thickness of 21 km. Gravity studies, chiefly those of Thompson and Talwani indicate a crust 22 km thick under the central Coast ranges.

From a magnetic viewpoint, surface outcrops in this area in decreasing order of magnetic susceptibility are: serpentine, peridotite (and dunite and pyroxenite), basalt, altered submarine volcanics, acid igneous, and sedimentary rocks (Figure 19). Large exposures are found of three of the magnetically significant rock types, namely, submarine volcanics, serpentine, and granite. Serpentine is considerably more magnetic than its parent ultrabasic rock because of the magnetite formed during alteration of the anhydrous silicates to serpentine minerals.

Some of the ultrabasic rocks such as serpentine and particularly the uncommon peridotite are thought by some (Oakeshott, 1966) to be examples of the non-granitic basement or even subcrustal material which underlies most if

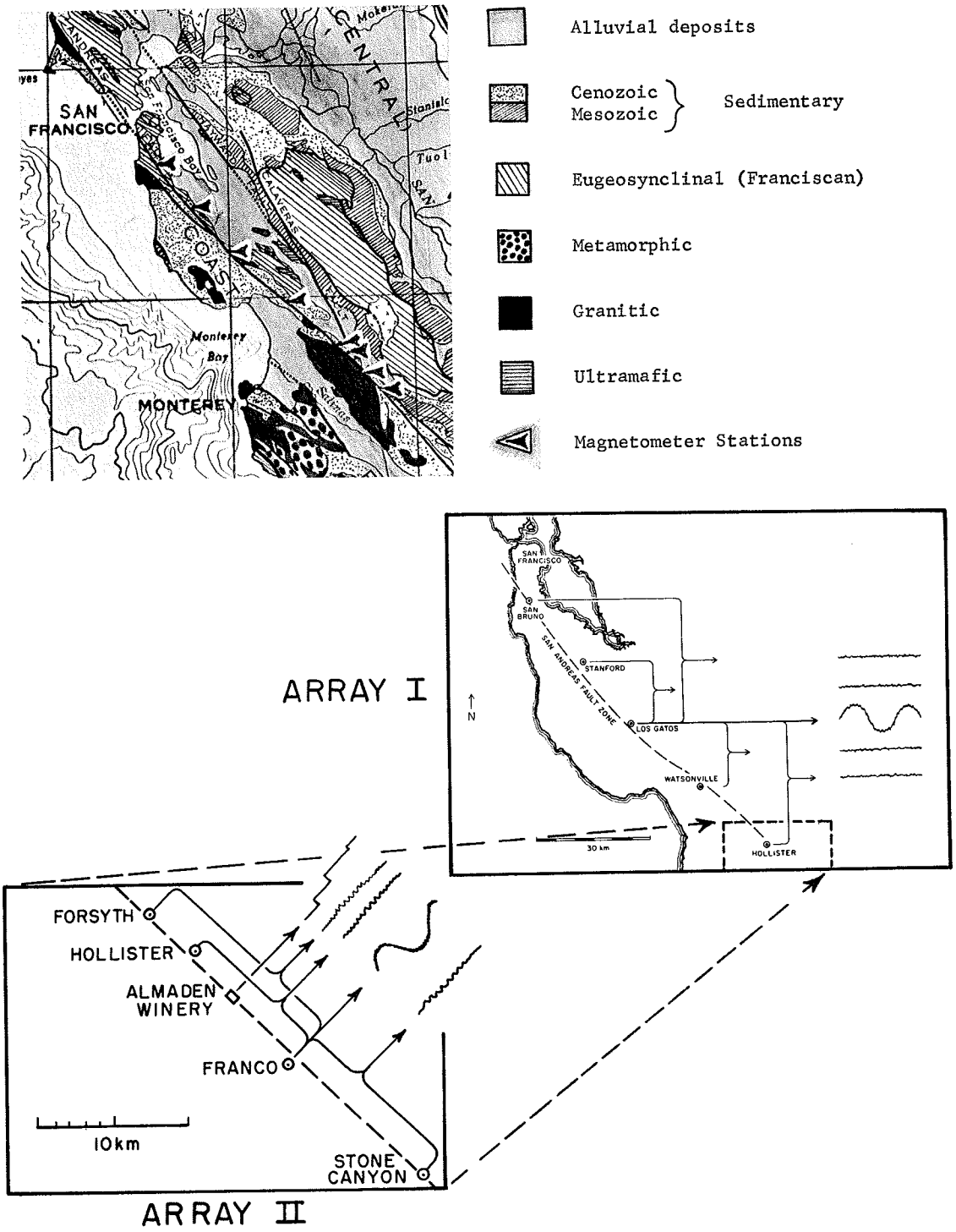

Figure 19. Geologic map and location map of San Andreas differential magnetometer arrays I and II.

not all of this region. Moreover, the base of the Franciscan formation has nowhere been observed, and the ultrabasic rock or its altered equivalent, serpentine, may represent the basement rocks on which the Franciscan rests (Page, 1966). From inclusions in the Franciscan serpentines, Bailey et al., (1964) suggest that the basement of the Franciscan formation and therefore the major basement under the area of this study may be peridotite, basalt, or serpentine. The lower limit of interest of these layers is based upon the depth of the Curie point isotherm which Griscom (1966) estimates to be at the bottom of the crust at 22 km. This value, however, could be 10 km deeper depending upon the assumed geothermal gradient.

Seismic and Strain History

The nature and magnitude of the displacement of the San Andreas fault through geologic history has not yet been clearly established. The estimates of the displacement vary from a few thousand feet (Taliaferro, 1943) to 350 miles (Hill and Diblee, 1953) of right lateral offset or a vertical displacement up to 50,000 feet (Oakeshott, 1966). The movement for at least the last several thousand years is right lateral at the rate during historic time of approximately 1 to 3 cm/year at the southern end of the area included in this study, i.e., as far north as Watsonville, (Burford, 1967; Meade and Small, 1966). The rate of displacement of the San Andreas fault from Watsonville to San Francisco has

not been determined with as much precision but it is certainly much less than the rate elsewhere on the fault.

Rupture creep displacement has been observed visually and instrumentally for several years across the San Andreas fault near Hollister, California. The displacement at the fault itself averages 1 cm per year, approximately one-half the total observed from the above geodetic observations. The instrumentally observed creep occurs almost completely in short spasms several minutes to days in length two or three times per year. There is no pattern nor regularity to the creep except that over several years time, the average rate is about 1 cm/year. Just how far northwest or southeast on the fault this intermittent creep occurs is not yet known. The geodetic observations, however, repeated every six months or so on other areas of the fault, also exhibit a spasmodic behavior in which most of the creep occurs between very few observations.

Several large earthquakes have occurred in this region of the San Andreas fault (excluding the Hayward fault) in historic time, the largest and best known being the San Francisco earthquake of 1906. Right lateral surface ruptures were visible from San Juan Bautista to Point Arena for a distance of 430 kilometers. The magnitude of the earthquake was approximately 8.3 with its epicenter near Olema in Marin County which is also the location of the largest displacement observed, 6.5 meters. As a result of investiga-

tions which followed, Reid (1910) formulated his elastic rebound theory.

There have been several other destructive earthquakes in this area such as San Francisco, 1836; San Jose, 1858; Santa Cruz Mountains, 1865; Monterey County, 1885; Hollister, 1897, and Monterey Bay, 1826; all were probably magnitude 5.5 or larger. The distribution of events of magnitude 4.5 or larger in recorded history is shown in Figure 20 (Eppley, 1961). During the past decade, earthquakes of magnitude 5.0 or larger have occurred near Watsonville, Pescadero, Daly City (San Francisco), Hollister, and Monterey Bay. As a rule, most of the earthquakes in this region, regardless of magnitude, are relatively shallow, generally 10 kilometers or less.

The seismicity over the past several decades as seen on a fine scale shows distinct anomalies in the distribution of earthquakes. The great majority of earthquakes in this portion of the San Andreas fault occur in five areas: near San Juan Bautista, in the Watsonville area, northwest and southeast of the Almaden winery near Hollister, northwest of the Pinnacles, and in the Santa Cruz mountains southwest of San Jose.

Correlation Instruments

Following the requirements for observation of the piezomagnetic effect, a correlation of local magnetic events

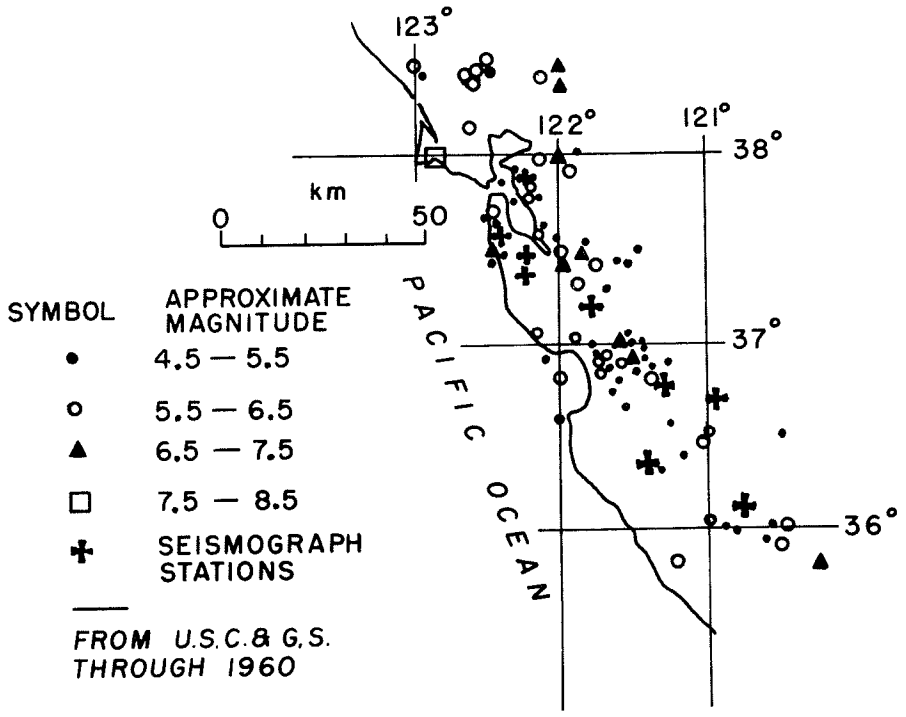

Fig. 20. Large earthquakes in the area of the array during historic time. (Eppley, 1961).

with other phenomena indicative of subsurface stress changes must be attempted particularly when seeking supporting evidence for the validity of the piezomagnetic effect. A network of seismographs operated by the University of California provides seismic coverage with an effective sensitivity to earthquakes of magnitude 2 or greater anywhere in the area under study. Three component seismograph stations are located at Pilarcitos Creek, Santa Cruz, Mt. Hamilton, and the Almaden Winery in Hollister (later moved 6 km northwest). In addition high gain three component seismographs were put in operation midway through the study by the Earthquake Mechanism Laboratory of the Environmental Science Service Administration at the Stone Canyon magnetometer site. A three component seismograph, formerly operated by the University of California, is located at Stanford University adjacent to the Stanford magnetometer site. Late in the program a seismograph was installed by the National Center for Earthquake Research of the U.S. Geological Survey at Black Mountain on the trace of the San Andreas fault. The locations of all seismographs are shown in Figure 20.

Rupture creep displacement is recorded in the Almaden Winery 10 km south of Hollister. The San Andreas fault zone is sufficiently narrow and the winery building so located that the structure straddles the fault trace. The displacement occurs betwen concrete foundation slabs and offsets in a right lateral sense not only slabs but the

walls, beams, and miscellaneous structures outside the building (Tocher, 1960). Under the direction of Dr. Don Tocher the slabs were instrumented, one set using an aneroid barometer movement and on another pair of slabs, a linear variable differential transformer. Using these devices, one mechanical and the other electromechanical, displacement of the slabs has been monitored since 1958 with a resolution of 0.01 mm.

Magnetometer Deployment and Installation

On the basis of the criteria outlined earlier sites were selected for magnetometer installations. A total of 5 rubidium vapor magnetometers were made available for this investigation. Maximum coverage lengthwise of the San Andreas fault was the first constraint. The distance between sites was such that the micropulsations at near stations were to be sufficiently coherent to allow the differential cancellation of these ionospheric time variations. Since the ionospheric current system is at an altitude of a few hundred kilometers, a station separation of a few tens of kilometers would be the maximum. Moreover, the separation of the magnetometers must be great enough to allow the magnetic effect of, say, a subsurface stress, to be much larger at one magnetometer than the other and therefore appear on the differential record. From the estimates of the piezomagnetic effect and the possible depths to the stressed

regions at earthquake foci, a separation no less than 20 kilometers was indicated. The distance selected considering all the above constraints was 30 kilometers.

One rubidium vapor magnetometer was already established and operated by Varian Associates as an observatory on Stanford University land near the San Andreas fault in Menlo Park. Since this site fit all other requirements, it was used as one of the sites and the other four were established at approximately 30 kilometer intervals along the San Andreas fault zone. Within several kilometers of these optimum points, exact locations were selected to be free of local man-made interference and with available power and telephone service. Without over-determining the constraints, sites were selected, if possible, on high magnetic susceptibility rocks fully realizing that the rocks at depth were the large stresses may originate are not actually known. The array was thus established on these criteria and will be described herein as Array I. The location of the sites are shown in Figure 19.

Each magnetometer was first completely overhauled and the optically pumped rubidium sensor modified for improved performance. The demodulator (frequency meter) and recorder were removed from the housing and the remainder, i.e., the sensor, its power supply, and crystal oscillator/mixer were brought to the site. A location was selected to be within reasonable electric cable distance to a source of ac power

but far enough away from any possible roadways, paths, or other source of even occasional human interferences. Hillsides, particularly brush covered, were ideal as they are not usually frequented by persons and the exposed instruments can be inconspicously placed. A hole 4 feet by 4 feet and 6 feet deep was dug and the sensor placed in a non-magnetic wooden box supported by three foot legs set firmly in the soil. A plywood top covered the hole. The sensor was thus firm, protected, and the diurnal temperature variations minimized. The installation at the Harris ranch near Hollister and the field site of San Bruno are shown in Figure 21 and is typical of the others.

A 150 foot multiconductor cable connected the sensor to the power supply, the latter mounted in its cabinet which in turn was contained in wooden canvas-covered boxes. The 240 kc Larmor frequency from the sensor is mixed with a stable crystal-controlled oscillator to produce an audio difference frequency. For reasons pertaining to the receiving equipment and telemetering restrictions, this audio frequency was specially determined by proper selection of the crystal. The crystal frequency was checked monthly with an accurate frequency counter to insure that any changes in the audio frequency were due only to changes in the Larmor precession frequency of the sensor.

A telephone line was obtained on a monthly lease basis from the local telephone service company and a termination

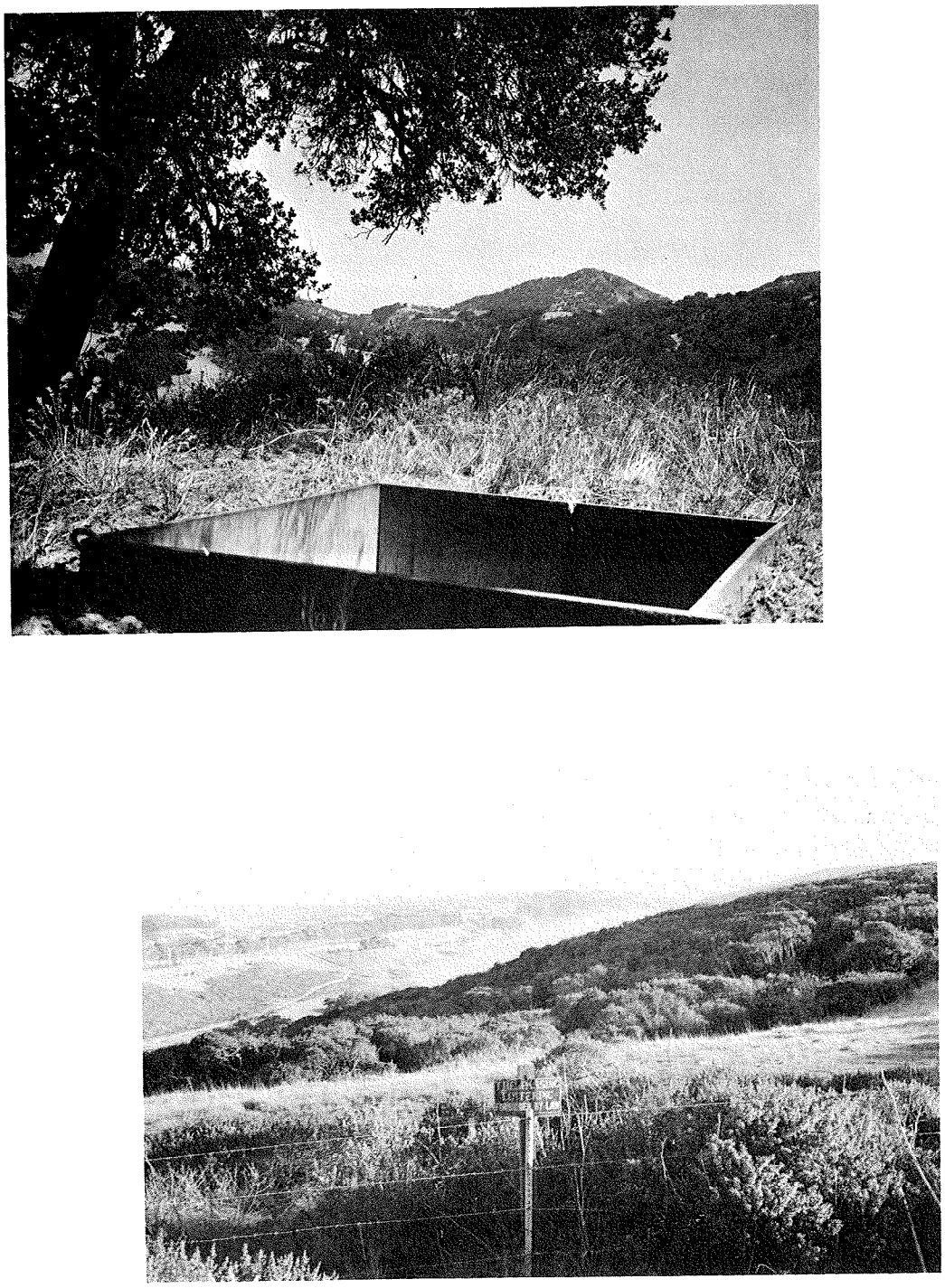

Figure 21. Typical magnetometer field sites for San Andreas array.

provided near the site with new pole installations, if necessary. The audio frequency signal was coupled to the telephone line through an impedance-matching transformer. The ac power cable was strung through the tress and the magnetometer connected to it through a voltage regulating transformer to insure that fluctuations in the local power would not affect the magnetometer. The magnetometer was complete and ready to operate with only two lines, telephone and ac power, leading from the usually-brush-covered site.

Each of the 5 signals were received at the Stanford University laboratory through as much as 100 miles or more of commercial telephone circuits and necessary amplifiers. The frequency-modulated information contained on the audio-frequency, however, remains unchanged with no loss of stability or resolution. Moreover, each signal was received as a frequency varying identically with each other, i.e. varying by the atomic-constant-determined frequency of 4.667 per gamma change in field intensity. The audio frequency signals were then each mixed with the signal from the site most centrally located in the array. In Array I this common reference was Los Gatos. The difference frequencies mixed through selected audio frequency telemetering filters were converted to a voltage in the frequency meters and recorded along with the demodulated reference magnetometer signal (Figure 22).

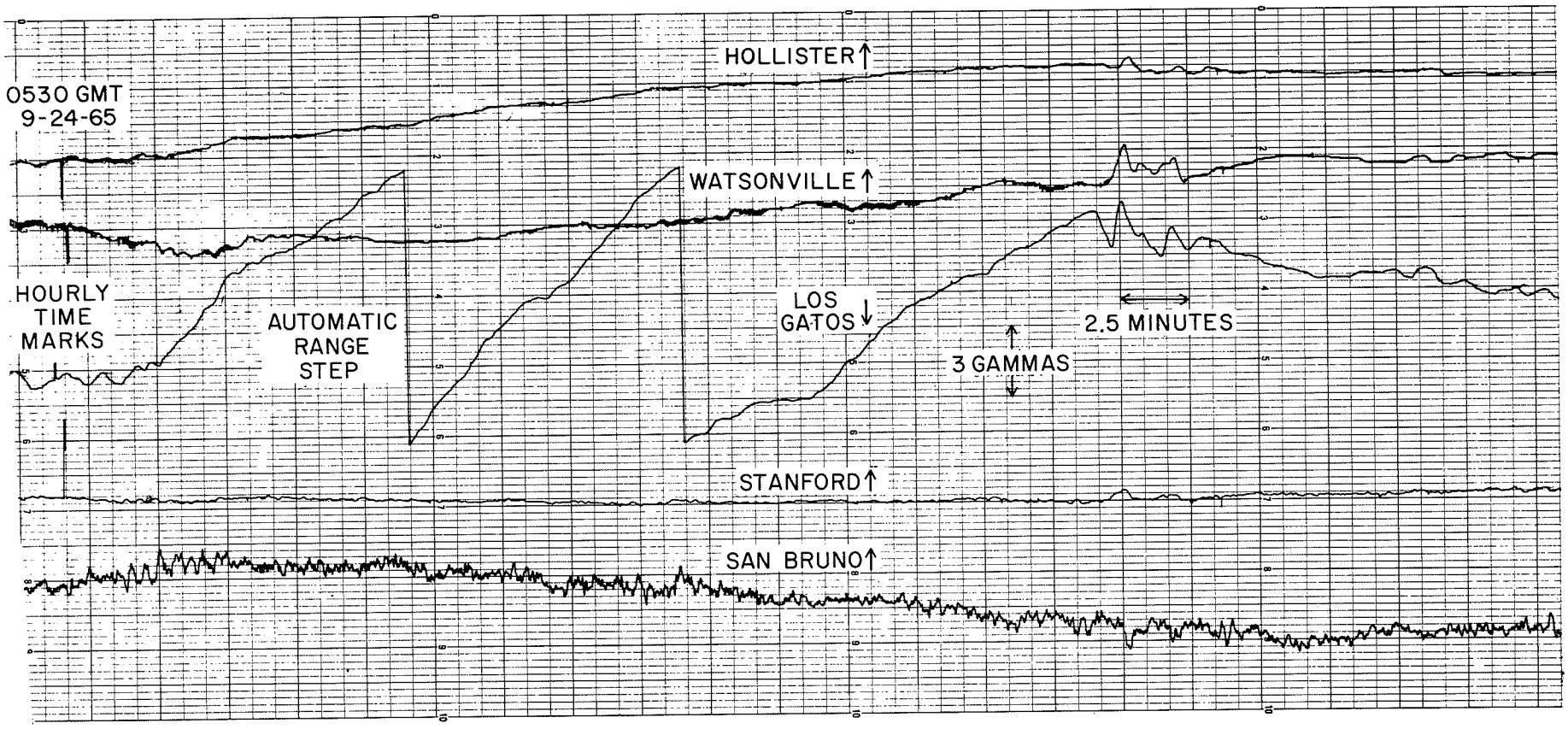

Figure 22. Differential and total magnetic intensity records from San Andreas array I.

Telemetering the atomic-constant-determined signals as described has the advantage of performing, in real time, the most important data processing step, namely, obtaining the differentials. The variations were also recorded on one chart to obtain a common time base. These steps thus precluded having to record in the field with accurate time references, replaced the otherwise needed high-stability recording equipment to insure that drift did not cause apparent events, by-passed the need for extensive computer time to obtain the differentials, and insured satisfactory magnetometer operation from the laboratory without having to go to the field sites. The telephone leased service was operable 99.5% of the time.

In the second phase of recording begun after 20 months, 3 magnetometers were relocated in a more dense array about the Harris ranch (Figure 19). This array will be referred to as Array II. The receiving and recording equipment described above was brought to the Harris ranch where the 3 differentials with respect to this centrally located Franco station were then obtained and recorded. In addition, each of the 3 differentials, the magnetometer signal itself, and a frequency analog of the creep recorder in the winery were sequentially telemetered to the Stanford Laboratory once each minute. In the Stanford Laboratory these signals were counted on a frequency counter calibrated in terms of gammas, the resultant count converted to a voltage in a

digital-to-analog converter, and recorded on a strip chart recorder. The complete sampling of each station was achieved once each minute. A digital printer also printed the count for one complete minute one minute out of each five minutes (Figure 23). The audio frequencies received at the Stanford Laboratory were also telemetered to the laboratory of one of the sponsoring groups, Varian Associates. There the frequencies were converted to a voltage in a synchronized switching apparatus and recorded on a strip chart recorder.

Interpretation of Magnetometer Records

Differential versus Total Intensity Variations

The purpose of differential recording is, of course, to reduce the effects of the ionospheric micropulsations. As an objective it is desired that the effects of a local change in field intensity from the piezomagnetic effect be observed on one magnetometer trace only, the other magnetometer being far removed from the source. If distant effects such as the ionospheric micropulsations were precisely the same at all stations, then the differential record would appear as a constant field. Any event present can then be said to be due to a local effect.

Such ordered results as described are not achieved, however, primarily because certain indirect sources of the ionospheric micropulsations are not actually at infinity

and are therefore not precisely the same at all stations. The actual variations on the differential records with respect to the common reference magnetometer record are shown in Figures 24 and 25 respectively for Array I with 30 kilometers spacing between sensors and Array II with an average 10 kilometer spacing for a period during typically 'quiet' magnetic conditions. The removal of the ionospheric pulsations is less efficient during periods of high activity as is evident in Figures 26 and 27.

It is evident that the differential records contain considerably reduced time variations but there the events which remain on the differential records would make it difficult or even impossible to resolve and recognize a similar event if it were of local origin. The reduction of ionospherically induced events on the differential records from the events as they appear on the total intensity record, is approximately 10:1 for Array I. This reduction is frequency dependent and follows approximately the dependence shown in Figure 28 where the ratio of an event on the differential record to the primary event as it appears on the total intensity record is plotted as a function of period.

Signal Enhancement of Differential Records

Various means of further enhancing the reduction of the pulsations on the differential record might be achieved, for example, by recording the ratio of the pulsations of

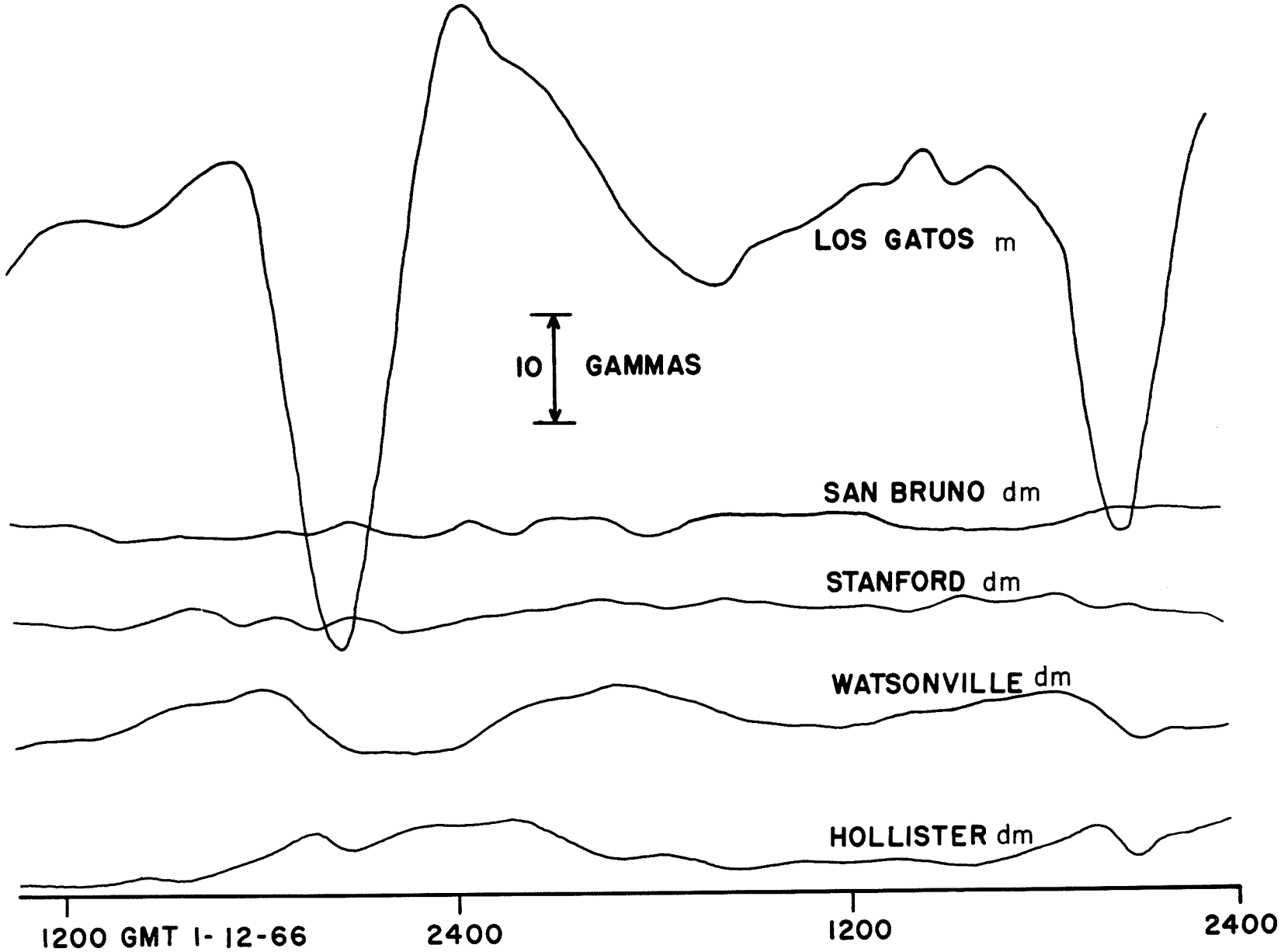

Figure 24. Variation in the total intensity and differentials of array I in a typical quiet period. m = magnetometer; dm = differential magnetometer.

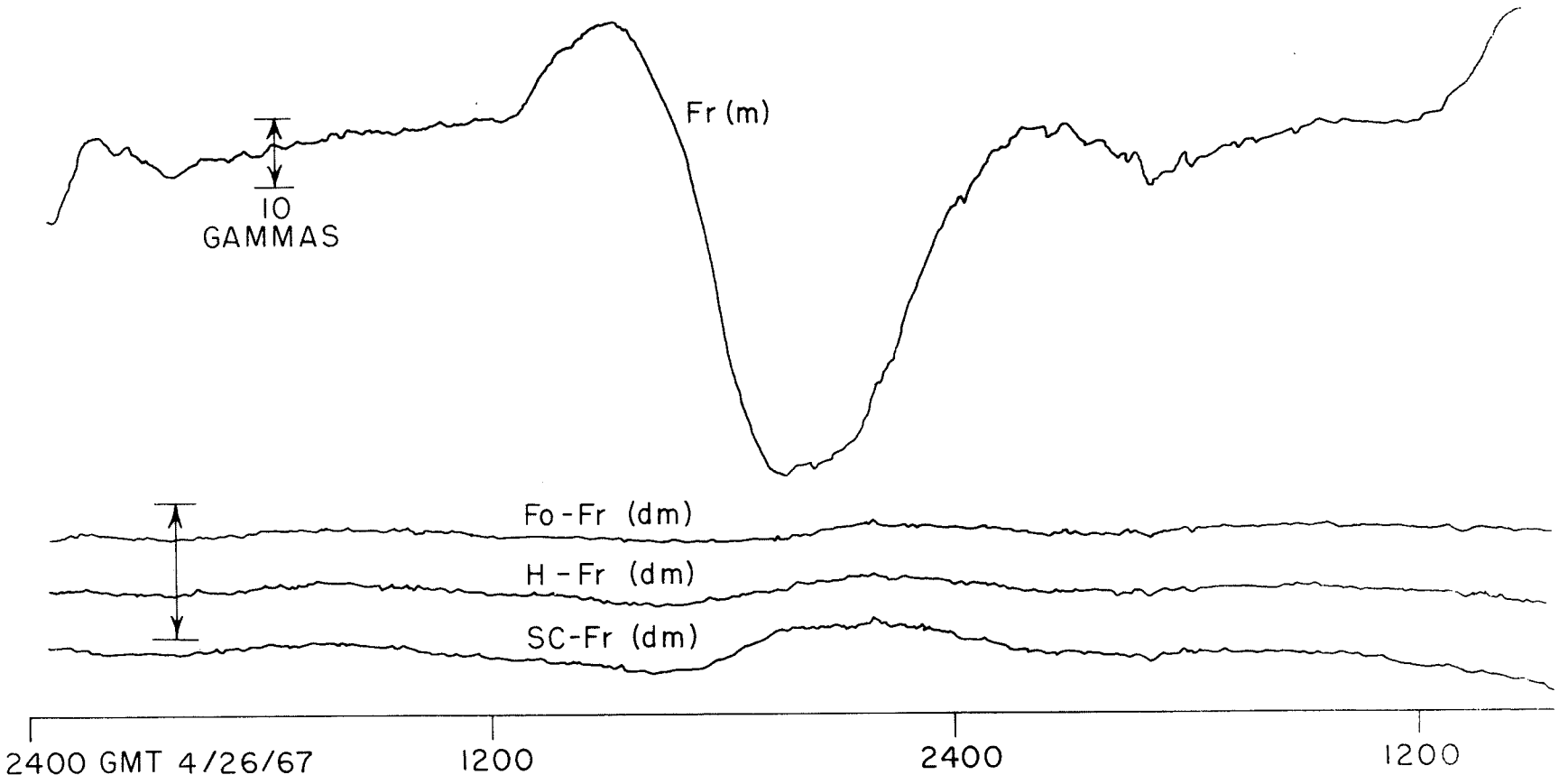

Fig. 25. Differential and total intensity variations of array II in a typical quiet period. Station symbols are abbreviated from names in Fig. 19.

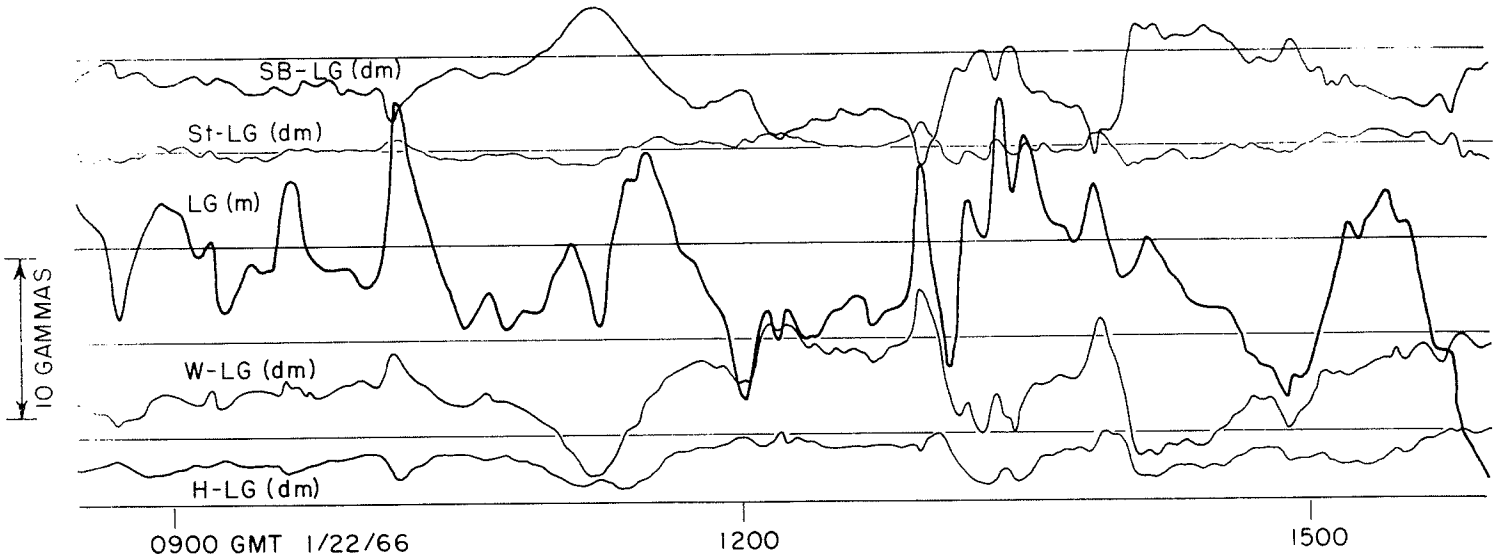

Figure 26. Differential and total intensity variations of array I during a magnetically active period.

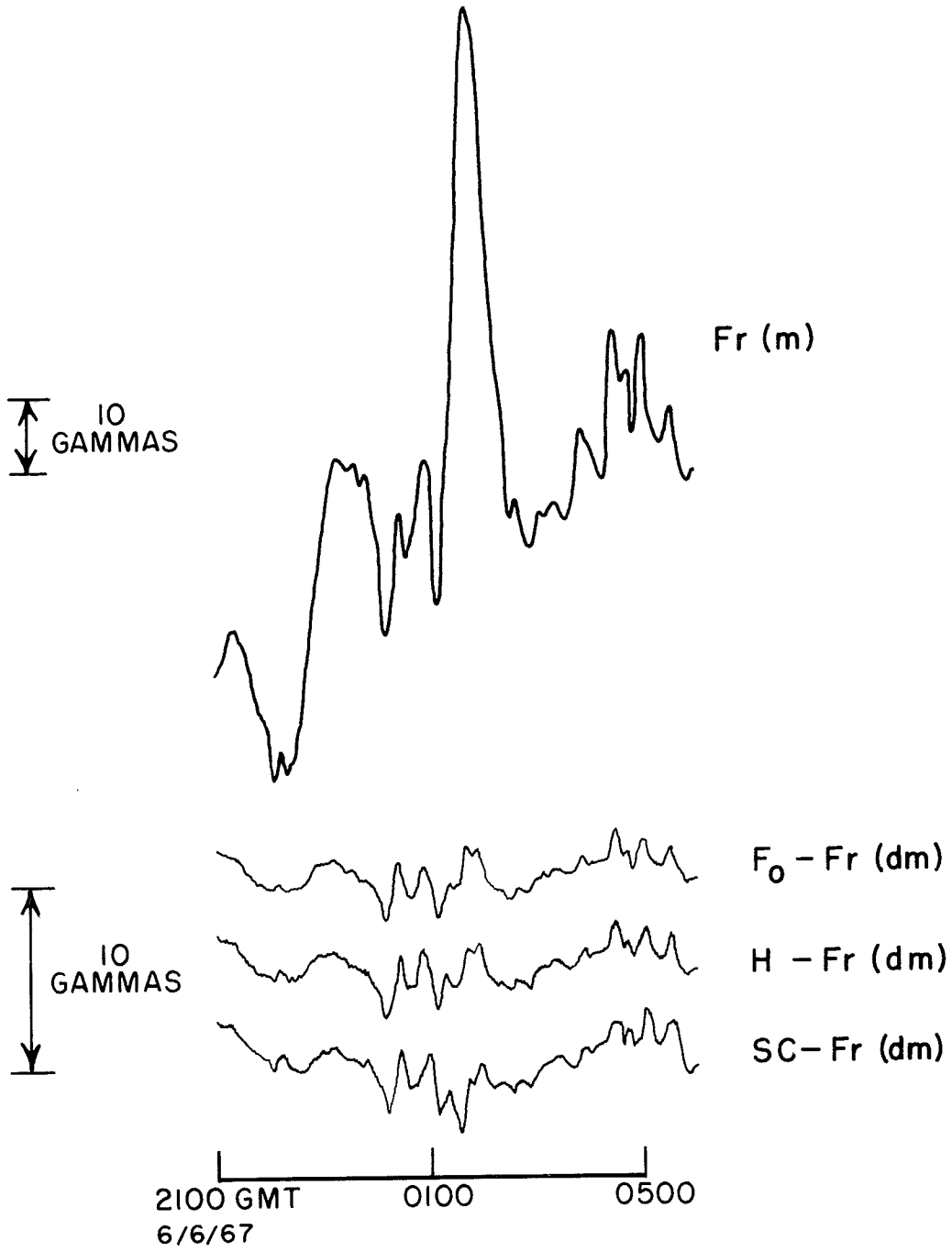

Fig. 27. Differential and total intensity variations of array II during a magnetically active period.

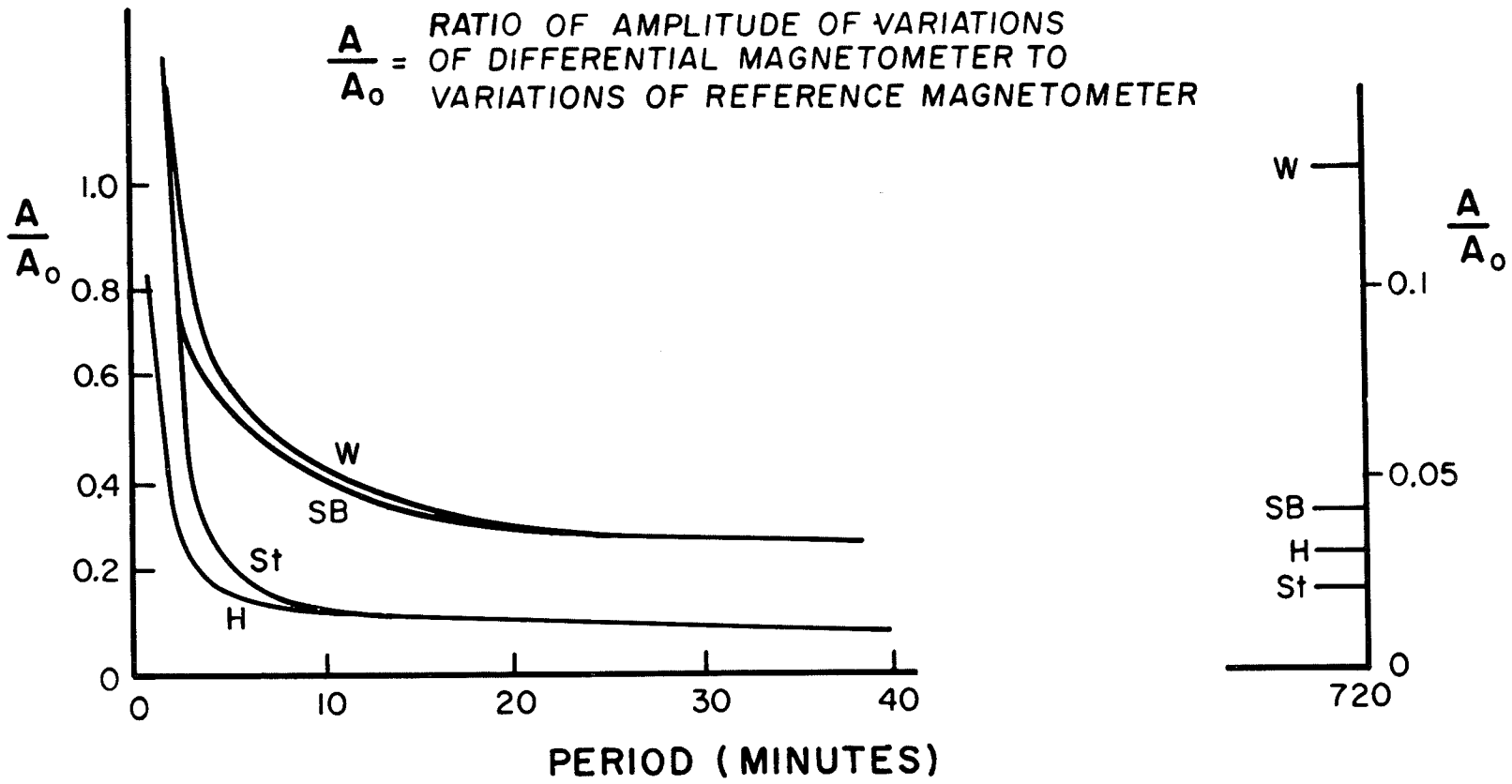

Figure 28. Frequency (period) dependence of the micropulsation events on the differential.

the total intensity to those of the differentials or the ratio of the differential variations to the time derivative of the total intensity variations. Moreover, the second differential, i.e., the difference of differential records, may enhance the resolution of local events but only if certain environmental conditions exist. In any case, the result of a second differential using various combinations are shown in Figure 29 for comparison with the normal first differential itself. Note that this technique does improve the resolutions of local events on Array II and on some second differentials of Array I.

Ionospheric Micropulsation Events on the Differential Records

Attempts to <u>remove</u> the effects of the micropulsations from the observations of local magnetic intensity variations at best result only in the <u>reduction</u> of the micropulsation events. Analysis of the assumptions of the array geometry and operational limitations indicate that sensors not immediately adjacent to each other will not, in fact, sense identical micropulsations. A given single pulsation will present itself with different amplitude and phase at two magnetometers several tens of kilometers apart. The observed difference in amplitude and phase is a function of frequency, the higher the frequency the greater the differences. The nature of this function is shown in Figure 28. Moreover,

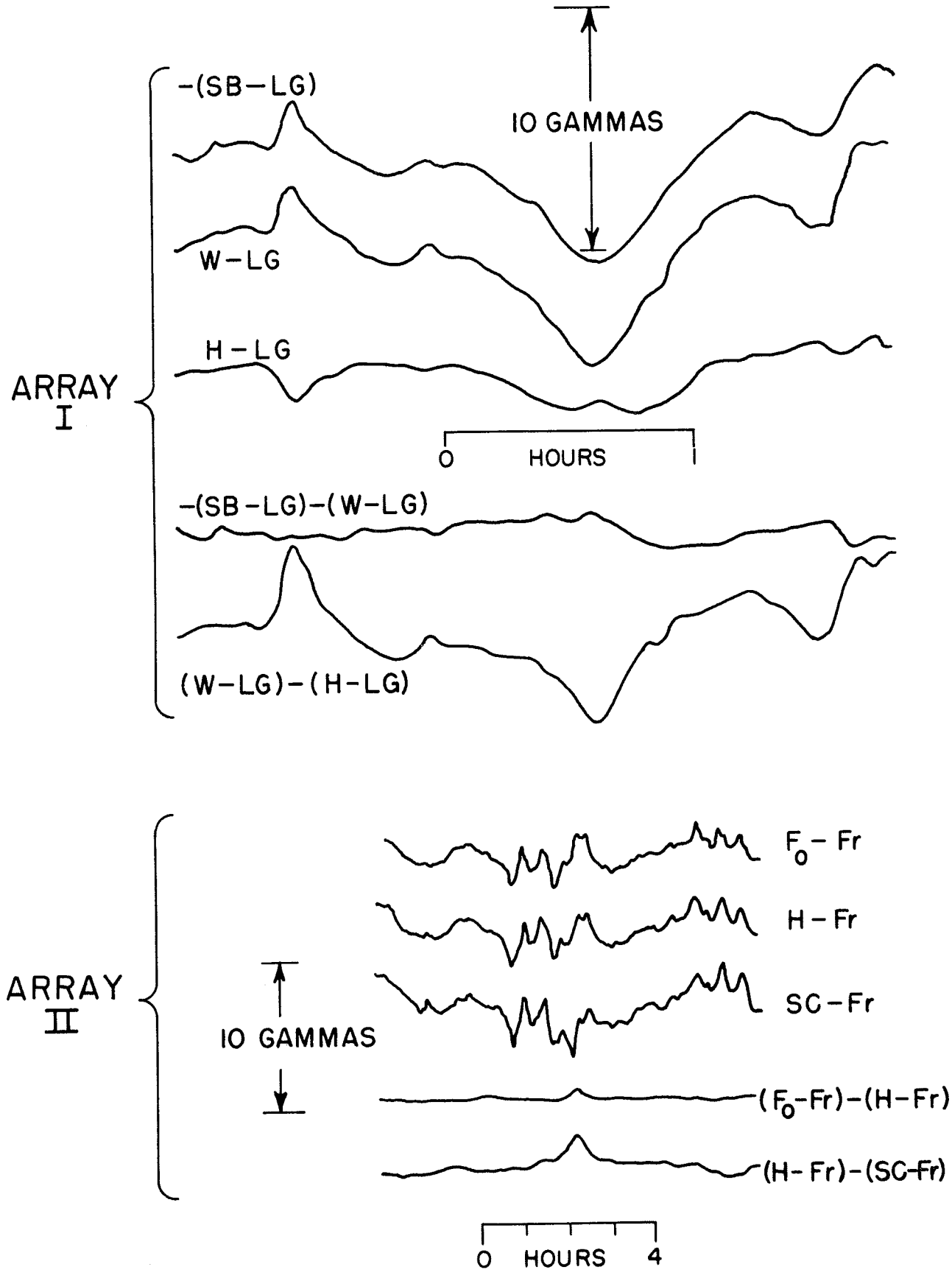

Fig. 29. 2nd differentials of variations in Figures 26 and 27 demonstrating improvement in removal of micropulsation noise.

the differences in amplitude are not as dependent upon the distance between stations as they are upon their location.

These phenomena are the consequences of the telluric current contribution to the geomagnetic micropulsations, anomalies in the subsurface conductivity at the continental margin, and the scalar intensity nature of the magnetometers used in the array. As outlined earlier, the observed micropulsations are largely the result of the varying magnetic fields of the overhead ionospheric current system and to a lesser degree the magnetic field associated with the local telluric current system. The magnitude and direction of the telluric currents are, in turn, determined by the conductivity of the subsurface. Both lateral, and vertical inhomogeneities in conductivity often exist across the contact of widely differing rock types. This is particularly true at the continental margins where the crustal thickness varies, the crustal and subcrustal properties vary, and the highly conductive ocean is present. The net result is a phenomena known as the "coast effect" (Parkinson, 1959; Schmucker, 1964; and Rikitake, 1964) where the vertical component of the time varying micropulsations is enhanced inland from the coast for several kilometers. Schmucker observed just such an anomalous behavior in the vicinity of two sites occupied during the present investigation, namely, Watsonville and San Bruno, both coastal sites.

The total intensity rubidium magnetometers are total-field magnetometers and as such measure only the components of the time variations in the direction of the total field. For all stations of the array, the inclination and declination are nearly identical and a micropulsation represented by a uniform plane wave would therefore have components identical at each of these stations. The direction of the pulsation changes at the near coast stations, however, and the projection of the pulsation vector on the total field is therefore not identical with the variations at the other stations. The pulsation is, in fact, larger at these anomalous coastal stations because the more vertical component of the pulsation presents a larger component on the somewhat vertical (65 degrees) inclination of the total field.

The frequency dependence of the variations present on the differential records is the result of the varying depth of penetration of the ionospherically induced telluric currents, i.e., the frequency dependence of the 'skin depth'. The depth where the currents will be deduced to 1/e of its value at the surface is given by

$$d = k \left(\frac{T}{\mu \sigma}\right)^{\frac{1}{2}}$$

where T = the period the micropulsation, μ = the magnetic permeability, and σ = the conductivity. Thus, the depth of penetration varies directly with the square root of the

period. The conductivity homogeneity, meanwhile, increases with depth, there being more massive and more uniform geologic conditions at depth. Therefore, the longer period micropulsations have more uniform telluric current contributions from one site to another and this uniformity is the principal determinant. The coherence is apparently proportional to the depth of penetration of the currents as expressed in the above expression, i.e., as the coherence increases, the ratio A/A_0, given by the ordinate from Figure 28, is

$$\frac{A}{A_0} \propto d^{-1},$$

then

$$\frac{A}{A_0} \propto (T)^{-\frac{1}{2}}$$

This ratio does, in fact, vary inversely as the square root of the period as shown in Figure 30 which in a qualitative manner supports the argument put forth above regarding the increase in conductivity homogeneity with depth.

The long period behavior of the ratio $\frac{A}{A_0}$ represented by the 720 minute period diurnal plot of Figure 28 is independent of period and attains a finite value of 0.02 to 0.04. It can be demonstrated that differential variations necessary to produce such values can be observed as a consequence of the diurnal variation and the field intensity dependence of induced magnetization over areas of different susceptibility.

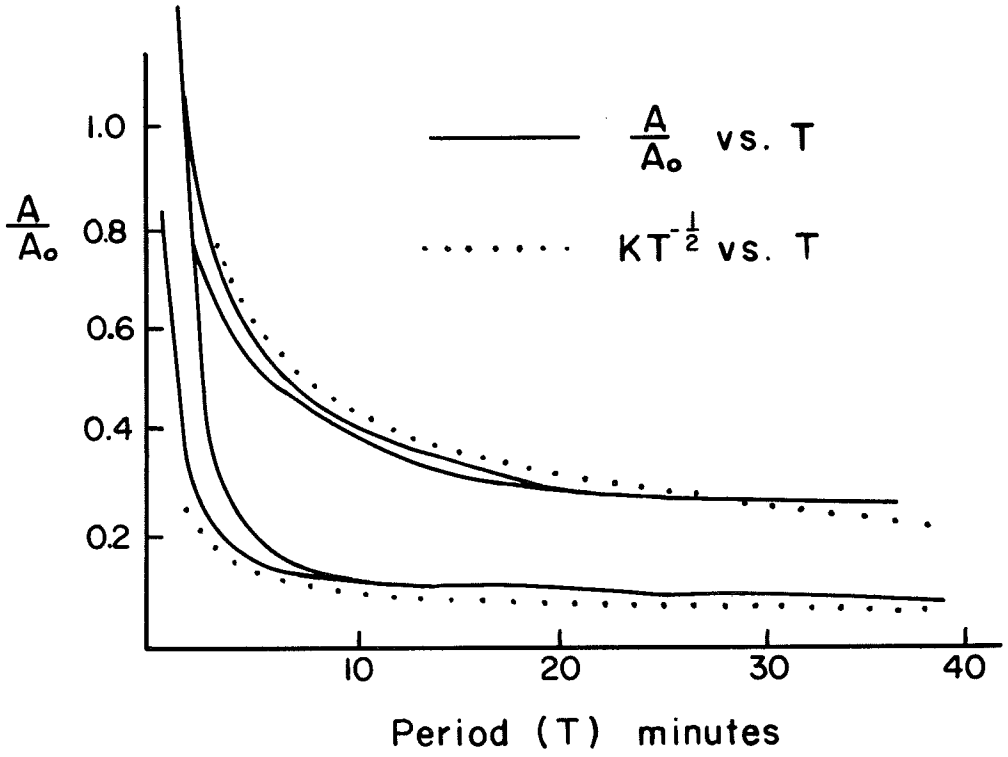

Fig. 30. Inverse square root of the period as a function of period plotted with the variables of Figure 28.

The long period ratio $\frac{A}{A_0}$ is, in fact, used to estimate the differential susceptibility for analysis of the piezomagnetic events disclosed herein.

Detectability of Local Events

Recognition of local events on a magnetometer within the array depends upon such factors as the amplitude, period, linear rate of change, signature, and areal extent of a local event. The recognition also depends upon the level of micropulsation activity during a given period; upon the particular site in which such an event is sought; and upon the spacing of the adjacent magnetometer stations.

From an exhaustive study of the records obtained from both the 120 km five station Array I and the higher density 25 km four station Array II, the approximate limits of detectability were determined. These limits are expressed graphically in Figure 31 as a function of the relevant variables listed above. In Figure 31a, the local event recognition limits for short periods are essentially the limits presented by the appearance of sinusoidal micropulsation effects on the differential record; at the long period dependence the limits are the stability of the instrument and the time rate of change of the differential secular change. This dependence can be compared to a normal power spectra plot of the total field as shown in Figure 32 (Herron, 1967).

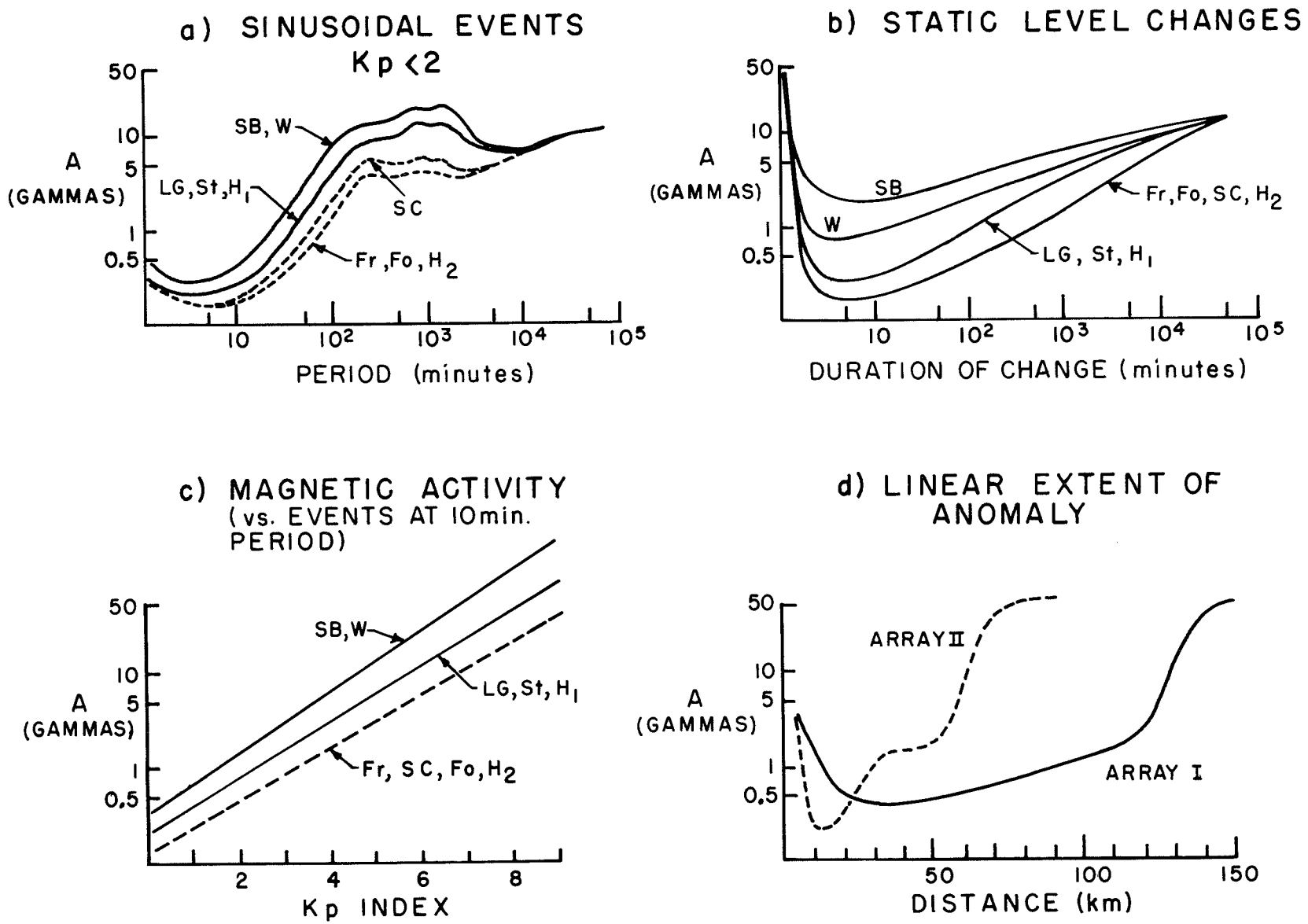

Fig. 31. Detectability of local magnetic events as a function of different variables. A is the minimum amplitude of a recognizable local event.

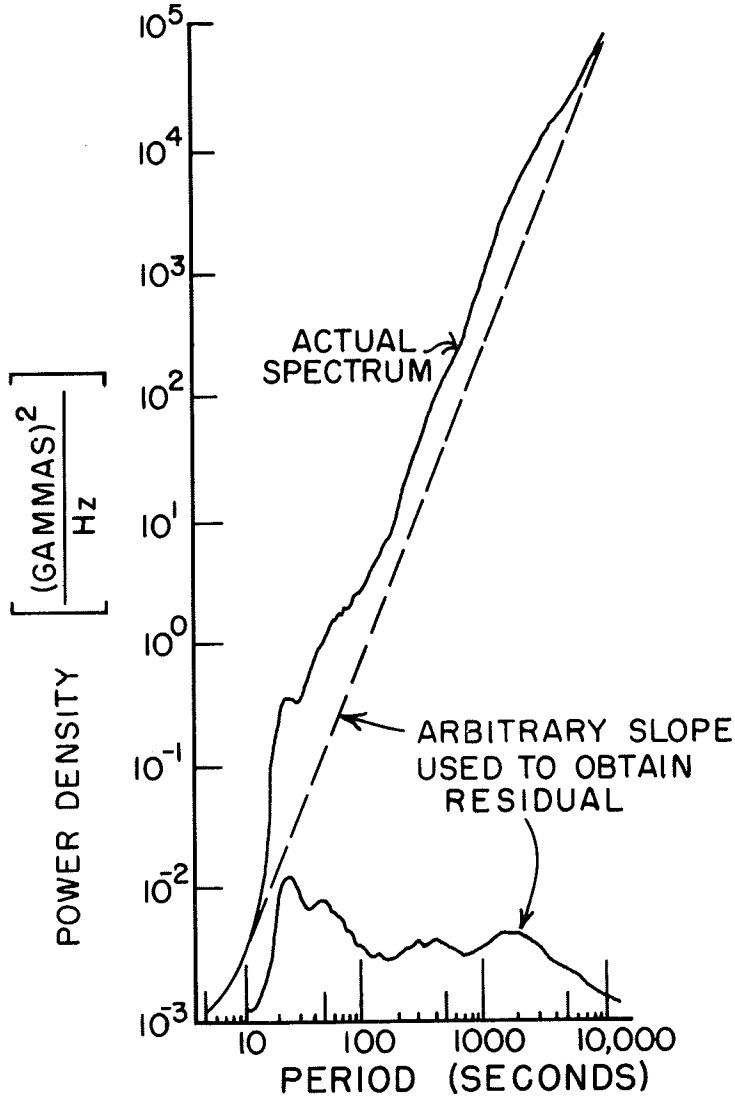

Fig. 32. Power spectrum of micropulsations of the total field (After Herron, 1967).

Figure 31b exhibits a sharp dependence at the short period region because of the possible confusion with electronic transients and cultural effects such as persons at the magnetometer and for the long period dependence the limits are the same as Figure 31a. The limits of detectability of local events set by the presence of high magnetic activity is indicated in Figure 31c as a function of the Kp index of magnetic activity (Lincoln, 1966, 1967). Essentially no local events of realistic amplitude can be seen during periods of high magnetic activity. The effect of the areal extent over which the 'local' event occurs on its detectability is expressed by Figure 31d. The change in slope nearest the origin of the local event indicates the relative probability of detecting an event whose areal (or linear) extent is much smaller than the distance between points of coverage. The other changes in slope are a consequence of the fact that small events which occur equally on all magnetometers might nevertheless be an event local to the array but will only be detected by comparison of these records with certain known instruments much more distant than the total extent of the array.

Telluric Records

Telluric current measurement apparatus was installed late in the experiment to investigate the existence of anomalous potentials associated with creep events. It has

already been shown that if conductivity were sufficiently altered during compression, the change in current flow would have associated with it a change in magnetic field. However, the calculated magnetic effect is orders of magnitude too small to be detected and the change in current flow might not be accompanied by a change in the parameter actually measured by the telluric apparatus, namely, potential. The time rate of change of flux density from the piezomagnetic effect itself would create a change in potential but that also is considerably smaller than could be detected. Nevertheless, an attempt was made to observe these effects should the estimates be incorrect.

Two electrodes consisting of lead sheets 0.5 cm thick by 40 cm by 60 cm were buried 2 meters deep in soil 100 meters apart across the San Andreas shear zone on the Harris ranch. The electrodes were connected to a high impedence strip chart recorder with a resolution of approximately 100 microvolts. The resolution of the potentials thus measured is 1 microvolt/meter. Drift of the potential as measured was unavoidable because of electrode potentials of the lead versus soil, changes of contact resistance, variations in soil moisture, and other factors.

The telluric current recorder unfortunately was operating only at the time of one possible piezomagnetic event on 31 October 1966. At that time there was no recognizable variations on the telluric recorder as large as 1 microvolt/meter

during the 30 minutes of that event. Telluric records were not obtained during the following observed piezomagnetic events. A single unexplained event of two opposite linear slopes which join at a discontinuity was observed on the telluric recorder at or just prior to an earthquake of magnitude 4.2 16 kilometers northwest of the telluric electrodes (Figure 33). The effect was not one caused by seismically induced variations in contact resistance, piezo-electric potentials or seismic-electric effect which exhibit the variation shown in Figure 34 recorded from another earthquake of similar magnitude approximately 25 kilometers to the southeast.

Seismic and Strain Events

The indicators of stress changes that were used for correlation with the magnetic records were seismicity and creep displacement. Seismic events occurring from September 1965 to April 1967 of magnitude 2.5 or larger whose epicenters were within 10 kilometers of the array are shown in Table 2 and Figure 35. Earthquakes of magnitude 3.0 or larger within 10 kilometers of the arrays when each was in effect occurred in July, October, November, and December, 1966 and April 1967. The seismic events were tabulated from the earthquake records of University of California for the stationsat Pilacitos, Santa Cruz, Mt. Hamilton, and Vineyard/SEGO (Figure 20).

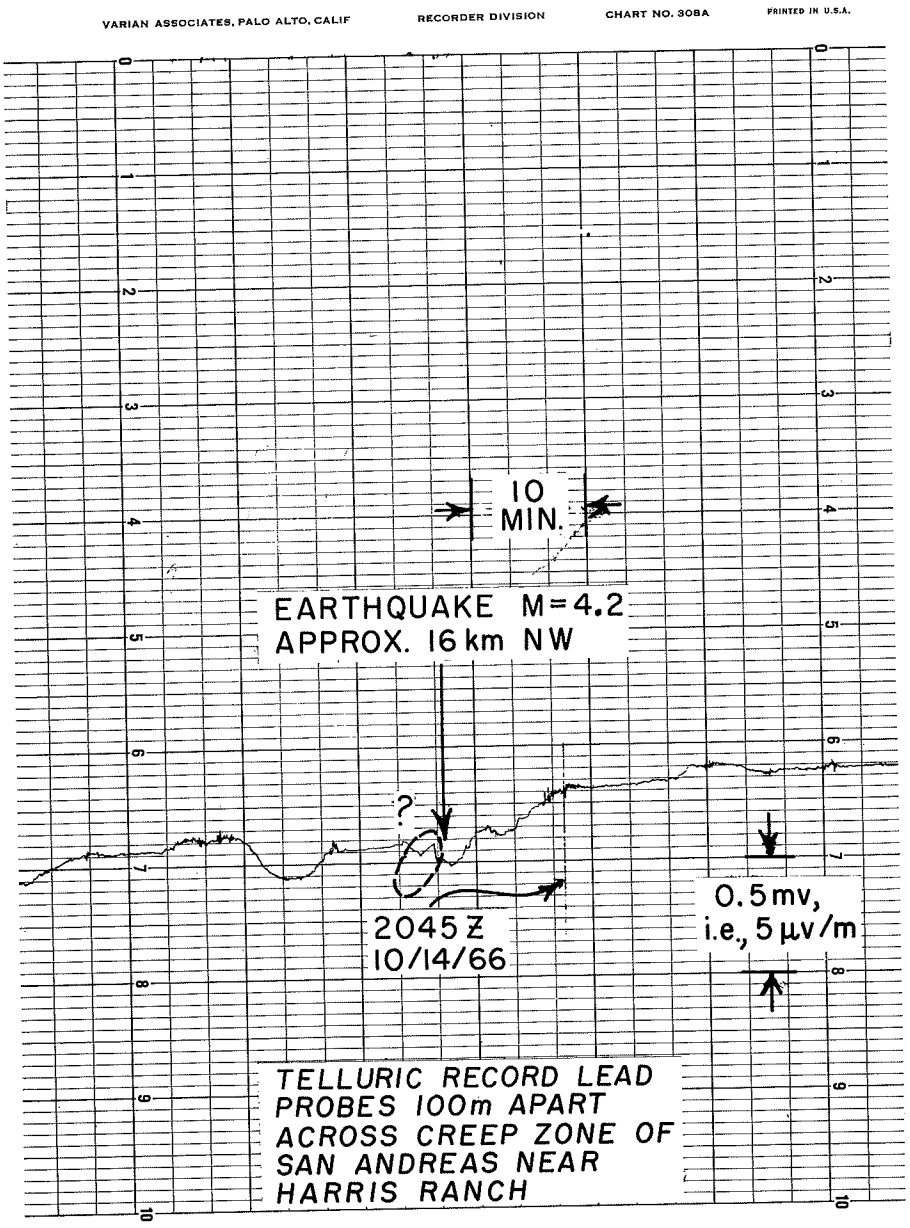

Figure 33. Telluric current record at Hollister at the time of a near earthquake.

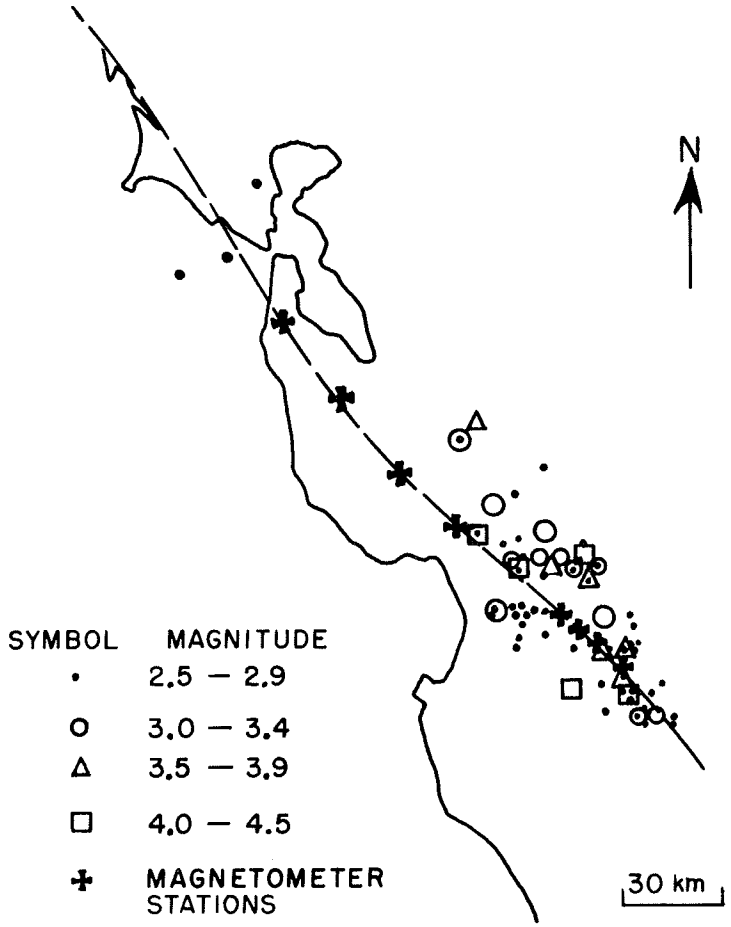

Figure 35. Earthquakes which occurred within array from August 1965 to April 1967.

Table 2. **Earth**quakes above M = 2.5 within San Andreas Array August 1965 through April 1967

Date	Time (GMT)	Latitude (degrees)	Longitude (degrees)	Magnitude
9-2-65	0803	36.6	121.2	2.8
9-2-65	0816	36.6	121.2	2.9
9-7-65	0130	36.8	121.6	2.8
9-12-65	0850	36.5	121.1	2.5
9-14-65	0909	36.6	121.4	4.0
9-25-65	0951	36.6	121.2	2.8
1-2-66	0759	36.5	121.1	2.5
1-3-66	2350	36.6	121.2	2.6
1-5-66	0555	37.0	121.5	3.0
1-9-66	0003	36.9	121.4	2.7
1-9-6	0008	36.9	121.4	3.3
1-14-66	0030	36.9	121.4	2.5
1-17-66	0148	37.0	121.5	3.3
1-17-66	0203	36.9	121.4	4.1
1-17-66	0223	36.9	121.4	2.9
1-17-66	0248	36.9	121.4	3.0
1-17-66	0623	36.9	121.4	2.8
1-21-66	0411	36.9	121.4	3.5
2-2-66	1308	37.4	121.7	2.9
2-8-66	0657	37.3	121.8	3.0
2-11-66	1857	36.8	121.5	2.5
2-13-66	1710	37.8	122.6	2.7
5-13-66	1946	36.9	121.6	3.2
5-15-66	1854	37.5	121.9	2.5
6-2-66	1312	36.9	121.6	2.5
6-5-66	2050	37.3	121.7	2.5
6-6-66	0723	37.3	121.8	3.8
6-11-66	1009	37.8	122.7	2.8
6-20-66	2300	36.3	121.0	2.6
7-3-66	0823	37.1	121.7	3.2
7-7-66	0411	36.8	121.7	2.5
7-11-66	1622	36.8	121.6	2.9
7-19-66	1044	36.7	121.3	2.7
8-5-66	0555	36.7	121.2	2.6
8-18-66	1137	37.0	121.2	2.5
(Franco magnetometer installed August 1966)				
10-10-66	0654	36.6	121.2	4.1
10-14-66	2034	37.0	121.7	4.2
10-20-66	1459	36.7	121.2	2.5
10-20-66	1511	36.7	121.2	2.8
10-25-66	2055	37.0	121.8	2.9
10-31-66	1631	36.5	121.2	2.5
10-31-66	1848	36.6	121.2	2.8
11-4-66	0454	36.5	121.2	3.2
2-16-66	0454	37.3	121.8	2.7
2-22-66	0351	36.6	121.1	2.5
3-7-66	0258	36.2	121.0	2.5
3-7-66	1829	36.8	121.6	2.7
3-10-66	2053	36.9	121.5	2.7
3-12-66	1659	36.8	121.6	2.5
3-12-66	1660	36.8	121.6	2.5
3-16-66	1821	36.9	121.5	3.0
3-16-66	1824	36.9	121.5	3.6
4-3-66	2118	37.0	121.8	2.7
4-10-66	0851	38.0	122.4	2.5
4-10-66	1533	36.7	121.6	2.6
4-14-66	0615	36.5	121.1	3.0
4-15-66	1719	36.9	121.4	2.5
4-15-66	1951	36.6	121.2	2.8
4-29-66	0809	36.6	121.3	3.8
5-2-66	1218	36.6	121.2	2.7
5-4-66	0633	36.8	121.2	2.7
5-5-66	1949	37.1	121.6	2.6
5-5-66	2230	36.9	122.5	2.5
5-12-66	1503	36.8	121.5	2.5
5-13-66	1726	36.9	121.5	4.5
11-22-66	2034	36.8	121.5	2.5
12-6-66	1035	36.8	121.5	3.3
12-18-66	0352	36.5	121.2	2.5
12-24-66	2057	36.5	121.2	2.7
1-14-67	0943	37.0	121.6	2.9
1-17-67	1114	36.6	121.3	2.6
1-28-67	0001	36.8	121.7	3.3
1-31-67	1826	36.5	121.3	2.5
2-1-67	2321	36.7	121.3	2.5
2-7-67	2200	37.0	121.7	2.8
2-18-67	0133	36.8	121.6	2.5
2-25-67	0201	36.8	121.6	2.9
3-1-67	1408	36.7	121.4	2.6
3-10-67	0629	37.2	121.5	2.7
3-14-67	0924	36.7	121.6	2.6
3-15-67	1648	36.9	121.5	2.8
3-26-67	0537	36.8	121.2	2.7
(Array II installed 1 April 1967)				
4-17-67	2047	36.8	121.6	2.5
4-21-67	1704	36.7	121.2	2.6
4-22-67	1640	36.7	121.2	3.6
4-27-67	0723	36.8	121.5	2.7

The creep displacement data was obtainted primarily from a converted recording aneroid barometer apparatus fixed in the Almaden Cienega Winery (Tocher, 1960). The record of displacement is written on a chart moving at approximately 1.6 mm/hr with sensitivity of 0.01 mm. The records are examined periodically and the distance measured with a micrometer screw adjusted to obtain absolute measurements of displacement. The observed creep averaged approximately 1 cm/year of right lateral movement, almost all of which occurred in 6 increments since August 1965. The duration of motion for each increment varies from minutes to days (Figure 36).

Earthquakes do not usually simultaneously accompany the creep displacement. The only earthquakes that occurred within the southern part of the array, however, occurred 4 days after a very large amount of creep (about 4 mm).

Creep displacement is also measured using an electro-mechanical transducer installed in the winery 50 meters from the mechanical transducer. From 1 April 1967, the dc voltage of the electromechanical transducer was used to drive a voltage-controlled oscillator for subsequent transmitting to the Harris residence and then to Stanford. The creep was thus recorded together with the magnetometer variations.

Local Geomagnetic Events and Correlation of Seismic/ Events

Within the limits of detectability set by the micro-

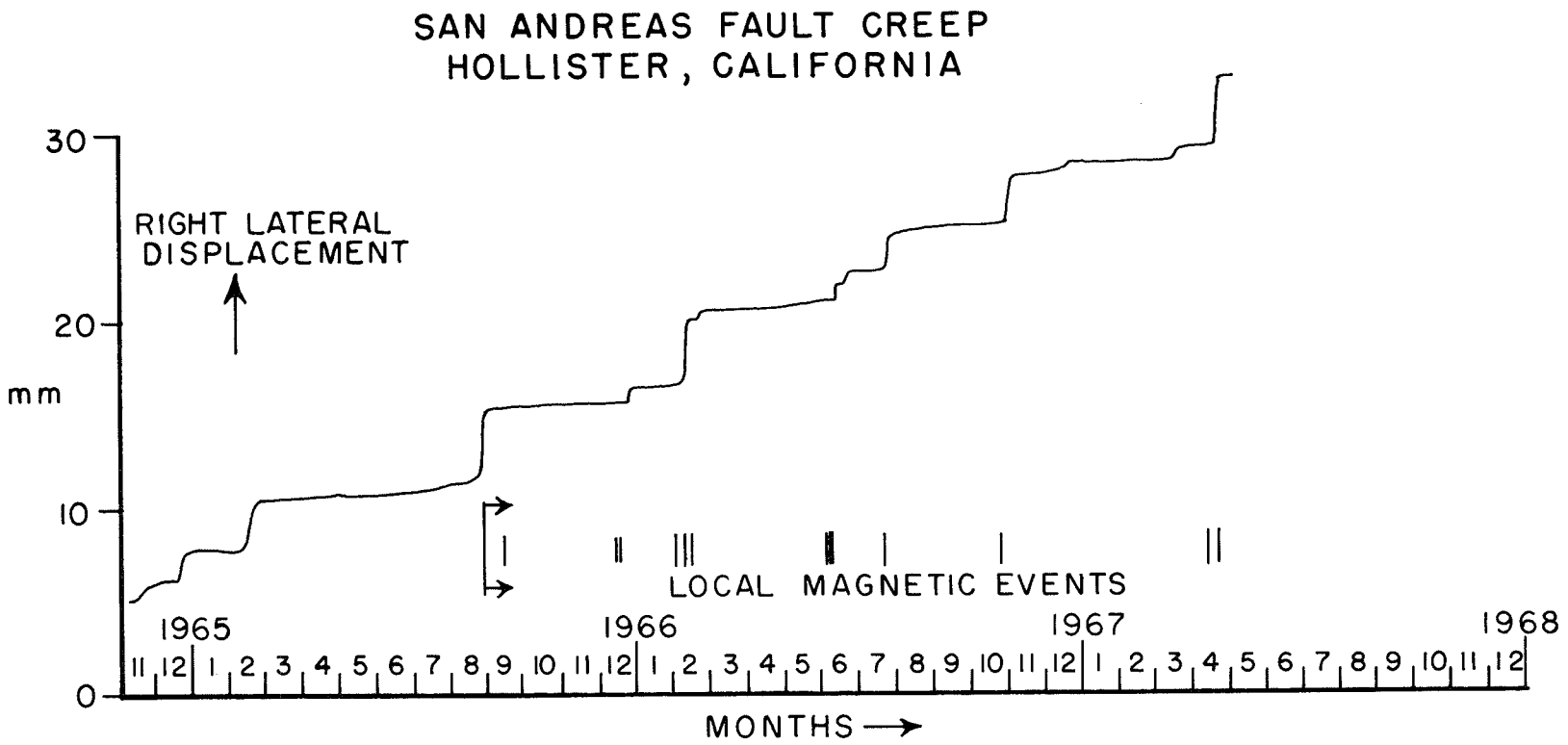

Figure 36. Creep of San Andreas fault at Almaden Winery, January 1965 through April 1967, plotted together with local magnetic events.

pulsations, the coast effect, the instrumental resolution, and spurious events, the records were visually examined for evidence of local changes in the geomagnetic field. Since the signature of the events were not initially known a criterion was established for a local event which can be stated as follows: any change on only one trace of the differential intensities which was within the limits set forth in Figure 31. It may certainly have been possible to have overlooked events which may have occurred during magnetically active times or which were subtle, low amplitude events of a sinusoidal nature. Moreover, if an event of subsurface origin (piezomagnetic) occurred throughout the entire array, then by the definition above, it would be classified simply as an ionospheric event. This limitation must be accepted as a shortcoming of this scheme for removing the micropulsation noise.

In general, five situations were found to occur: a change may occur on one differential trace only, indicative of a local magnetic effect. A change may also occur equally and in the same sense on all traces in which case the event would be local to the common reference magnetometer site (Figure 37). Most variations that appear on the differential traces which are of unequal amplitude and perhaps phase and are accompanied by a change (usually larger) on the references magnetometer are simply incomplete cancellation of the ionospheric pulsations. For periods longer than 30 seconds, a

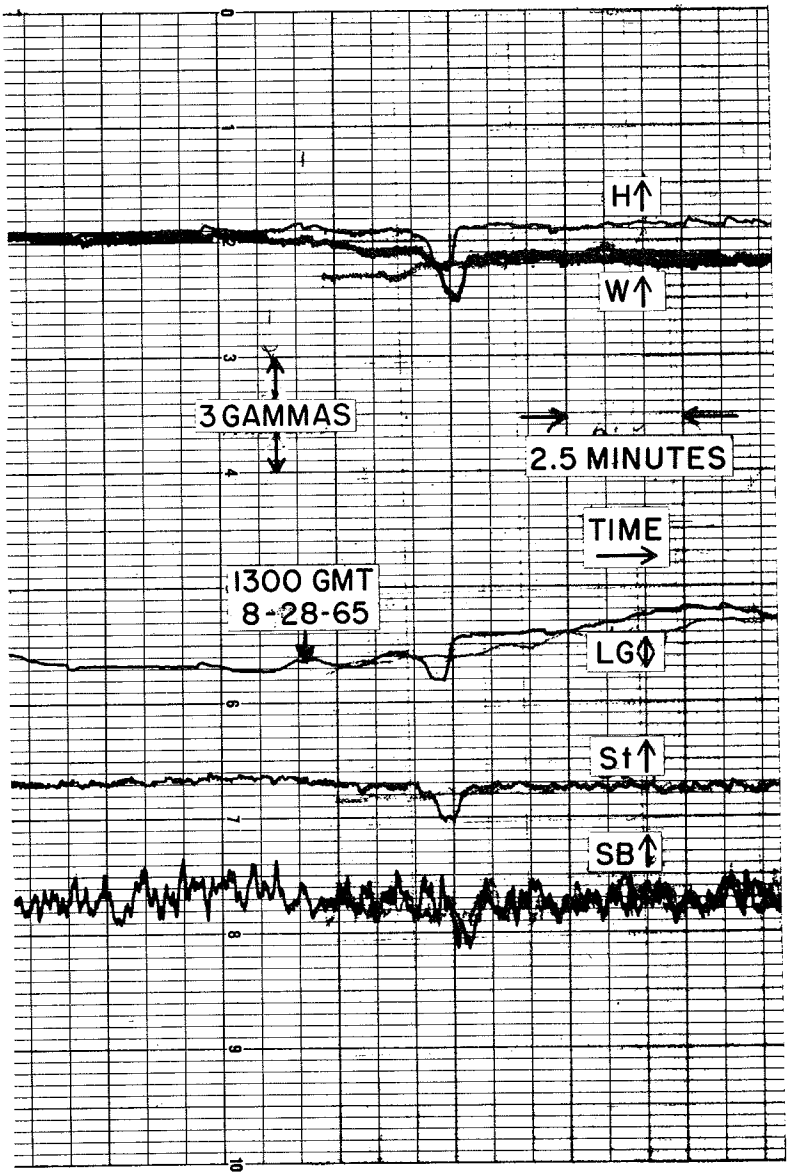

Figure 37. Local magnetic event at Los Gatos.

micropulsation will always be larger on the reference magnetometer trace than on any differential trace (Figure 38). This is another way of saying that the event itself, for periods longer than 30 seconds is larger than the differences between the event at the various sites. On the other hand, events local to the array have occurred on all stations of Array II and by the definition above would not be classified as a local event. The events were long period, larger on the differentials than on the total intensity, and of unequal amplitude and were thus recognized. Subsequent comparison with magnetometers more distant (two array lengths away) confirmed their local nature. The fifth situation is simply the appearance of a micropulsation event on the reference magnetometer trace without any expression of this event on the differential traces. This occurence is the result of perfect coherence between all stations including the reference station with the result that the differentials are truly constant (Figure 39).

Under these conditions, the records of the differential and total intensity were analyzed. All events shorter than 30 seconds were considered to be in the noise region and ignored. By doing so the selection of local events was placed on a more objective basis. The sources of noise in this part of the spectrum could arise from the following: 1) the permanent daytime micropulsation peak at 20 to 30 seconds with a typical amplitude of 0.1 gamma; 2) man-made

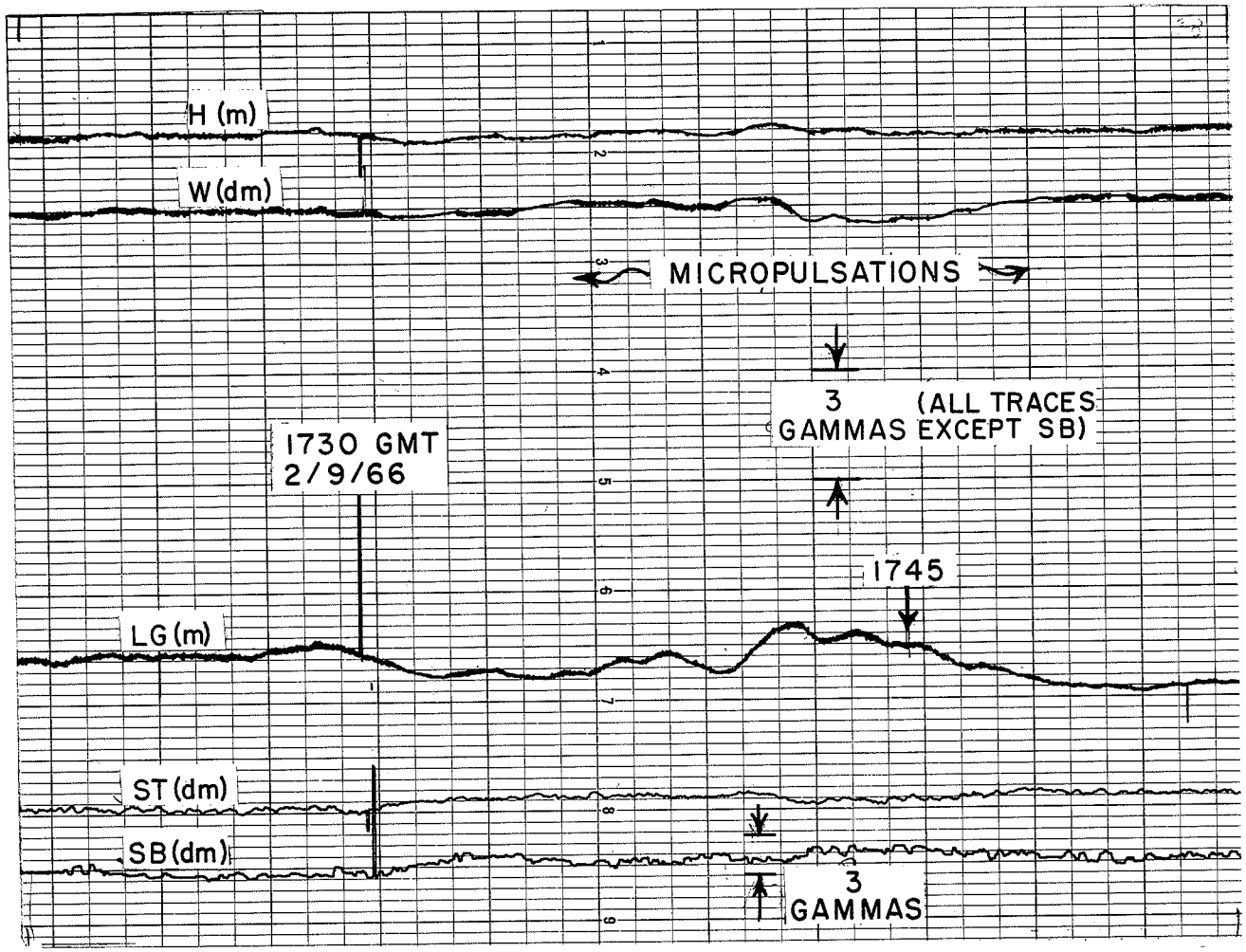

Figure 38. Typical incomplete cancellation of micropulsations on differential array I.

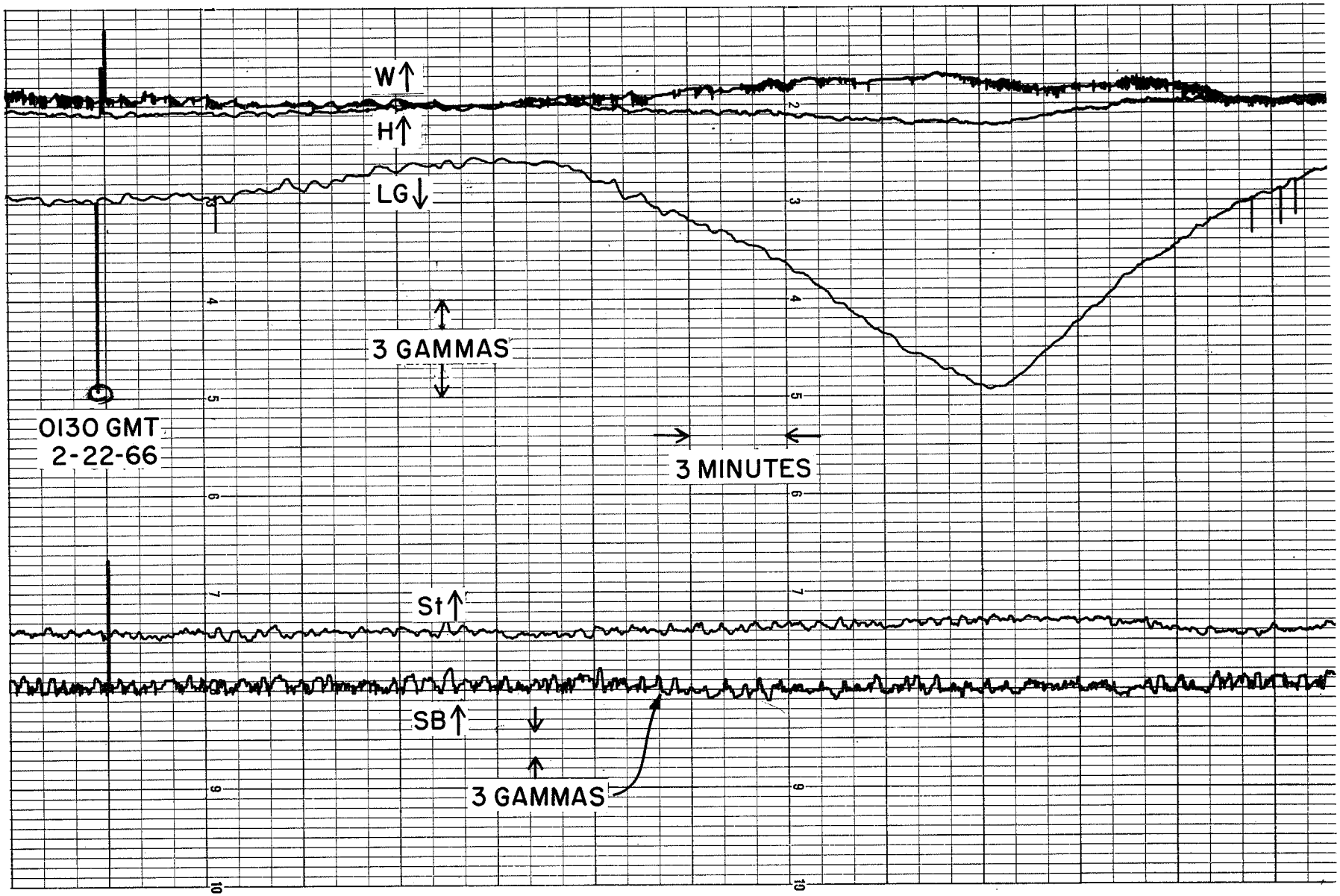

Figure 39. Long period micropulsation event which exhibits efficient cancellation on differential channels of array I.

activity which was observed and confirmed on the differential traces and which because of their proximity to the sensor always had frequency components in this band. Transient events which take place in less than several seconds were considered to be instrumental errors and thus ignored. An event which was expressed as a permanent change in the local field was considered as a long period event, however.

The array became operational in late August 1965. Unfortunately the magnetometers were not quite functioning properly during the large creep event beginning on 19 August. A local event of rather short duration was observed at the Los Gatos reference magnetometer site on 28 August 1965 (Figure 37). An earthquake of magnitude 4.5 occurred on 7 September on the Hayward fault 40 kilometers to the northeast of the northern portion of the array. On 14 September a magnitude 4.0 earthquake was recorded with its epicenter 30 kilometers southeast of the Harris station on the San Andreas fault. There were scattered small seismic events throughout the northern part of the array during the following few weeks. On 22 September a local increase in field intensity was noted on the Stanford trace followed some 3 hours later by a similar change at Hollister with the Hollister change partially returning to its former value 1 hour later (Figure 40). Neither creep nor local earthquakes were observed precisely at these times. (All magnetic, creep, and seismic events are plotted on a common time scale in

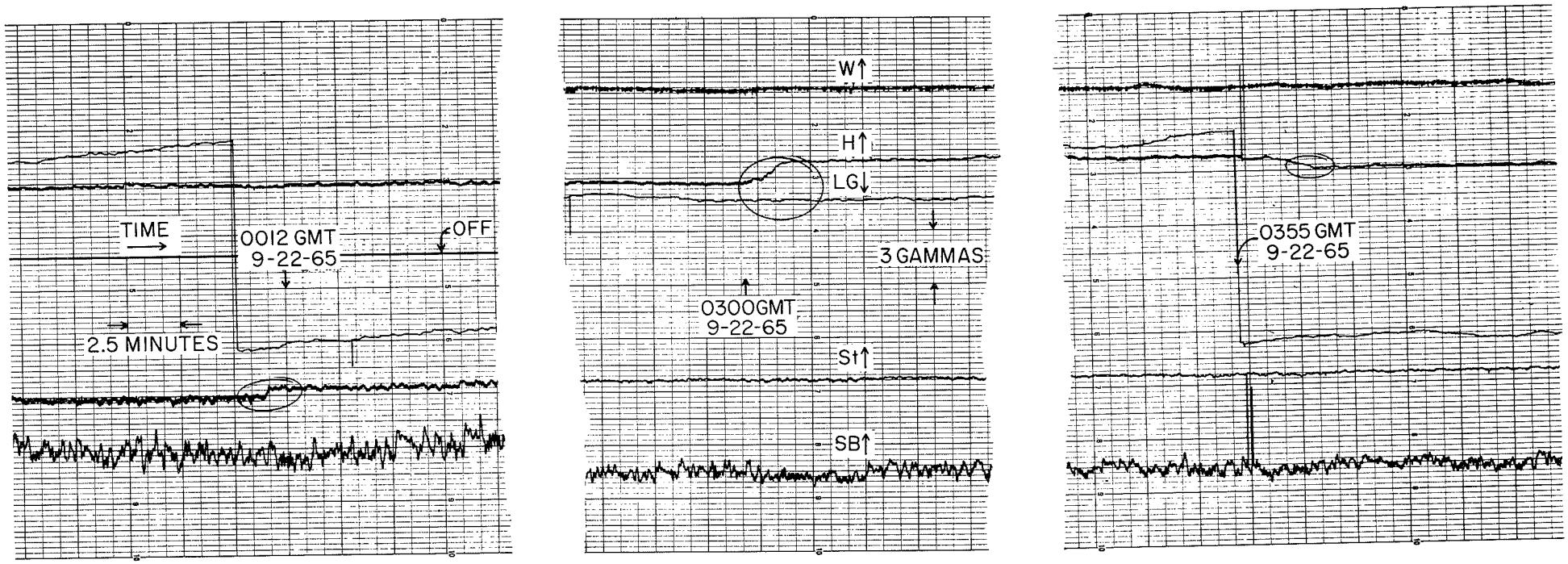

Figure 40. Local events at Hollister and Stanford on array I.

Figure 36.

The next local magnetic events was observed at Hollister on the 20th and 21st of December 1965. Both events were local increases of approximately 1.5 gamma (Figure 4a and 41). Within the long term resolution of the trace, these events did not appear to have risen to this value or to return to their former value. Ten hours following the second event, creep was observed at the winery near Hollister (Figure 36).

No further local magnetic events nor creep events were observed until 7 February 1966 when a local quasi-sinusoidal change in field intensity was observed at Hollister (Figure 42). The event was primarily a decrease returning to its former value at a much greater rate than the initial rate of change. Two days later the first significant creep occurring since 21 December 1965 was observed. The rate of creep increased the following day and a local earthquake of magnitude 2.5 occurred a few kilometers to the west. This was the only local earthquake as large as 2.5 magnitude occurring within the array to that time. (A small unexplained local transient event was observed at Hollister 2 hours prior to this earthquake but nothing at the time of the earthquake (Figure 43). Such short period effects, however, as stated earlier are not included as significant local magnetic events. On 16 February, a local increase in intensity was observed at Hollister and finally on 21 February an event very similar to the first are on this series

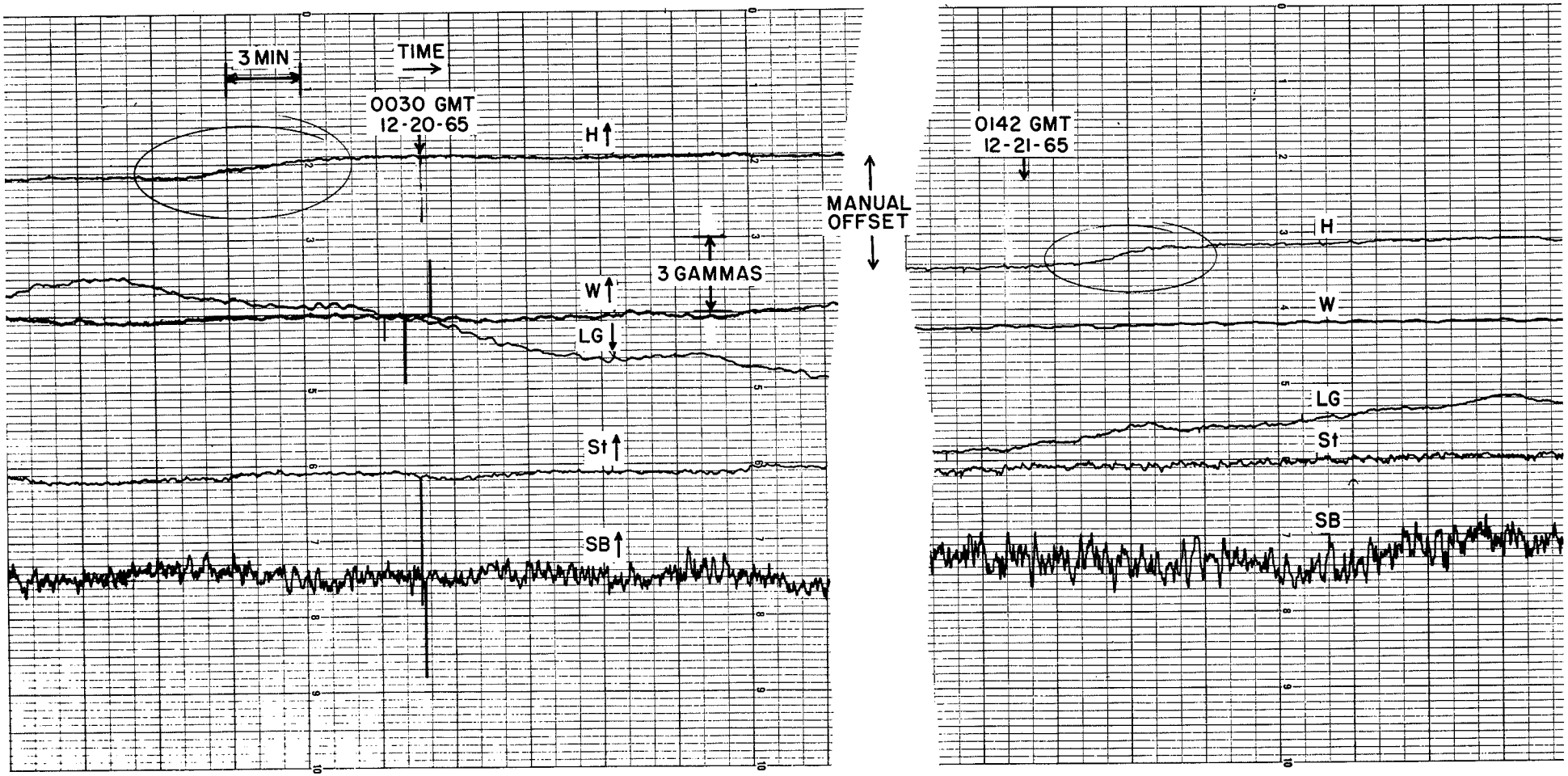

Figure 41. Local magnetic events at Hollister.

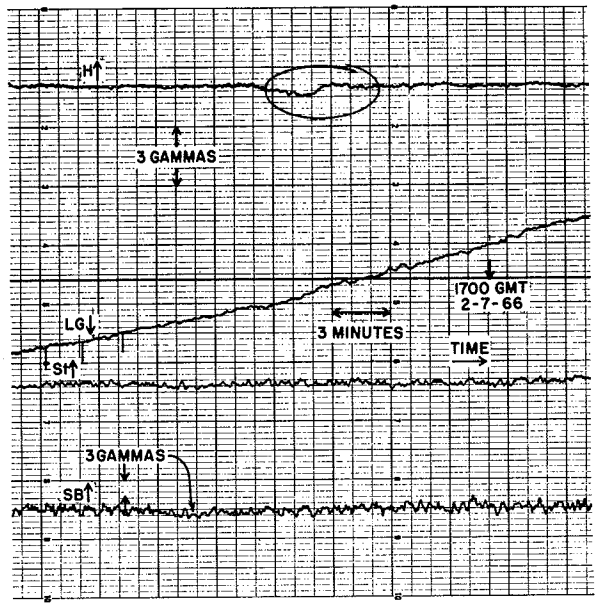

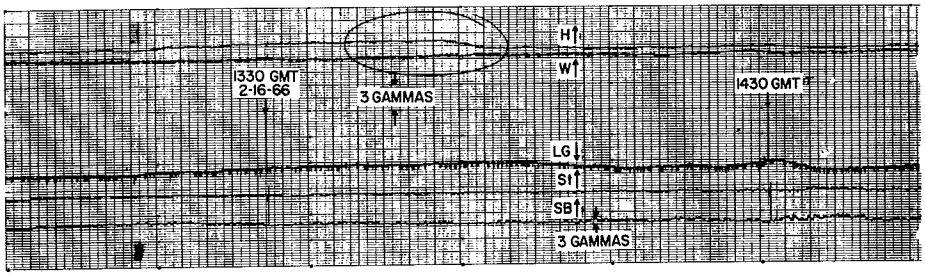

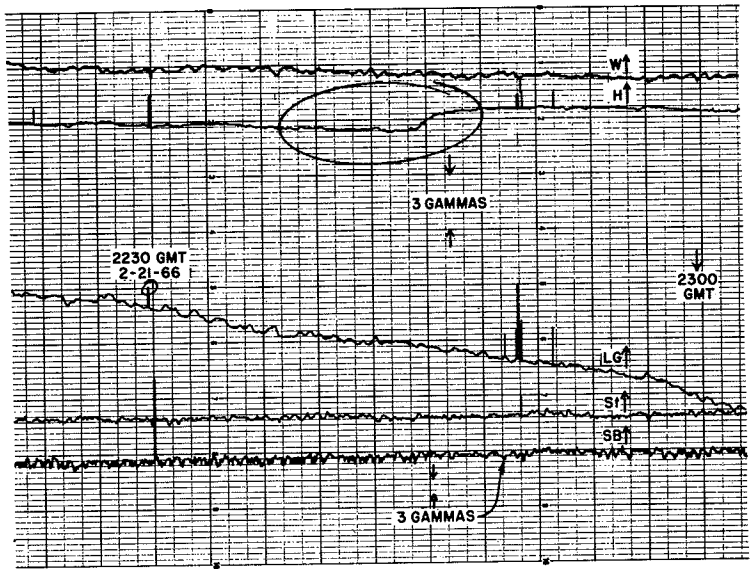

Figure 42. Local magnetic events at Hollister which span in time a major creep displacement of the fault and local earthquakes.

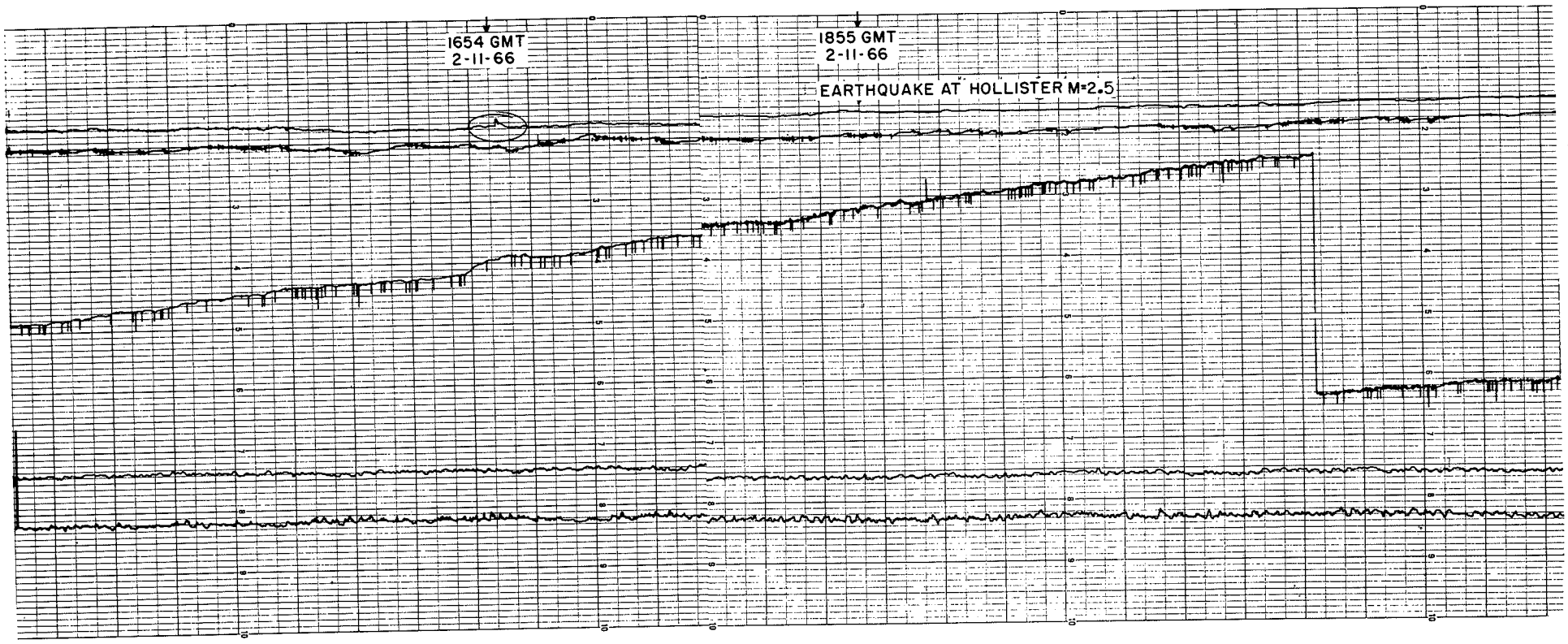

Figure 43. Differential magnetometer records during a local earthquake of magnitude 2.5.

occurred but of much larger amplitude and of longer duration (Figure 42). From 9 February to 21 February creep was occurring for a total displacement of 3.5 mm. Two earthquakes of magnitude 2.7 occurred near the Watsonville magnetometer on 16 March 1966 but there were no recognizable local magnetic events. An earthquake of magnitude 3.8 was recorded on 29 April 1966 whose epicenter was 25 kilometers southeast of the Hollister magnetometer on the San Andreas fault. No creep was observed, however. On 8, 13, and 14 June 1966, local events were again observed at Hollister identical to those observed in December 1965 (Figure 44). On 13 June the first creep since the major displacement in the previous February began and continued over a period of 10 days for a total of 1.5 mm.

A local magnetic event was again observed at Hollister on 26 July as shown in Figure 45. Creep was observed beginning on 30 July and continued until 15 August for a total of 2.09 mm.

In October 1966 two local earthquakes were observed, one of magnitude 4.2 with its epicenter very near the Watsonville magnetometer and the second of magnitude 4.1, 20 kilometers southeast of Franco. At the time of the first event, no local magnetic events were observed simultaneously even as small as 0.05 gamma at the Watsonville site (Figure 46). In fact, the magnetometer as predicted, did not even respond mechanically to the motions of the earthquake whose

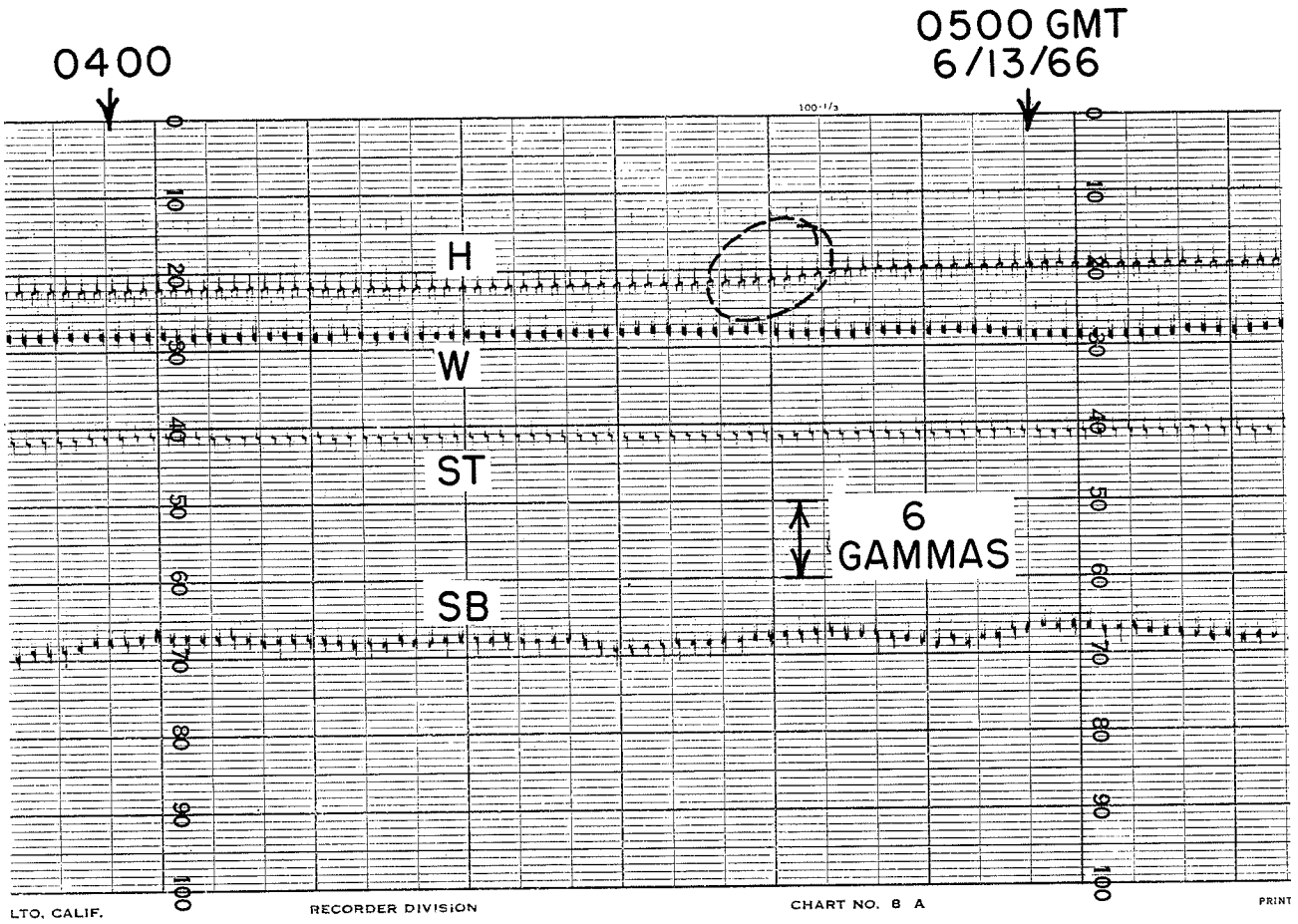

Figure 44. Local magnetic event at Hollister.

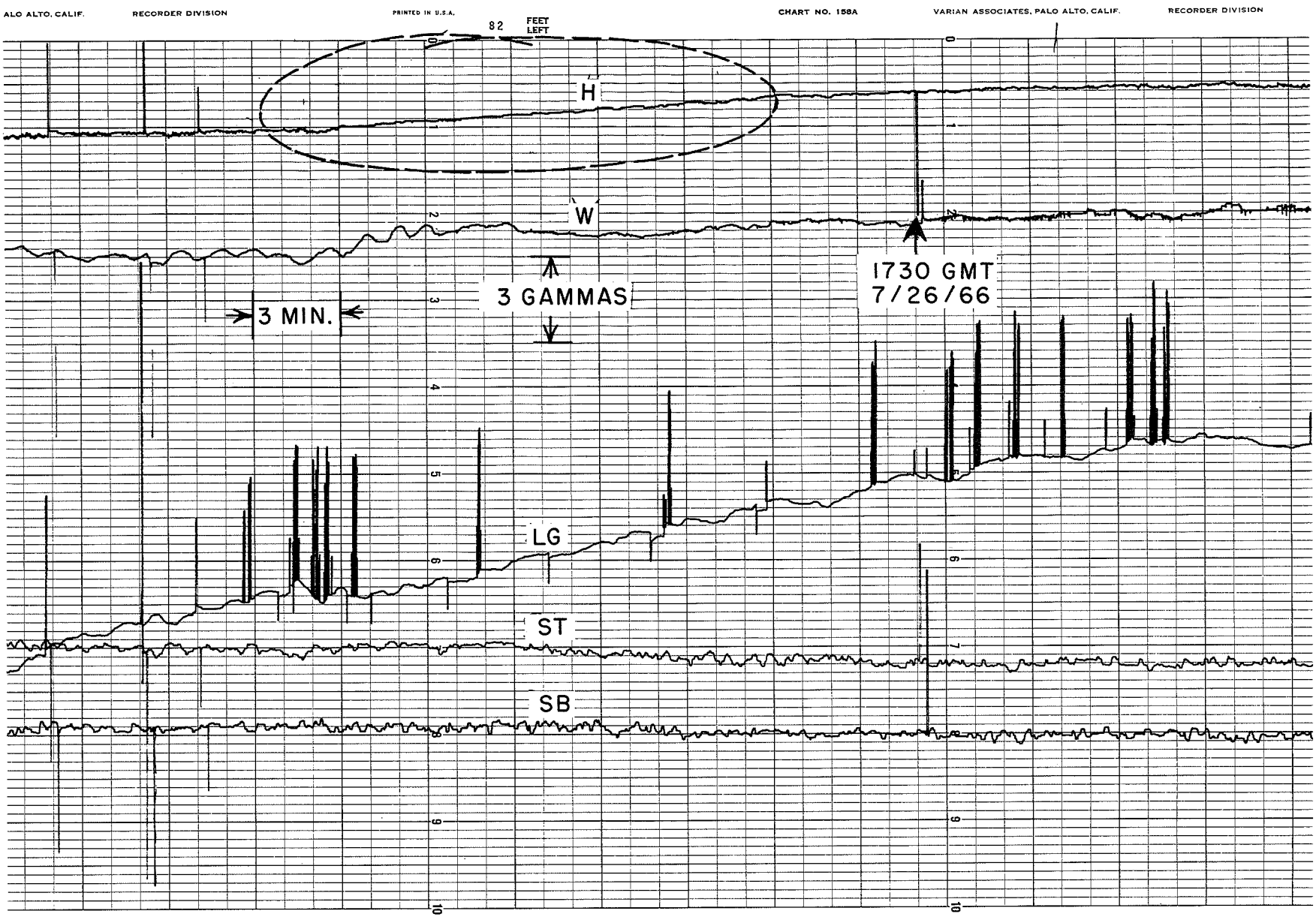

Figure 45. A local magnetic event at Hollister.

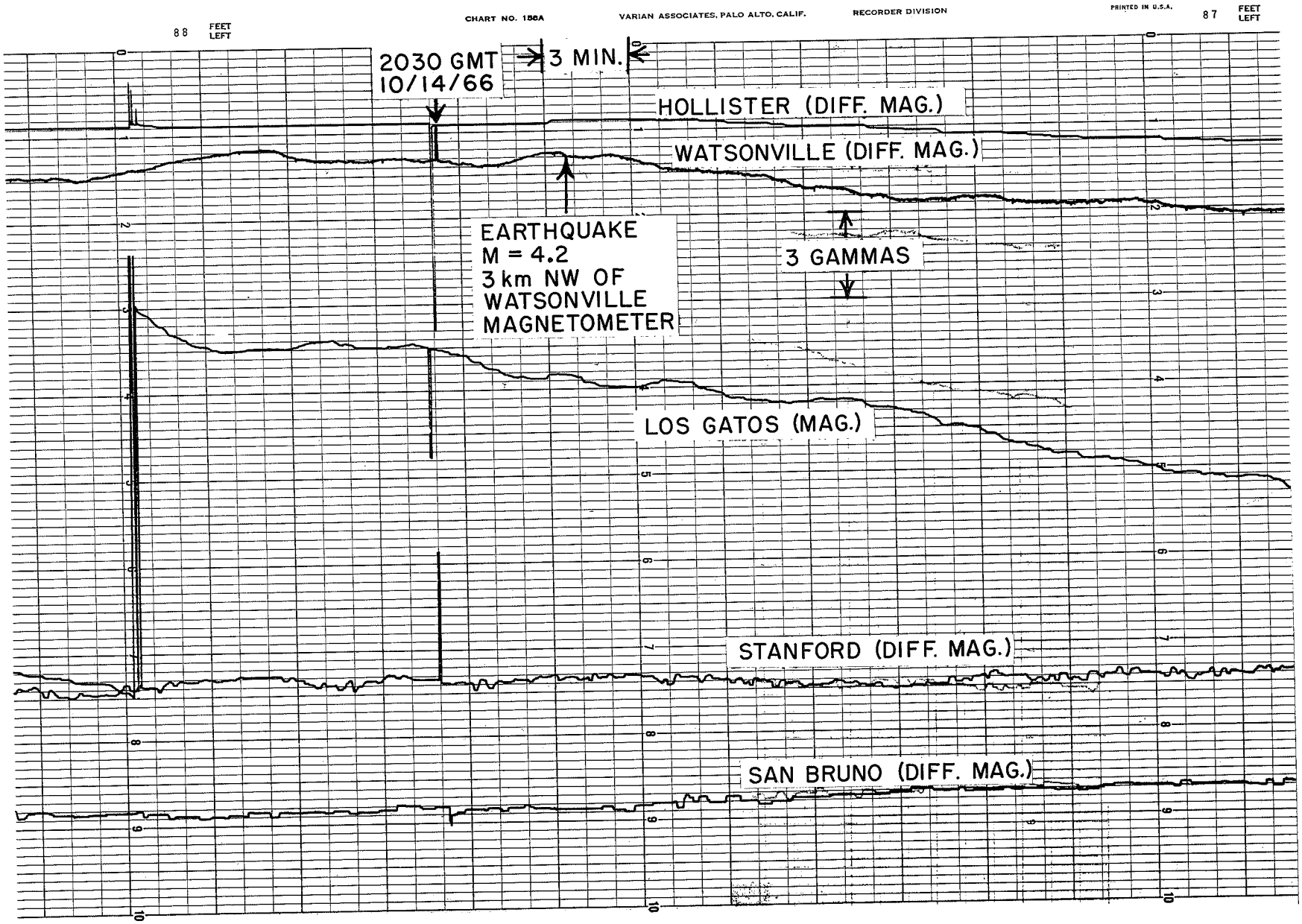

Figure 46. Record of differential magnetometer during a very local earthquake at Watsonville.

epicenter was determined to be in the immediate vicinity of the sensor. There was a pair of local changes of short duration 14 hours before the earthquake, however, as shown in Figure 47 but not within the defined period limits of the correlatable local magnetic events. There was a local increase of magnetic intensity at Franco 3 hours before the second earthquake (Figure 48) and a local decrease 9 days later. Micropulsation activity increased, especially in the short, non-cancelling periods of the micropulsation spectrum during the last few days of October. A possible local event occurred on 31 October at Hollister (Figure 49). The qualification as a local event, though, is marginal because of the presence of micropulsation activity. It is clear that if the event is indeed local and had occurred during less disturbed times, identification would have been positive. Creep was observed beginning on 1 November and by 5 November resulting in 2.4 mm displacement.

No significant creep nor magnetic events were observed for several months. In the latter part of March 1967, the array was reorganized into a more dense net in the area of Hollister for the following reasons:

1) to confirm the reality of the previously described events by observing them on redundant magnetometers
2) to investigate the spatial occurrence of these events
3) to investigate the relative times of such local events should they propagate

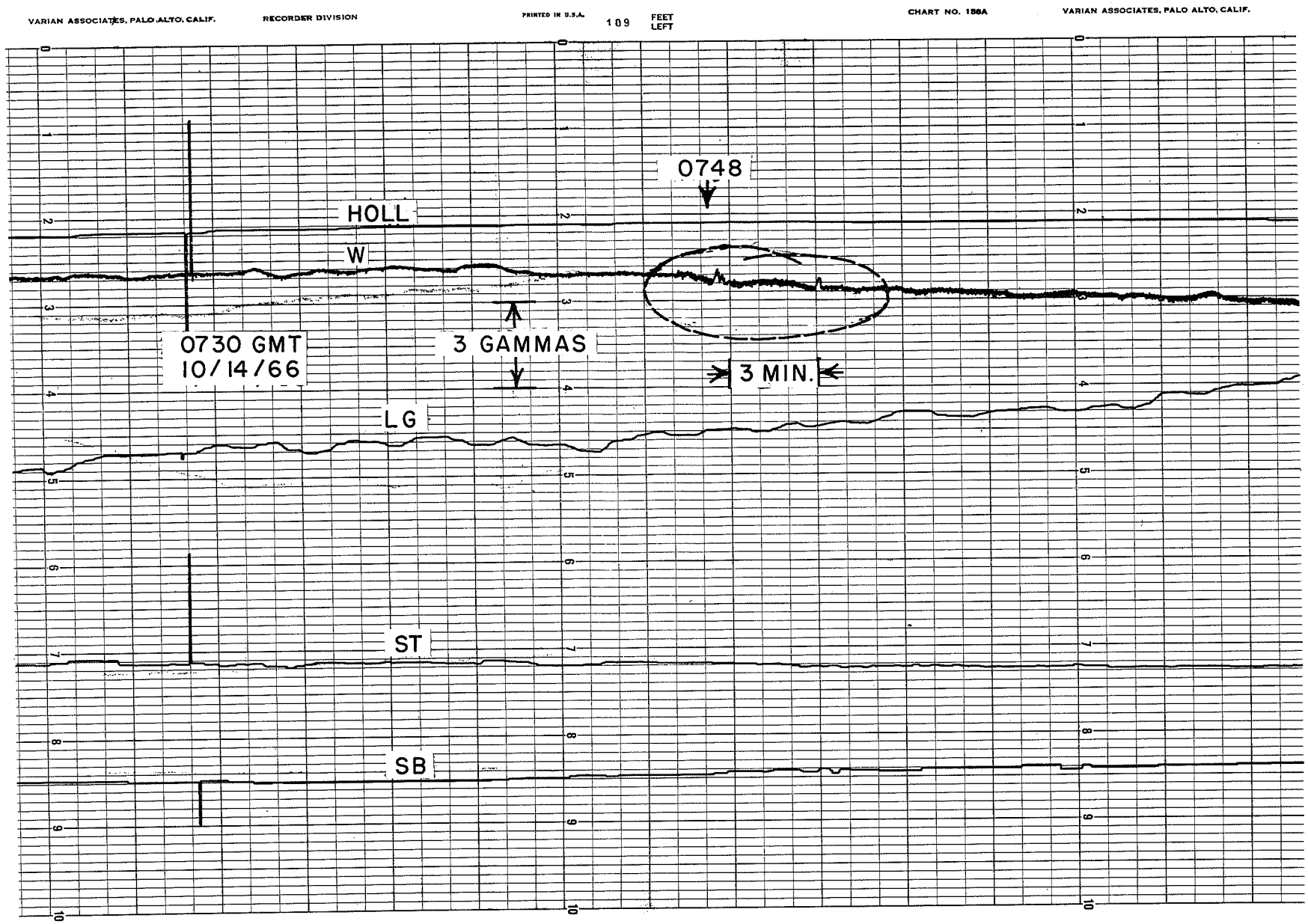

Figure 47. Possible local events at Watsonville 13 hours before the earthquake in Figure 46.

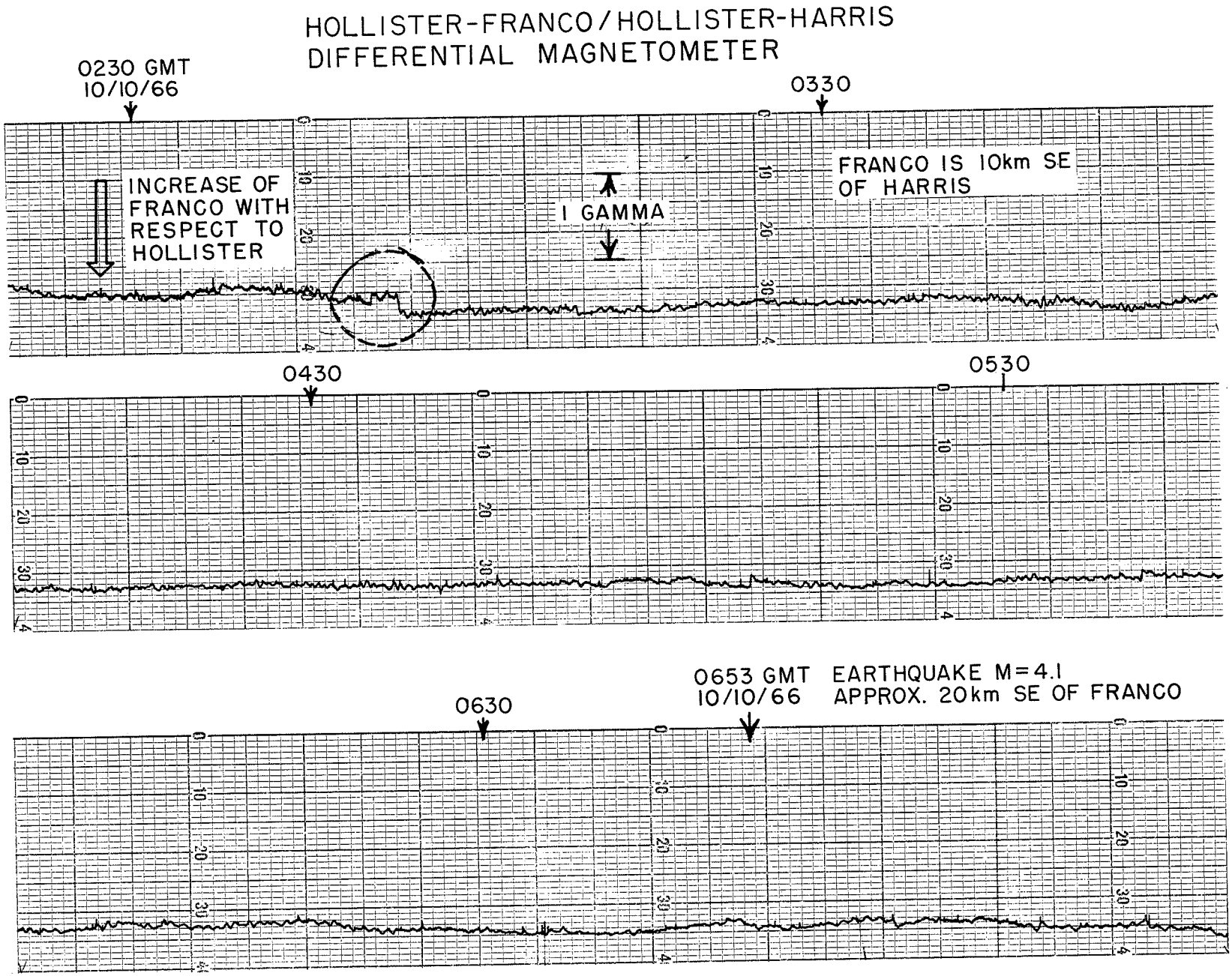

Figure 48. Local increase in field intensity at Franco 3 hours before near earthquake.

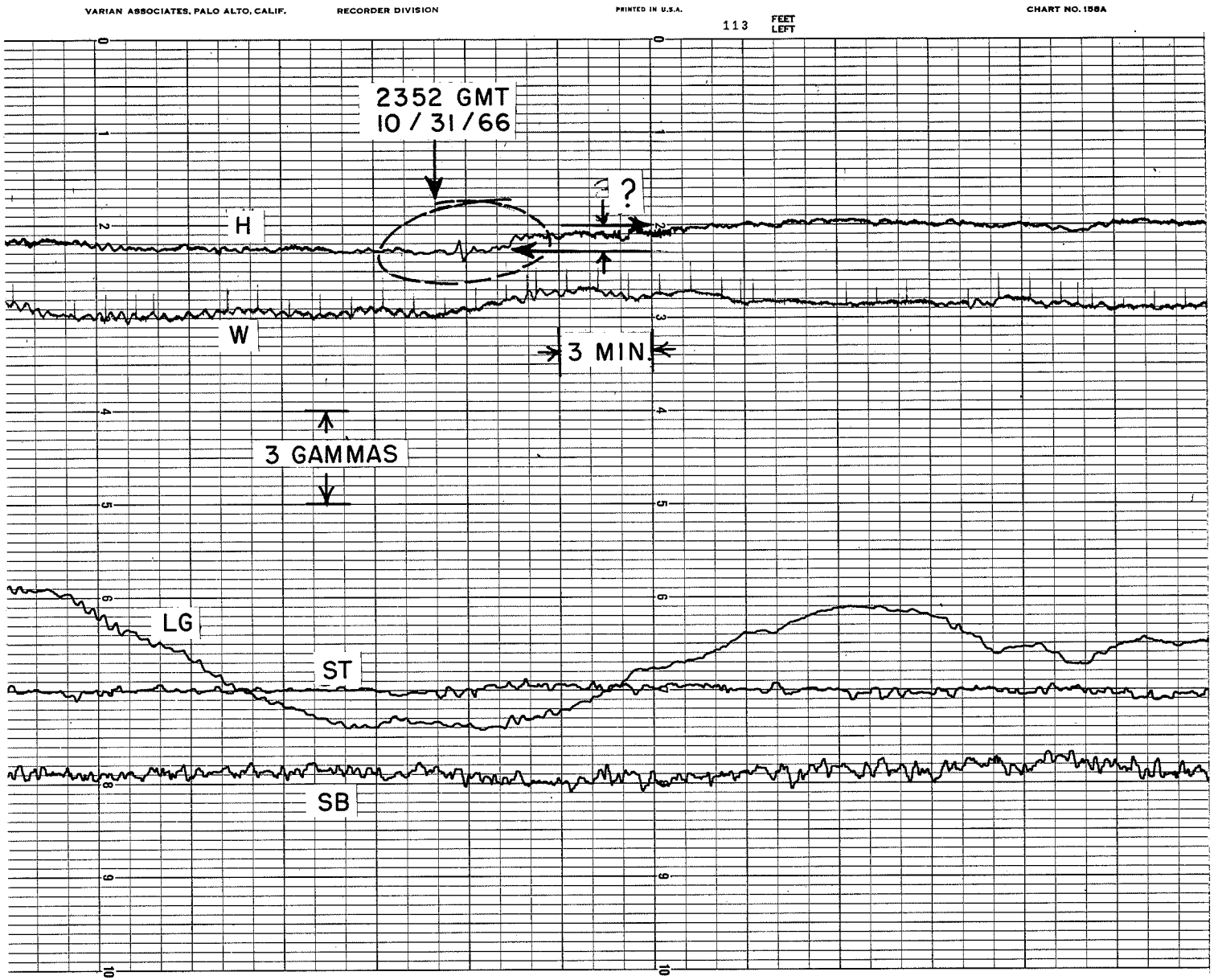

Figure 49. Possible local magnetic event at Hollister.

The deployment and manner of data acquisition of the re-established array have been described in Section 3B.

A series of very interesting local magnetic events were observed on all magnetometers of the Hollister array on 18 April 1967. The form, sense of change, and sequence of events was similar to the events observed in February, 1966, at the Hollister magnetometer of the earlier array. At 16h 33m GMT on April 18, 1967, a local decrease began simultaneously at each station (Figure 50a, b). Fortunately, the event was of different amplitude at each station, for it might have been overlooked simply as an ionospheric event. The event exhibited peak amplitudes at 16h 50m. The largest excursion, by more than a factor of 2, was observed at Stone Canyon where the event persisted for 90 minutes, or almost three times longer than observed at the other stations of the array. The other stations gradually returned to near pre-event values in about 36 minutes. The reference magnetometer at Franco also exhibited the local event, verified by using the magnetic records from the Castle Rock Observatory as a reference (Figure 50c). The event at each differential station represents only the amount by which the intensity differs from that at Franco. The Franco intensity, however, was also changing during the event. Therefore, the complete event at each station was determined by adding to it the simultaneous event at Franco reconstructed in the manner shown in Figure 50c.

The evidence that this event is of local origin is that

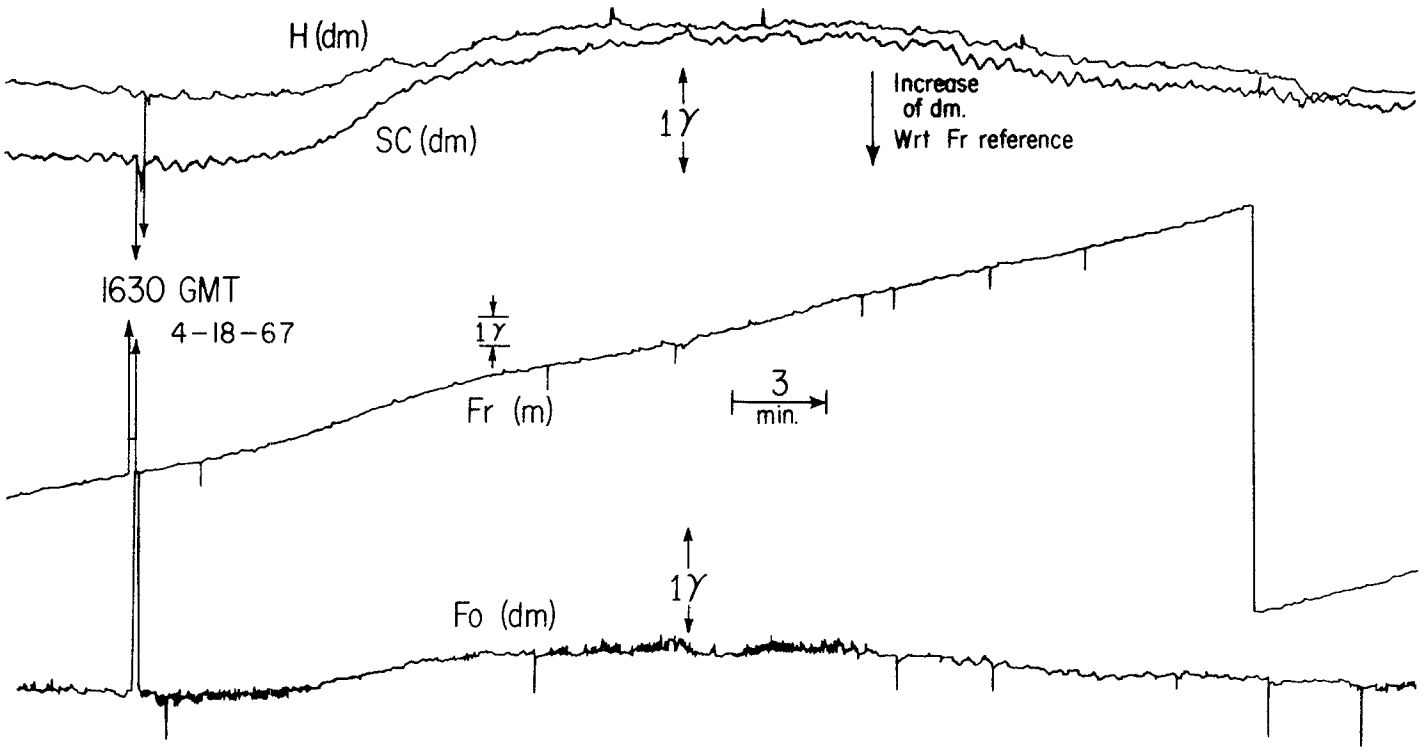

Fig. 50. a) Local magnetic events on array II. 4 mm creep displacement of the San Andreas fault occurred at 0830 4-19-67.

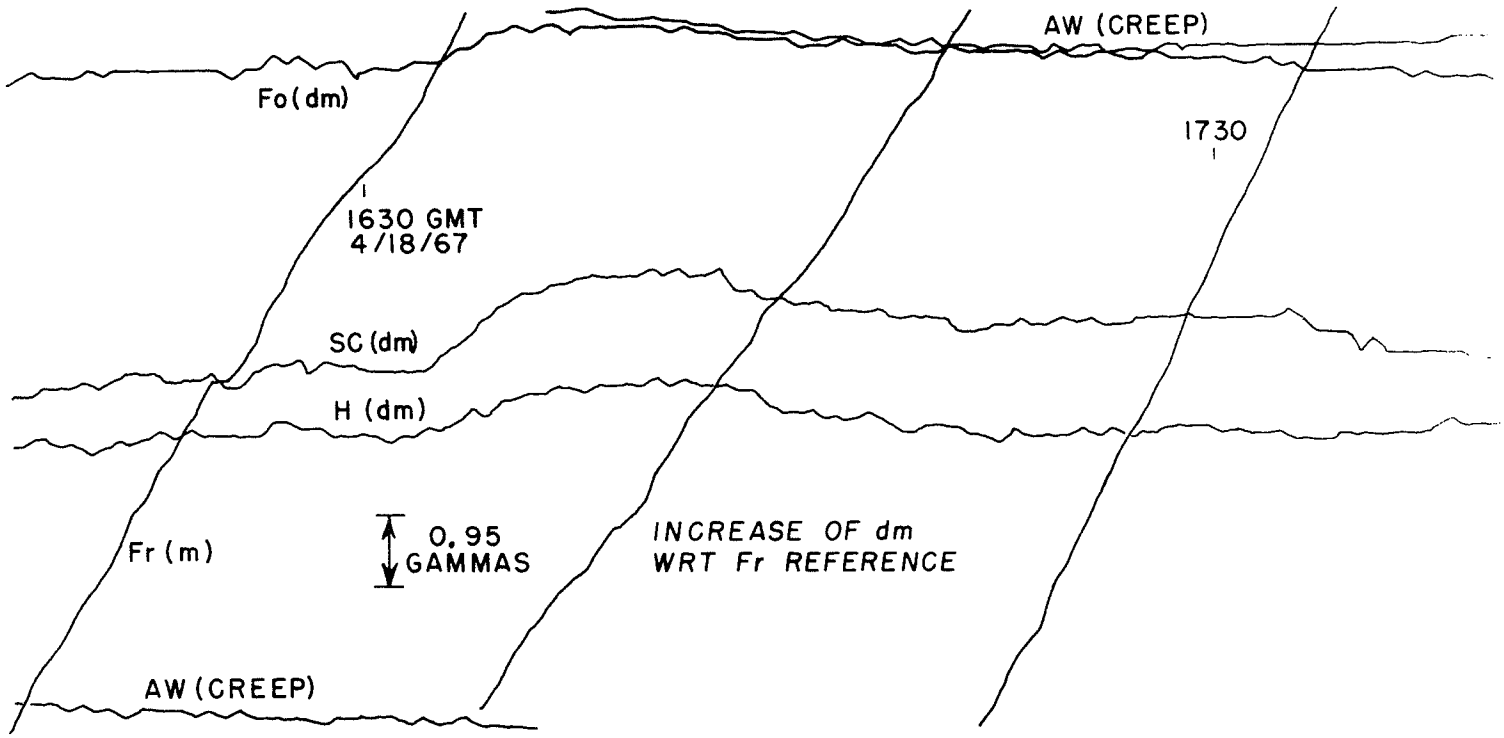

Fig. 50. b) Local event in array II recorded at Stanford University. Steps in data are automatic range switching.

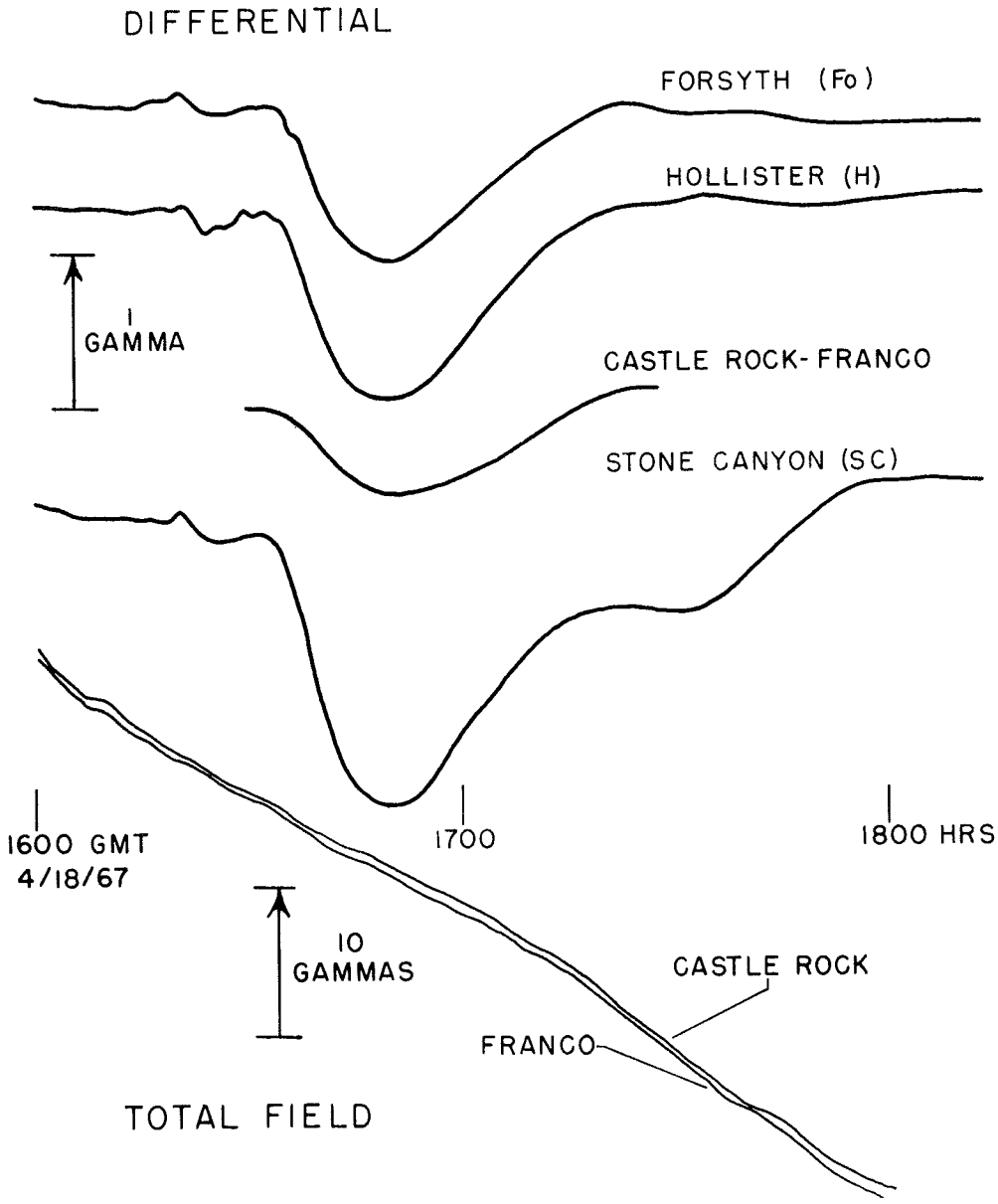

Fig. 50. c) Local magnetic event on array II. Replotted from Figures 50 a) and b) to account for the observed effects at the common reference magnetometer at Franco. The upper 4 traces represent the complete amplitude of the event at each site.

such differences in the intensity observed at nearby stations are not observed except accompanying ionospheric activity, where the amplitude of a pulsation is 5 to 10 times larger than the difference observed, for periods longer than 3 minutes. Also, the Castle Rock (and Stanford) total field magnetometers showed no event during this time. It is perhaps surprising that this observed event was so widespread. If this had been expected, the reference magnetometer might have been placed at a more distant site.

A large amount of creep was observed on the mechanical recorder in the Almaden winery near Hollister beginning on 19 April 1967. The electromechanical transducer being recorded along with the magnetometers showed rapid creep beginning at 0830 GMT on this data (Figure 51). The total amount of creep displacement was 3.92 mm.

A series of local earthquakes also occurred from 20 April to 22 April 1967, the largest of which was of Richter magnitude 3.6 on 22 April occurring in the central part of the array. A magnetic event possibly associated with this local earthquake is shown in Figure 52.

A second local geomagnetic event occurred at 16h 40m GMT 29 April 1967 (Figure 53). This event was also observed at all stations of the array but represents, instead, an increase in field intensity. The amplitude of this event is larger than the first event observed at each station. Subtracting the Castle Rock total field variations from the

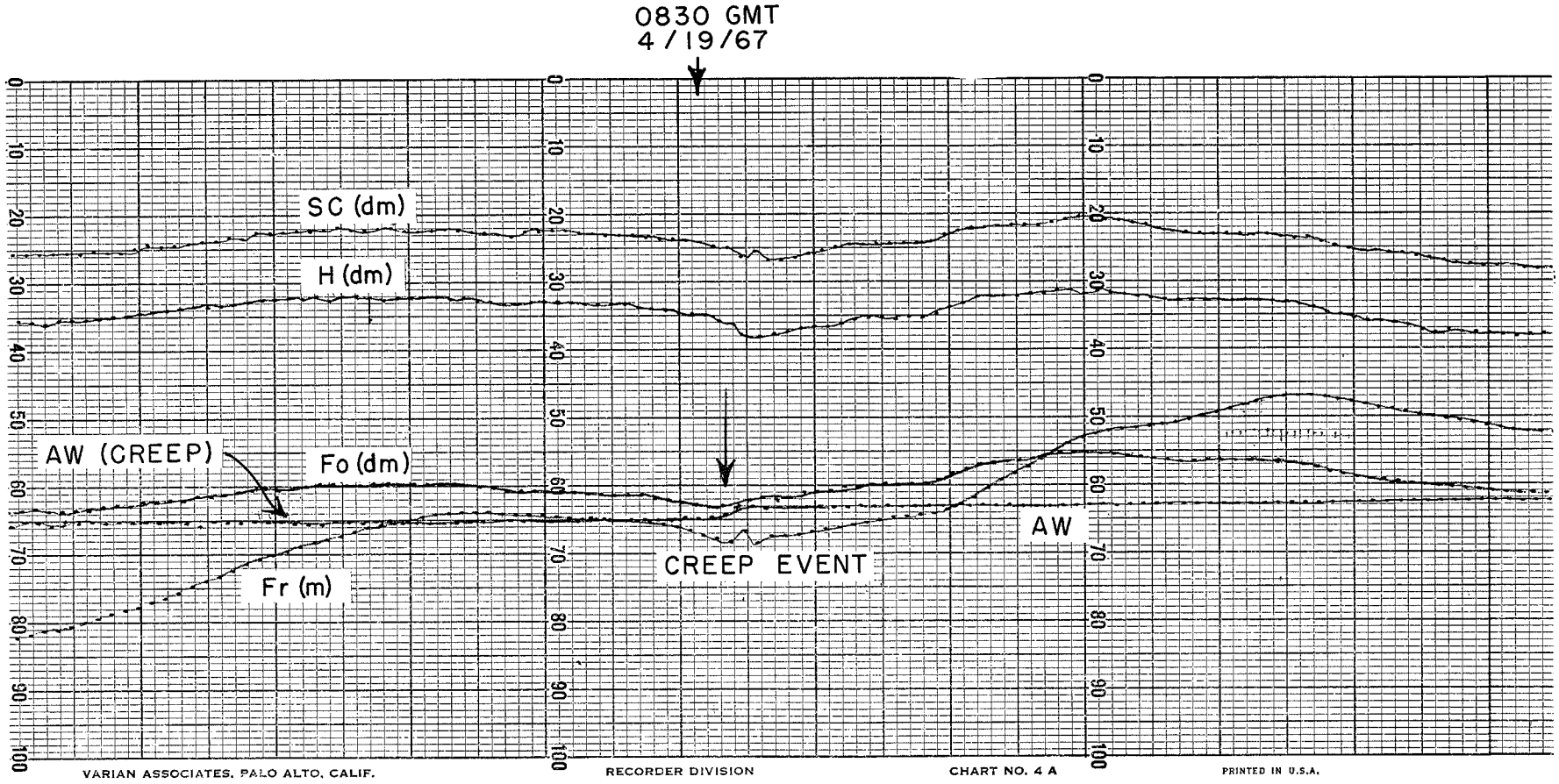

Figure 51. The creep event which followed the magnetic events of Figure 50a, b, and c.

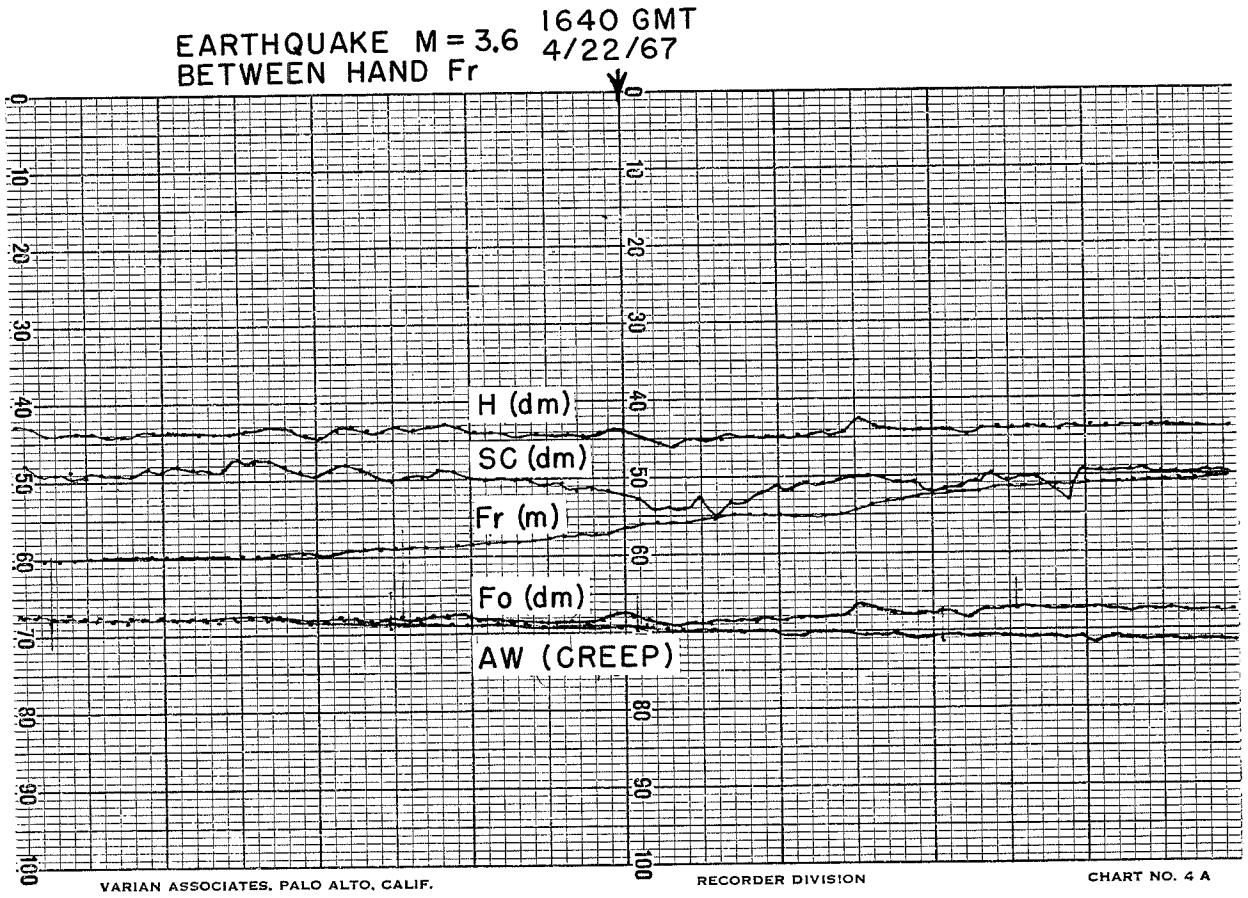

Figure 52. A local long period magnetic event on Stone Canyon which might be associated with a local earthquake of magnitude 3.6.

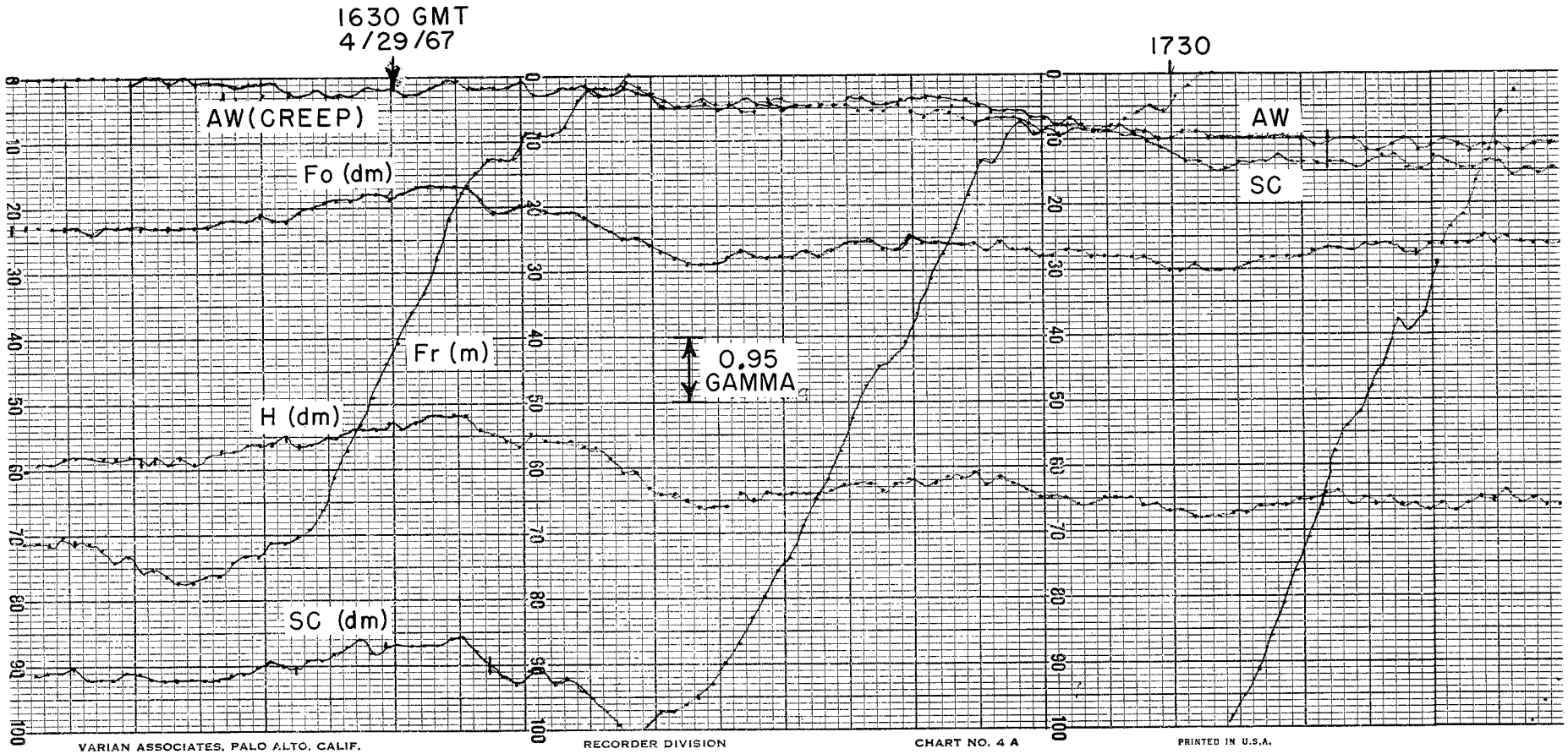

Figure 53. A second local magnetic event of opposite sense 11 days following the one in Figures 50 a-c.

Franco record shows that the traces probably returned to pre-event values in approximately 1 hour although the differential traces do not exhibit this.

It is interesting to compare these events with the sequence of magnetic, creep, and seismic events which were observed on the single Hollister sensor 14 months earlier: assigning the time of the first event of 7 February 1966 as the beginning of day 1, we observe the following response: at day 2 creep was observed; at day 3 there were local earthquakes, M = 2.5; at day 9 a local increase in field intensity of much larger duration; and finally at day 14 another local decrease. During all of this time creep was occurring at the winery.

Prior to the establishment of the array, magnetometers were operated in the vicinity of the Stanford site for over 4 years. However, they were not operating in a differential mode and consequently local changes on the record would normally be undetected if they have the general character of the micropulsations as it appears that they do. One magnetometer actually was the present Stanford instrument, a rubidium vapor magnetometer, in approximately the same location as used in the array. A second magnetometer was located 2 kilometers to the east and was a horizontal torsion-wire variometer. The latter instrument consists of a torsion-wire suspended horizontal magnet whose rotation from magnetic north is sensed by a photo cell/light assembly causing a

current to flow in a coil about the magnet. The current which maintains the magnet in a fixed position is displayed on a chart recorder.

The largest earthquake in several years in this area of the San Francisco Peninsula had a magnitude of 4.6 and occurred on 22 May 1963 with its epicenter 19 kilometers south of the horizontal component magnetometer. The magnetic records were examined 1 week before and after the earthquake for obvious deviations from the quiet background. Four hours before the earthquake increased approximately 15 gammas returning to its undisturbed value in approximately 1 hour as shown in Figure 54. The horizontal intensity from the Tucson Magnetic Observatory was used as a reference by adjusting the time of the records for the differences in diurnal phase between the longitude of Tucson and the longitude of Stanford. The magnetic activity was sufficiently quiet to produce a very constant difference as shown in Figure 54. The arrival of the surface waves of the earthquake caused full scale excursions on the record.

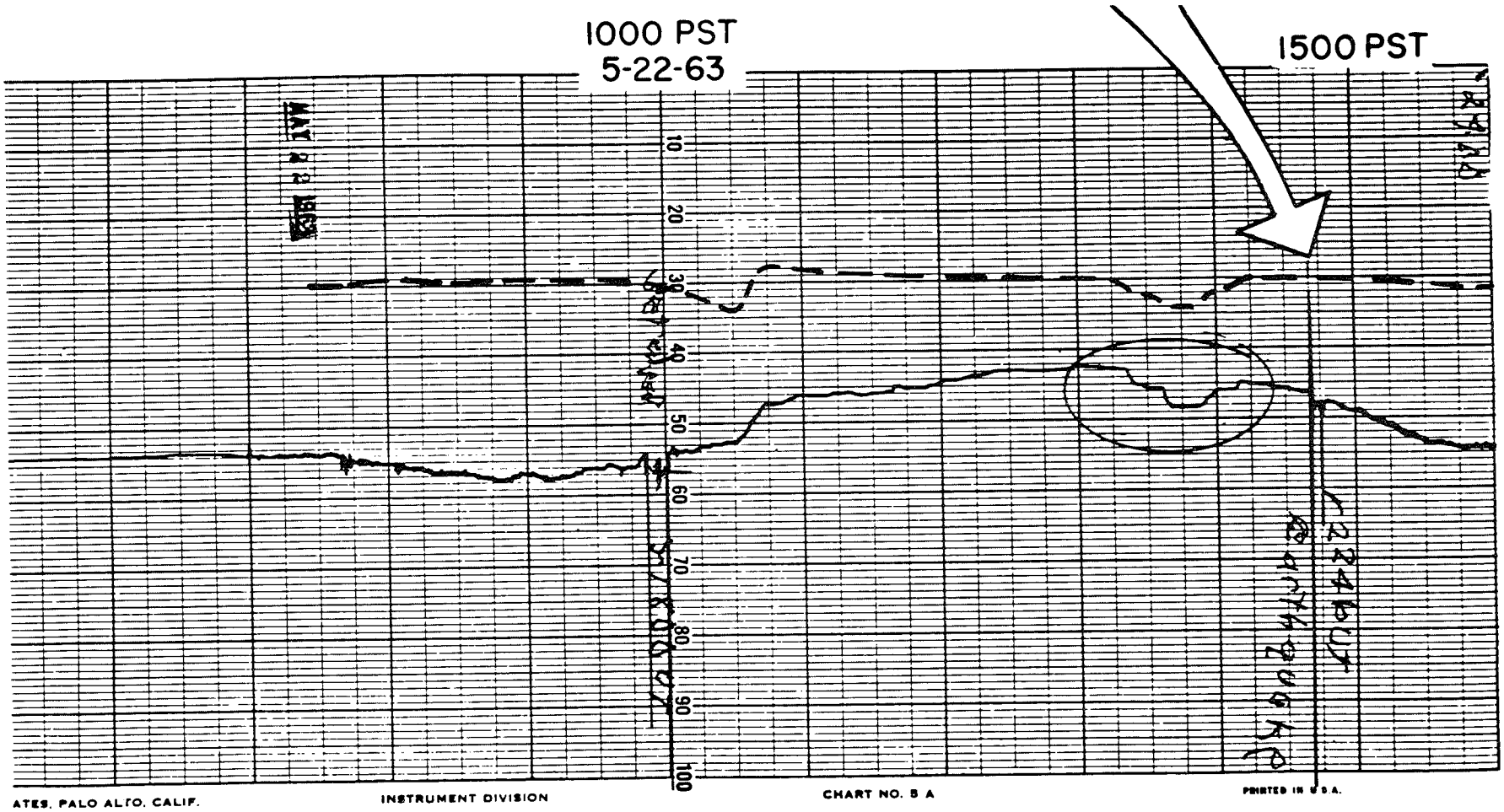

Figure 54. A local magnetic event on a horizontal force variometer one hour and four hours before a magnitude 4.6 earthquake 19 kilometers south of the station.

C. Fairview Nevada Array

Setting

Geology

The area is in the Basin and Range Province and centered about a north-south elongate mountain, Fairview Peak. The mountain is capped by flows and intruded by dikes of Tertiary volcanics. In the southern part of the mountain are metasediments, chiefly slate. The principal structural features are the normal faults which bound Fairview Peak on the east and west, therefore constituting a typical horst and graben structure.

Seismicity and Strain History

The region is well known seismologically because of a series of relatively recent earthquakes, the largest of which was a magnitude 7.1 earthquake in December 1954. The earthquake was associated with movement for several tens of kilometers on the normal fault on the east side of the mountain creating a scarp up to 6 meters high. The region still exhibits very high seismicity as do many of the ranges in western Nevada.

Magnetometer Deployment

Two rubidium magnetometers were set up 14 kilometers apart as shown in Figure 55 so that each one would serve as

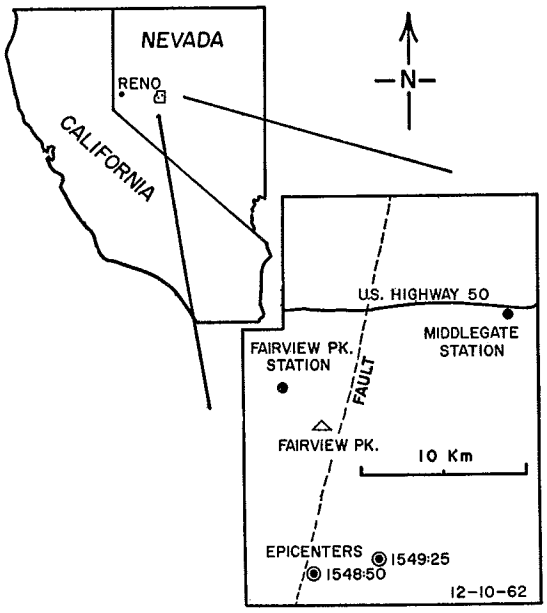

Figure 55. Location map of the Fairview, Nevada magnetometers.

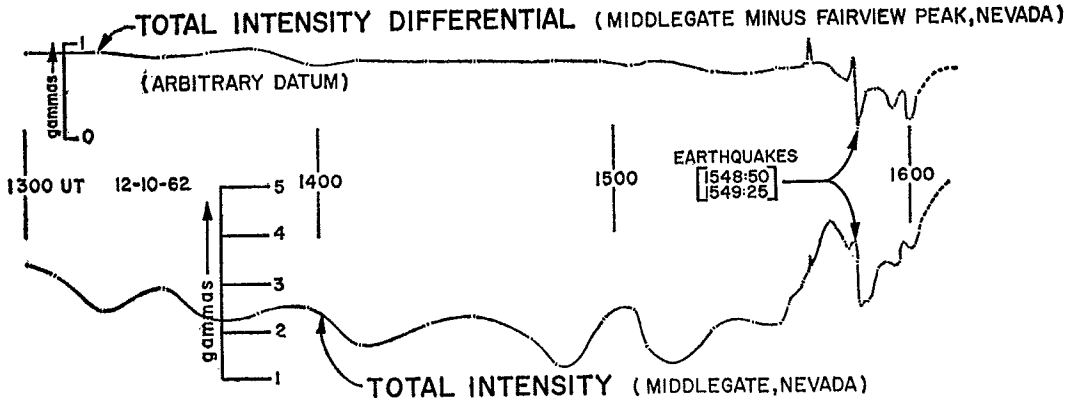

Figure 56. A local magnetic event at the time of a pair of local micro-earthquakes.

a reference for the other to remove the micropulsations and diurnal variations. Each magnetometer was operated by itself without telemetering links and the analog records subtracted afterwards to obtain differential variations.

Correlation Instruments

A network of portable, high gain seismographs was set up by Stanford Research Institute at 3 locations around Fairview Peak. The epicenters and depths of the larger events were automatically computed from the seismic tapes.

Seismic Events

An average of 20 to 30 micro-earthquakes were recorded daily around Fairview Peak. The epicenters of some of the events were more distant, up to 60 kilometers away. The seismic events recorded during the 4 days of operation from 9 - 12 December 1962 appear in Table 3 with notations indicating their relative size. An accurate magnitude was not determined for these seismic events but they are certainly less than magnitude 2. Their small magnitude precluded an accurate determination of their epicenters.

Local Geomagnetic Events and Correlation

The most significant geomagnetic event is reproduced in Figure 56 and is one which occurred in a manner suggested by elastic rebound theory. The intensity increased steadily and reached a maximum, returning abruptly to some former value

Table 3. Seismic Events: Fairview, Nevada, December, 1962

Date	Time (GMT)	Relative Intensity
12-10-62	0134:00	s
"	0207:20	s
"	0238:50	w
"	0522:50	m
"	0117:12	w
"	1548:50	s *
"	1549:25	s *
"	1555:30	m
"	2306:30	w *
12-11-62	0943:58	w *
"	0947:18	m
"	1047:20	w
"	1226:20	m
"	1429:50	ms
"	1516:20	ms
12-12-62	0052:10	m *
"	0106:50	s
"	0816:50	w *
"	1004:20	m
"	1605:40	m

s = strong
m = medium
w = weak
* = seismic events preceeded by magnetic events

at the moment of a microearthquake (less than Richter magnitude 2). The differential plot shows that the geomagnetic field change was indeed local and more pronounced at one station. Furthermore, the rate of change of intensity that occurred simultaneously with the earthquake follows the qualitative time dependence suggested by Stacey (1962a). A quantitative justification of the magnitude of the observed event as a piezomagnetic anomaly was given by Breiner (1964).

Other local magnetic events were observed at Fairview Peak which did not occur precisely at the instant of local earthquakes but rather just before them. On every instance of the four groups of magnetic events shown in Figure 57, a local earthquake followed thereafter at an average time of 10 to 20 minutes. On the other hand, there were many earthquakes not associated with any magnetic events. However, since there were 20 earthquakes in 4 days the probability of there being an earthquake in any one of the four 20 minute intervals is approximately 1 in 72. The observed coincidence of 1 in 5 and the fact that no magnetic events were observed at other times on this magnetometer suggest that the magnetic events may be associated with the local microearthquakes.

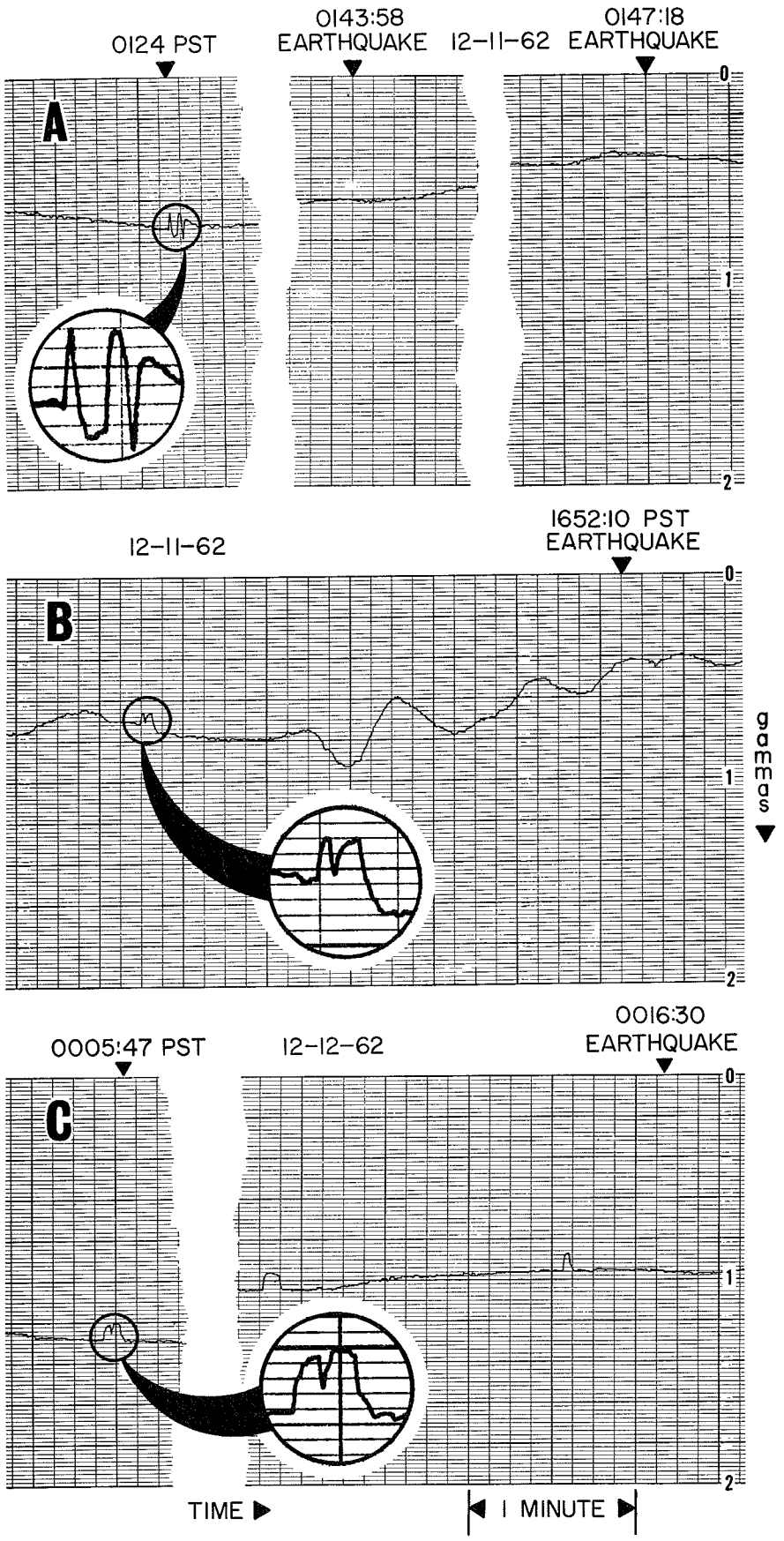

Figure 57. Possible local magnetic events at Fairview, Nevada which appeared only just before local micro-earthquakes.

D. Whitecloud Mountains, Idaho Array

Setting

Geology

The area in which the magnetometer array was set up is in central Idaho at Robinson Bar on the Salmon River approximately 30 kilometers east of Stanley, Idaho (Figure 58). The geology is known from reconaissance mapping only and the resultant maps show very little of any structural features which may be the cause or result of the local seismic events. The center of the seismically active area is the Whitecloud Mountains, a small group of barren peaks composed entirely of granite. The granite is bordered on the northeast by low grade metasediments. Only one fault has been mapped in the entire 200 square kilometer area about the peaks and that is a thrust fault which strikes northeast through the central peaks of the Whitecloud Mountains.

Seismicity

Attention was drawn to the area by the annual occurence of a few magnitude 4 or 5 earthquakes whose location is always in the general area between the Whitecloud Mountains and the Salmon River. High gain seismographs set up by the Stanford Research Institute for several weeks at a time in 1964 produced epicentral locations near the Whitecloud Mountains and

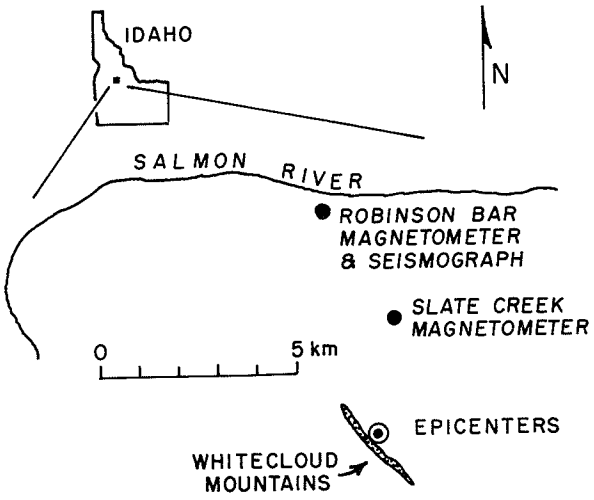

Figure 58. Location map of Idaho magnetometer array.

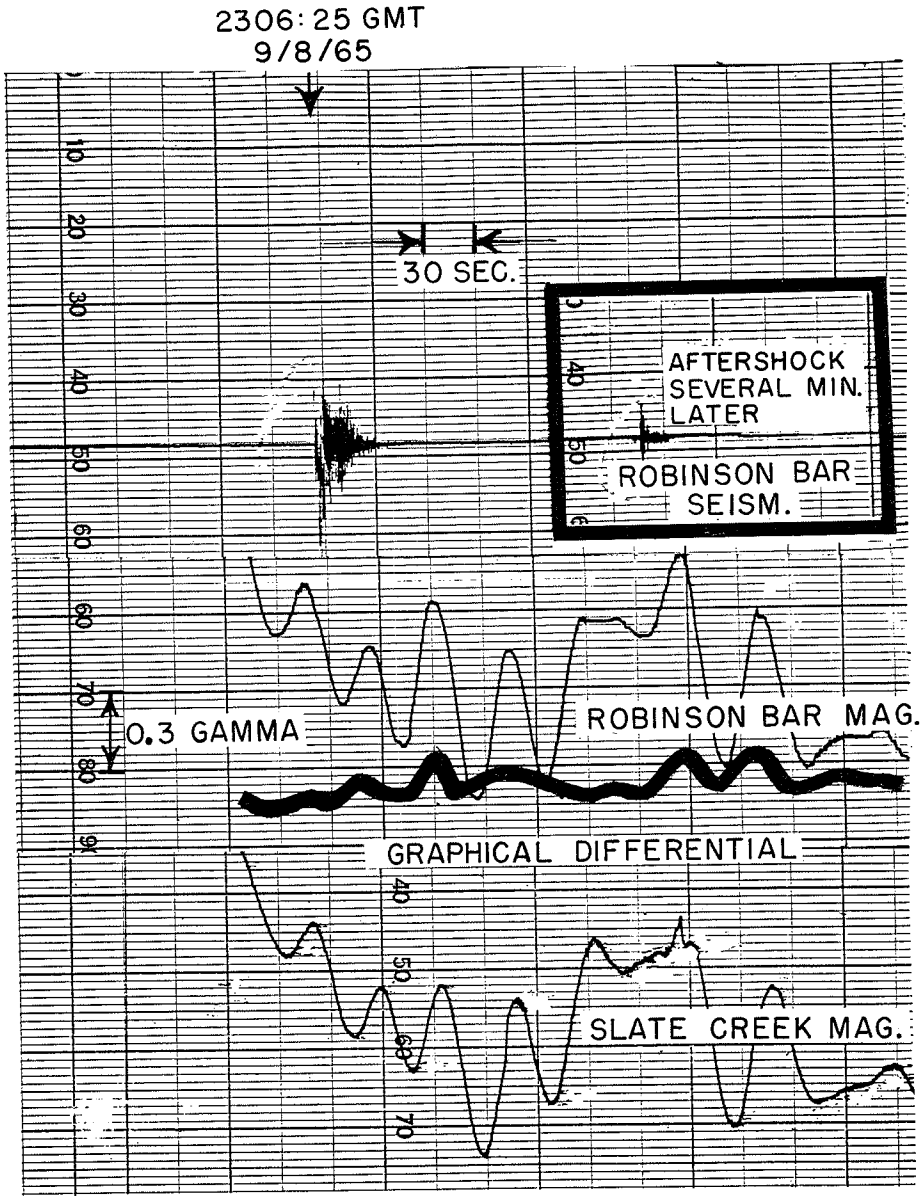

Figure 59. Magnetometer and seismometer recordings on a common time scale during a local earthquake large enough to be felt.

showed the area to be very seismically active.

Magnetometer Deployment

Two rubidium magnetometers were set up 16 km north and 8 km east north-east of the epicentral area (Figure 58). Each magnetometer was operated independently on generator or commercial power continuously for 8 days. Time marks were placed on the records twice daily.

Correlation Instruments

A single seismometer was set up at the location of the Robinson Bar magnetometer and operated alongside the magnetometer recorder to obtain a common time base for the two records. The S - P times were used for epicentral distance determinations.

Interpretation of Records

The two magnetometer records, since they were operated independently, had to be used graphically to obtain the differential variations. Prominent 0.3 gamma peak-to-peak sinusoidal activity of 40 second period was present during much of the time masking any such local events.

Seismicity

During the 8 day period 3 local earthquakes on 1, 3, and 8 September were recorded together with their aftershocks and a few other smaller isolated events. An S - P time of

3.5 seconds was noted on all detectable events. Campers at the Whitecloud Mountains felt one of the earthquakes while others at Robinson Bar did not. This evidence together with the previously localized seismic events in the area suggest that the epicenters are indeed in the vicinity of the Whitecloud Mountains.

Local Geomagnetic Events

No obvious local geomagnetic events were observed during the 8 days even with the extremely high sensitivity achieved on each magnetometer trace, i.e., 0.03 gamma. An example of the two magnetometer traces at the time of a small local earthquake are shown in Figure 59. Long period events were also sought in the graphically determined differential traces but no local events were recognized.

E. Matsushiro, Japan

While assisting the Earthquake Research Institute of the University of Tokyo a differential rubidium magnetometer was set up and operated near the town of Matsushiro in Nagano Prefecture, Japan.

Setting

Geology

The center of the seismically active area is a Pleistocene volcanic cone represented topographically as a prominent hill 250 meters high on the surrounding flat plain. The mountain, named Minakamiyama, is composed primarily of volcanic flows of unknown susceptibility but with a measured remanent magnetization of approximately 6×10^{-3} cgs units. The major rock type in the area around the mountain is diorite.

Seismicity and Strain History

The Matsushiro area is very seismically active, there having been at least 10 earthquakes between magnitude 5 and 8 in Nagano Prefecture during recorded history. In August 1965 a swarm of earthquakes began occurring in the vicinity of Minakamiyama at an average depth of 4 kilometers. At least 20 earthquakes of magnitude 4 to 5 were recorded in the following year.

Level surveys and tiltmeter records showed that during

this same year, Minakamiyama tilted as a block so that the surface north of the mountain was 1 meter lower than the south, for a strain of 10^{-3} per year (Kasahara, personal communication, September 1966).

Magnetometer Deployment

In the process of installing a rubidium differential magnetometer atop Minikamiyama, a single magnetometer was operated through the evening of 13 September 1966. The purpose of the single magnetometer recording was to observe the effects of a direct current electric railway only 4 kilometers from the site through the town of Matsushiro. The following morning the second magnetometer was connected to the first to provide the differential recording. The sensors were 11 meters apart in a north-south line.

Correlation Instruments

Numerous seismographs and tiltmeters were operating in the vicinity of Minakamiyama. For the purpose of this report, however, only the location of the hypocenter of one earthquake is of consequence.

Interpretation and Correlation of Records

The recordings of the single magnetometer exhibited an abruptly changing level of 4 gammas peak-to-peak at intervals of tens of seconds. This effect is due to the changing current in the electric railway 4 kilometers away. The frequency of

the variations decreases somewhat during the night. Local events smaller than 4 gammas or even twice this amount when more engines are put into service anywhere in this electric circuit of the train route are impossible to recognize with assurance using a single magnetometer.

The second sensor which was operating but not recording through the evening was connected in a very-short-baseline differential mode to examine the reduction of the effects of the railway current on such an arrangement of sensors. With the sensors only 11 meters apart, no changes of tens of seconds duration were observed as large as 0.008 gammas. Various sensitivity settings and chart speeds were tried in the process of examining the high sensitivity aspects of this array.

At one point, it was decided to simply let the recording apparatus operate undisturbed to observe the nature of the long term recordings. Immediately upon recording, the differential intensity was observed to be increasing. The chart speed was changed from 2 inches/minutes to 6 inches/hour to observe this 'drift'. All instruments had been operating the entire night and were thus at operating temperature. The sensors were fixed firmly to tripods so that they would not move. The variation, then, was probably not an instrumental error. Two minutes later with the gradient of the field still drifting, a strong earthquake was felt which was later determined to be of magnitude 4.8, with its

hypocenter 1 kilometer to the north and 7 kilometers deep. The varying intensity asymptotically reached a plateau 30 minutes later (Figure 60).

Two distinct magnetic changes were observed during this time. The principal event is the variation which apparently began at an unknown time and with unknown prior signature before the undisturbed differential recording began. This event was a 1.8 gamma change over the 11 meter distance in the 32 minutes in which it was observed. The secondary event was an abrupt 0.2 gamma increase which was observed visually to have occurred during the earthquake. That the abrupt change was due to a shift of the sensor in the gradient atop the mountain is possible but not probable. The magnetic event occurred at the beginning of the 10 second period during which the earthquake was felt.

The two events may both be the result of stress-induced piezomagnetic effects. Because the events have the same sign and occurred in the local subsurface, they should represent in part, the decreases in stress associated with the seismic event. Moreover, the magnetic event follows the same logarithmic time dependence as the local events of the San Andreas fault attributed to the release of stress. The Matsushiro event is replotted as a function of log t in Figure 60 for comparison with Figures 5 and 6. The earthquake may thus represent a brittle fracture equal to 0.2 of the total stress release, the remaining stress release

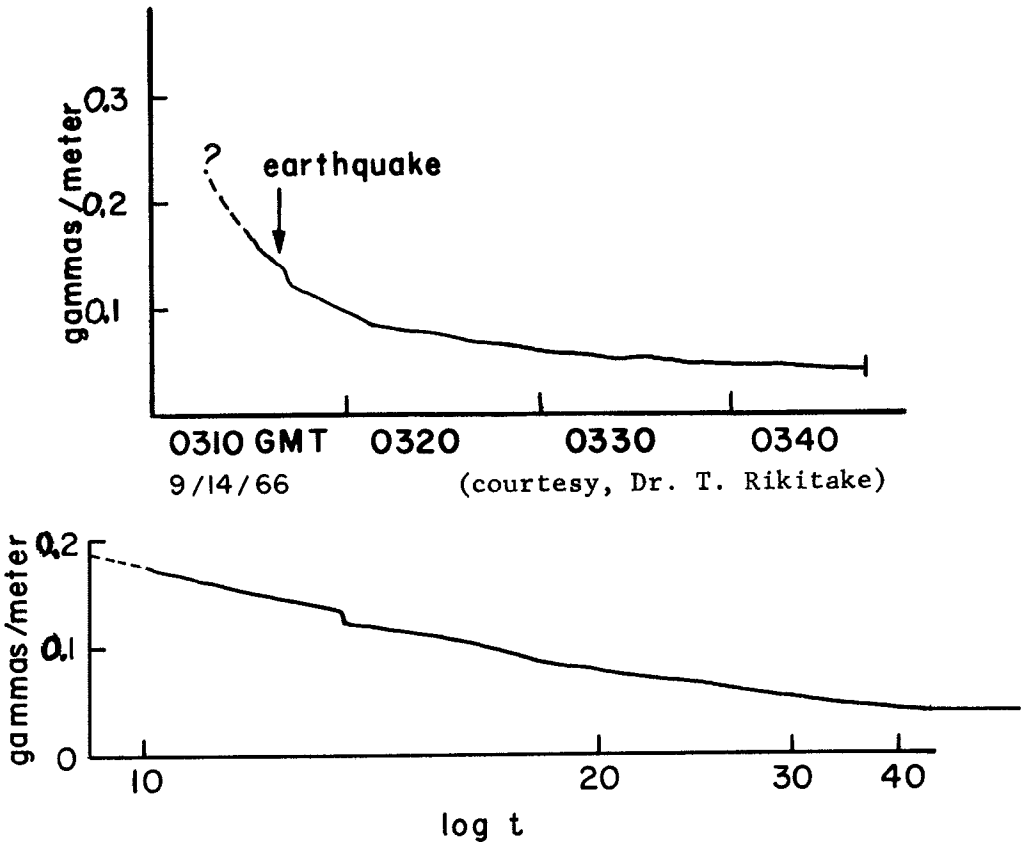

Figure 60. Differential rubidium magnetometer at Matsushiro, Japan during an earthquake of magnitude 4.8 whose hypocenter was almost directly beneath the sensors.

begin the result of creep deformation.

The observation represents a differential measurement only. The actual total intensity change is unknown but would be larger and its estimate would depend upon the assumed distance to the source. To examine the possible total intensity-anomaly/depth dependence, consider the effect of a 10 kg/cm^2 stress drop over the mountain of the stated magnetization. The mountain produces an anomaly of 2.5×10^3 gammas at the position occupied by the sensors (Rikitake, et al., 1966). The stress is reported to be primarily tensional in the N-S direction (Kasahara, private communication). From piezomagnetic considerations, the effect of tensional stress is to increase the susceptibility and remanent magnetization by the fraction

$$(10 \text{ kg/cm}^2)(6 \times 10^{-4} \text{ cm}^2/\text{kg}) = 6 \times 10^{-3}$$

The change in the spatial anomaly is therefore approximately

$$6 \times 10^{-3} \times 2.5 \times 10^3 = 15 \text{ gammas}$$

In the horizontal N-S deployed 11 meter differential magnetometer array, the sensors are actually 8 meters apart along the line of the earth's field which dips 45° to the north. If the local source is a dipole, say, in the center of the mountain at a depth of 150 meters, then the differential anomaly can be determined by

ΔF_N = 15 gammas, 150 meters from north sensor

$\Delta F_S = (\frac{150}{158})^3 \Delta F_N$ = 13 gammas, 158 meters from south sensor

$\Delta F_N - \Delta F_S$ = 2 gammas

which is comparable to the observed value of 1.8 gammas. If the source were at 300 meters, then the anomaly would have to have been approximately 25 gammas. Because the stress drop, total intensity anomaly, and depth to the source are all unknown such calculations serve only to establish a functional relationship and not the actual piezomagnetic conditions.

F. Nevada Test Site

In an attempt to observe the piezomagnetic effect of the stress relaxation about a large underground explosion, differential magnetometers were used to monitor a nuclear explosion at the Nevada test site in cooperation with the U.S. Geological Survey. Laboratory experiments of sharply applied stresses to rock samples demonstrated that the susceptibility changes and returns to a pre-stress value with an exponential decay (S. H. Ward, personal communication). The time constant for hand samples is on the order of milliseconds. It was expected that a large undergound explosion might exhibit similar behavior but with the time constant of seconds or minutes.

Two rubidium magnetometers were arranged differentially with one sensor mounted firmly 1500 meters from ground zero of a nuclear device at a depth of 600 meters. The second sensor was operating 2700 meters away and its signal telemetered on a cable to permit differential recordings at a sensitivity of 0.02 gammas.

The explosion was of low intermediate yield (expected energy of 20 - 100 kilotons of TNT). The geologic conditions were not ideal for the experiment for the area was underlain by sediments and Tertiary volcanics of low susceptibility.

No local magnetic events were observed at the time of the explosion which persisted longer than a second and which

were larger than a few hundredths of a gamma. Further experiments were planned but not performed.

4. CONCLUSIONS

The principal objective of this work, i.e., to detect local changes in the geomagnetic field, was achieved. Such events were observed at 3 sites: San Andreas fault, Fairview, Nevada; and in Matsushiro, Japan. Moreover, on the San Andreas fault array, these local geomagnetic events were noted on several occasions and even on redundant instruments insuring their reality at least as a change in the field.

The secondary objective of this investigation is to determine what significant correlation exists, if any, between these magnetic events and local earthquakes or strain events. It was expected that if any local field changes would be observed, they would occur as an abrupt change in the static level of the field accompanying a local earthquake. For lack of empirical data on the stress changes in seismically active areas, this approach was not only the simplest but had some foundation in fact following Reid's elastic rebound theory. With the exception of the principal Fairview, Nevada magnetic event which was not actually abrupt and the minute sudden shift on the Matsushiro, Japan event which might have been the result of a physical shift of the sensor in the gradient, no such abrupt change in the static field was definitely observed accompanying an earthquake. The correlation of local geomagnetic events with local earthquakes observed within the San Andreas array

is, in fact, zero. This is not to say that there would be no positive correlation if the monitoring is continued or if larger earthquakes occur nearer the magnetometer sensors. From a comparison of the 30-minute local excursion of the field at Matsushiro and the transient nature of the stresses which accompany earthquakes, it appears that the magnetic event and the earthquake are associated only through a third phenomena - perhaps a major change in the tectonic stress. Unfortunately the recordings had not begun soon enough to observe the earlier phenomena.

The rupture creep displacement of the San Andreas fault, on the other hand, closely correlated with the local geomagnetic events (Figure 36). It was because of the excellent agreement between these phenomena that the major emphasis of this work is placed on the piezomagnetic analysis of a strike-slip fault and that the San Andreas fault array was maintained for over 24 months.

If the various local geomagnetic events are associated with these creep events and perhaps indirectly with the stresses accompanying the earthquakes in Japan and Nevada, then are these geomagnetic events truly piezomagnetic events? A rigorous but impractical proof of such a fact would involve a measurement of the stress changes affecting the magnetic properties of rock at depth. The source of these effects, however, is probably deeper than it is now possible to measure stresses. At the very least, the sources of error

can be evaluated and certain non-piezomagnetic contributions eliminated.

With regard to the San Andreas events only, the events were shown to be local magnetic events because of their magnitude and appearance on only one part of the array. Local geomagnetic events whose signature and period resemble the prevalent micropulsations, events which are very long period, or events which may have occurred in periods of high magnetic activity will all have passed unrecognized as local events. From this standpoint there may have been more events than those reported. The reality of the events which were resolved were confirmed by the multiple local magnetometers which recorded the events. The long period and again the redundant instruments eliminated mechanical motion of the magnetometer as a source of the events. Stress-induced effects on the telluric currents and displacement of the structural blocks with respect to the magnetometer were shown to be much smaller than the piezomagnetic effects for the same stress change.

Movement at depth of the Curie point isotherm in several minutes time over a distance sufficient to add or remove a volume of ferrimagnetic rock necessary to produce the observed magnetic change can also be eliminated. Another possible explanation of the local geomagnetic events, though not considered likely here, is the loss or gain by a mineralogical phase change of a quantity of spinel or other mineral at

depth sufficient to cause the observed anomaly. Phase changes have been observed in the laboratory which occurred in seconds (Adams and Davis, 1962) and which have been suggested as a possible earthquake generating mechanism (Ringwood, 1962; Evison, 1963).

An examination of the quantitative aspects of the piezomagnetic effect over a strike slip fault with the environment of the San Andreas fault has provided a range of possible values for the anomaly. If the mechanism of stress changes which produce the creep displacement is correct and if these magnetic events are truly piezomagnetic effects, then one or more of the anomaly determinates expressed in Figure 7 would be higher than was expected from the assumed stress sensitivities, predicted subsurface stress changes, or the observed susceptibility of surface outcrops. The remanent magnetization, for example, which was not taken into account because of its unknown variability, might be of significance in producing the observed effects. The stress sensitivity constants, S_c and S_t, theoretically increase with temperature (Kern, 1961) which might also explain why the effects were apparently originating at considerable depth.

The validity of the spasmodic nature of the creep observations used for correlation with the local geomagnetic events have been doubted by some who contend that the concrete blocks in the winery over which the creep is measured

move only when sufficient shear stress has been applied across a continuously moving fault block. That is to say, that the actual creep is continuous and the creep observations are artficially discontinuous. The one-to-one correlation of the local geomagnetic events and the observed creep events, however, tend to confirm the validity of this discontinuous behavior. The magnetic and creep events taken together, in fact, lend support to each other. It is possible to conceive a short time lag in the reaction of the concrete blocks to a suddenly applied shear stress to account for the 10 to 20 hour lead of the magnetic event over a creep event. A sensitive quartz extensometer installed in a tunnel 2 kilometers northwest of the winery, however, exhibited the same time lag between the local geomagnetic event and the creep displacement as did the winery creep recorder.

If stress changes are indeed the source of these local geomagnetic events, then these reported observations represent a significant contribution to the knowledge of the stress variations involved to crustal deformation, at least in this particular area. First the stress changes were observed to begin simultaneously within the 1 minute resolution afforded by the April 1967 event over a distance of at least 25 kilometers. It appears that the source of the magnetic changes is at a depth between 5 and 20 kilometers because of the lack of surface strain changes and because the sources cannot be deeper than the depth of the Curie point isotherm

at approximately 20 to 25 kilometers. The time signature of these stress changes was also observed for the first time and, in the most general sense, found to exhibit certain repeatable characteristics. One type of signature occurred stepwise as a local increase in intensity varying as the logarithm of time and is suggestive of the release of stress. The other signature which preceeded the larger creep events decreased linearly with time and returned to its prior level varying as the logarithm of time. Magnetic changes were observed to occur, at least in this area of study, before surface creep, other strain changes, and seismic events so that some phenomenon does indeed occur before creep deformation and perhaps before many seismic events are observed in the upper layers of the crust. Such a phenomenon might be a regional stress release initiated by creep acceleration at depth (Orowan, 1960). The signature that is observed might then be the result of the stress release as it passes through the Curie point isotherm only above which can the magnetization be stress sensitive. Furthermore, the lack of seismic events at the time of the magnetic event can be attributed to aseismic strain changes at a depth where the hydrostatic stress allows the rock to deform by creep behavior. The local earthquake that followed the initial magnetic and creep events both in February 1966 and April 1967 by 4 days and approximately 2 days for the magnetic and creep events respectively are suggestive of local

readjustments to a new strain environment and as such may simply be aftershocks of a 'zero frequency' earthquake.

REFERENCES

Adams, L. H. and B. L. Davis, Rapidly running transitions at high pressure, Proc. Natl. Acad. Sci., 48, 982-990, 1962.

Andrade, E. M. DaC., Viscous flow in metals, Roy. Soc. London Proc, ser A. 84, 1-12, 1910.

Bailey, E. H., W. P. Irwin, and D. L. Jones, Franciscan and related rocks, and their significance in the geology of western California, Calif. Div. Mines Geol. Bull. 183, 177 pp. 1964.

Bauer, L. A., Magnetograph records of earthquakes with special reference to the San Francisco earthquake of April 18, 1906, Terr. Magn. II, 1960.

Benioff, H., Earthquakes and rock creep, Bull. Seismol. Sci. Am., 41, 31-62, 1951.

Benioff, H., Earthquake source mechanisms, Science, 143, 1399-1406, 1964.

Bolt, B. A. and W. C. Marion, Instrumental measurement of slippage on the Hayward fault, Bull. Seismol. Soc. Am., 56, 305-316, 1966.

Bozorth, R. M., Ferromagnetism, Van Nostrand, N. Y., 1951.

Brace, W. R., Electrical resistivity changes in saturated rock under stress, Science, 153, 1525-1526, 1966.

Brace, W. F. and Byerlee, J. D., Stick-slip as a mechanism for earthquakes, Science, 153, 990-992, 1966.

Breiner, S., Piezomagnetic effect at the time of local earthquakes, Nature, 202, 4934-4937, 1964.

Breiner, S., The piezomagnetic effect in seismically active areas, Ph.D. thesis, Stanford University, 1967.

Brune, J. N. and C. R. Allen, Low-stress drop, low-magnitude earthquake with surface faulting, paper presented at the Seismol. Soc. Am. Meeting, 24 March 1967.

Burbank, J. E., Earthquake disturbances recorded on the magnetographs at the Observatories of the U.S. Coast and Geodetic Survey, Terr. Magn. 10, 113, 1905.

Burford, R. C., Recent strain changes across the San Andreas fault and coast ranges at Hollister and Cholame, California, unpublished paper, U.S. Geol. Survey, March 1967.

Chapman, S. and J. Bartels, Geomagnetism, Vol. 1, Clarenden Press, Oxford, 1951.

Chinnery, M. A., The stress changes that accompany strike-slip faulting, Bull. Seismol. Soc. Am., 53, 921-932, 1963.

Eaton, J. P., Crustal Structure from San Francisco, California, to Eureka, Nevada, from seismic refraction measurements, J. Geophys. Res., 68, 5789-5806, 1963.

Eppley, R. A., Earthquake history of the United States, Part II, U.S. Gov't printing office, 1961.

Evison, F. F., Earthquakes and faults, Bull. Seismol. Soc. Am., 53, 873-891, 1963.

Gouin, P., Coincidence of magnetic disturbances with local earthquakes recorded from the Ethiopian rift system, Nature, 208, 541-543, 1965.

Grabovsky, M. A., Changes in the magnetic properties of magnetite under mechanical stresses, Bull. (Izv.) Acad. Sci. USSR, Geograph, and Geophys. Ser. 13, 2, 1949.

Grabovsky, M. A., and E. I. Parkhomenko, Changes in the magnetic properties of magnetite under high compression, Bull. (Izv.) Acad. Sci, USSR, Geophys. Ser. 5, 405-417, 1953.

Graham, J. W., The role of magnetostriction in rock magnetism, Adv. in Phys. 6, 1957.

Griggs, D. T. Creep of Rocks, J. Geol. 47, 225-251, 1939.

Griggs, D. T., High pressure phenomena with application to geophysics, in Ridenour, L. M., Editor: Modern Physics for the Engineer: McGraw Hill, N. Y., 272-305, 1954.

Griggs, D. T. and J. Handin, Observations on fracture and a hypothesis of earthquakes, Geol. Soc. Am. Mem. 79, 347-373, 1960.

Griscom, A., Magnetic data and regional structure in northern California, Geology Northern California, Calif. Div. Mines Geol. Bull. 190,407-417, 1966.

Hagiwara, T., Example of land deformations witnessed by the people before a great earthquake and of those detected by the leveling just before strong earthquakes, abstract, paper presented at U.S. - Japan Conference on Research related to Earthquake Prediction, Tokyo, March, 1964.

Hasoyama, K., Characteristic tilt of the ground that preceeded the occurrence of the strong earthquake of March 7, 1952, J. Phys. Earth, 1, No. 2, 75-81, 1952.

Hazard, D. L., The relation between seismic and magnetic disturbances, Bull. Seismol. Am., 8, 1918.

Healy, J. H., Crustal structure along the coast of California from seismic refraction measurements, J. Geophys. Res., 68, 5777-5788, 1963.

Herron, T. J., An average geomagnetic power spectrum for the period range 4.5 to 12,900 seconds, J. Geophys. Res., 72, 759-761, 1967.

Hill, M. L. and T. W. Diblee, Jr., San Andreas, Garlock, and Big Pine faults, California - a study of the character, history, and tectonic significance of their displacements, Geol. Soc. Am. Bull., 64, 444-458, 1953.

Judd, W. R. Ed., State of stress in the Earth's Crust, Elsevier, N. Y., 337-553, 1964.

Kalashnikov, A. G. and S. P. Kapitsa, Magnetic susceptibility of elastically stressed rocks, Proc. (Doklady) Acad. Sci. USSR, 136, 3, 1952.

Kalashnikov, A. G., Prospective magnetometric methods to detect forerunners of earthquakes, Trans. (Trudy) Geophys. Inst. No. 25 (152), 162-180, 1954.

Kapitsa, S. P., Magnetic properties of igneous rocks under mechanical stresses, Bull. (Izv.) Acad. Sci. USSR. Geophys. Ser. No. 6, 1955.

Kato, Y., Investigation of the changes in the earth's magnetic field accompanying the earthquake or volcanic eruption, Science Rep. Tohoku Imp. Univ. Series 1, 28, 1, 1938-

Kato, Y., Investigation of the changes in the earth's magnetic field accompanying earthquakes or volcanic eruptions, Sci. Rep. Tohoku Imp. Univ. 29, 315, 1940.

Kato, Y. and S. Utashiro, On the changes of the terrestrial magnetic field accompanying the great Nankaido earthquake of 1946. Science Rep. Tohoku Univ., 1, No. 1, 40-41, 1949.

Kato, Y., On the changes of the terrestrial magnetic field accompanying the Tohochi earthquake of 26 December 1949, Science Rep. Tohoku Univ. Fifth Ser. 2, No. 2, 149-152, 1950.

Kato, Y., and A. Tokachi, Further note on the investigation of the changes in the earth's magnetic field accompanying earthquake and volcanic eruption, Science Rep. Tohoku Univ. Series 5, Geophys. 6, 67-68, 1953a.

Kato, Y., J. Ossaka, and K. Noritomi, On the change of the earth's magnetic field accompanying the Tokachi earthquake of 4 March 1952, Science Rep. Tohoku Univ., Fifth Series Geophys. 4, 146-148, 1953b.

Kern, J. W., The effect of stress on the susceptibility and magnetization of a partially magnetized multidomain system, J. Geophys. Res. 68, 3807-3816, 1961.

Kitamura, T., Paper presented at Earthquake Res. Inst., Univ. Tokyo, September 1964.

Koch, J. W., Analysis and effects of current movement on an active thrust fault in Buena Vista Hills Oil Field, Kern County, California, Bull. Am. Assoc. Petr. Geol., 17, 694-712, 1933.

Lapina, M. I., Geomagnetism and seismic phenomena, Bull. (Izv.) Acad. Sci. USSR, Geophys. Ser. No. 5, 393-404, 1953.

Lincoln, J. V., Geomagnetic and Solar data, J. Geophys. Res. Vols. 71-72, 1966, 1967.

Lommitz, C., Creep measurement in igneous rocks, J. Geol. 64, 473-479, 1956.

Meade, B. K. and J. B. Small, current and recent movement on the San Andreas fault, Geology of Northern California, Calif. Div. Mines, Bull. 190, 385-391, 1966.

Milne, J., Earthquakes, earth current, and magnetic phenomena, Trans. Seism. Soc. Japan, 15, 135, 1890.

Milne, J. Seismic. magnetic, and electric phenomena, Seismol. J. Japan, 3, 23-33, 1894.

Miyakoshi, E., Study on some phenomena foretelling the occurrence of destructive earthquakes, Bull. Disaster Prev. Res. Inst. No. 6, 27-38, 1953.

Moore, G. W., Magnetic disturbances preceeding the 1964 Alaskan earthquake, Nature, 203, No. 4944, 508, 1964.

Nagata, T., Rock Magnetism, 2nd ed., Maruzen, Tokyo, 1953.

Nagata, T., H. Kinoshita, Studies on piezomagnetization (I), J. Geomagn. Geoelectr. 17, No. 2, 121-135, 1965.

Nagata, T., Magnetic susceptibility of compressed rock, J. Geomagn. Geoelectr. 18, No. 1, 73-80, 1966.

Neel. L., Influence de la pression sur l'aimantation remants des roches, Paper presented at conference at Newcastle, Eng., 4 May 1959.

Oakeshott, G. B., San Andreas fault in the California Coast Ranges province, Geology of Northern California, Calif. Div. Mines Geol. Bull. 190, 357-373, 1966.

Omer, C. C., Seismic areas and secular magnetic variations, Bull. Seism. Soc. Am. 36, 21, 1946.

Orlov, A. P., Earthquakes and their relations to other natural phenomena, Kazan, 1887.

Orowan, E., Mechanism of seismic faulting, Geol. Soc. Am. Mem. 79,]23-345, 1960.

Page, B. M., Geology of the Coast Ranges of California, Geology of Northern California, Calif. Div. Mines Geol. Bull. 190, 255-276, 1966.

Parkinson, W. D., The influence of continents and oceans on geomagnetic variations, Geophys. J., 6, 441, 1959.

Press, F., Determination of crustal structure from phase velocity of Rayleigh waves, 2, San Francisco Bay region, Bull. Seismol. Soc. Am., 47, 87-88, 1957.

Pekeris, C. L., The seismic buried pulse, Proc. Natl. Acad. Science 41, 629, 1955.

Reid, H. F., The mechanics of the earthquake, The California Earthquake of April 10, 1906. Report of the State Earthquake Investigation Commission, Vol. 2, (Carnegie Inst. of Washington, D.C.) 1910.

Reid, H. F., The free and forced vibrations of a suspended magnet, Terr. Mag., June and December, 1914.

Rikitake, T., Changes in magnetic dip that accompanied the activities of Volcano Mihara, Bull. Earthquake Res. Inst., 29, 161. 1951.

Rikitake, T., Outline of the anomaly of geomagnetic variations in Japan, J. Geomagn. Geoelect., 15, 181-184, 1964.

Rikitake, T., Y. Yamazaki, Y. Hagiwara, K. Kamada, M. Sossi, T. Watanabe, K. Momose, T. Yoshino, K. Otani, K. Ozawa, and Y. Sanzai, Geomagnetic and geoelectric studies of the Matsushiro earthquake swarm, Bull. Earthquake Res. Inst., 44, 363-408, 1966.

Ringwood, A. E., A model for the upper mantle, J. Geophys. Res., 67, 857-867, 1962.

Robertson, E. C., Creep of Solenhofen limestone under moderate hydrostatic pressure, Geol. Soc. Am., Mem. 79, 227-244, 1960.

Rothé, J. F., Deformitions des anomalies magnetiques, Serie a travsux scientifiques Pub. du Bureau Central Seism. Int. 1950.

Sassa, K., and E. Nishimura, On phenomena forerunning earthquakes, Disast. Prevent. Res. Inst. Kyoto, Bull. 13, 1956.

Schumucker, U., Anomalies of geomagnetic variations in the southwestern United States, J. Geomagn. Geoelect., 15, 193-221, 1964.

Shapiro, V. A., The seismomagnetic effect, Izv., Earth Physics, No. 8, 61-73, 1966.

Stacey, F. D., A note on the possibility of earthquake forewarning from geomagnetic measurements, Geomagnetica, (Servico Meteorologico Nacional, Lisbon), 109-119, 1962a.

Stacey, F. D. Theory of magnetic susceptibility of stressed rock, Phil. Mag., No. 7, 551-556, 1962b.

Stacey, F. D., Seismomagnetic effect and the possibility of forecasting earthquakes, Nature, 200, p. 1083-1085, 1963.

Steketee, J. A., On Volterra's dislocations in a semi-infinite medium, Can. J. Phys., 36, 192-205, 1958.

Taliaferro, N. L., Geologic history and structure of the central Coast Ranges of California, Calif. Div. Mines Bull. 118, 119-163, 1943.

Thompson, G. A., M. Talwani, Crustal structure from Pacific Basin to Central Nevada, J. Geophys. Res., 69, 4813-4837, 1964.

Tocher, D., Creep rate and related measurements at vineyard, California, Bull. Seismol. Soc. Am., 50, 396-404, 1960.

Watanabe, H., The occurrence of elastic shocks during destruction of rocks and its relation to the sequence of earthquakes, Special contributions, Geophys. Inst. Kyoto Univ. 3, 297-302, 1963.

Whitten, C. A. and C. N. Claire, Analysis of geodetic measurement along the San Andreas fault, Bull. Seism. Soc. Am., 50, 404-415, 1960.

Wilson, E., On the susceptibility of feebly magnetic bodies as affected by compression, Proc. Roy. Soc. (London) H 101: 712-722, 1922.

de Zafra, R. L., Optical pumping, Am. J. Phys., 28, 1960.

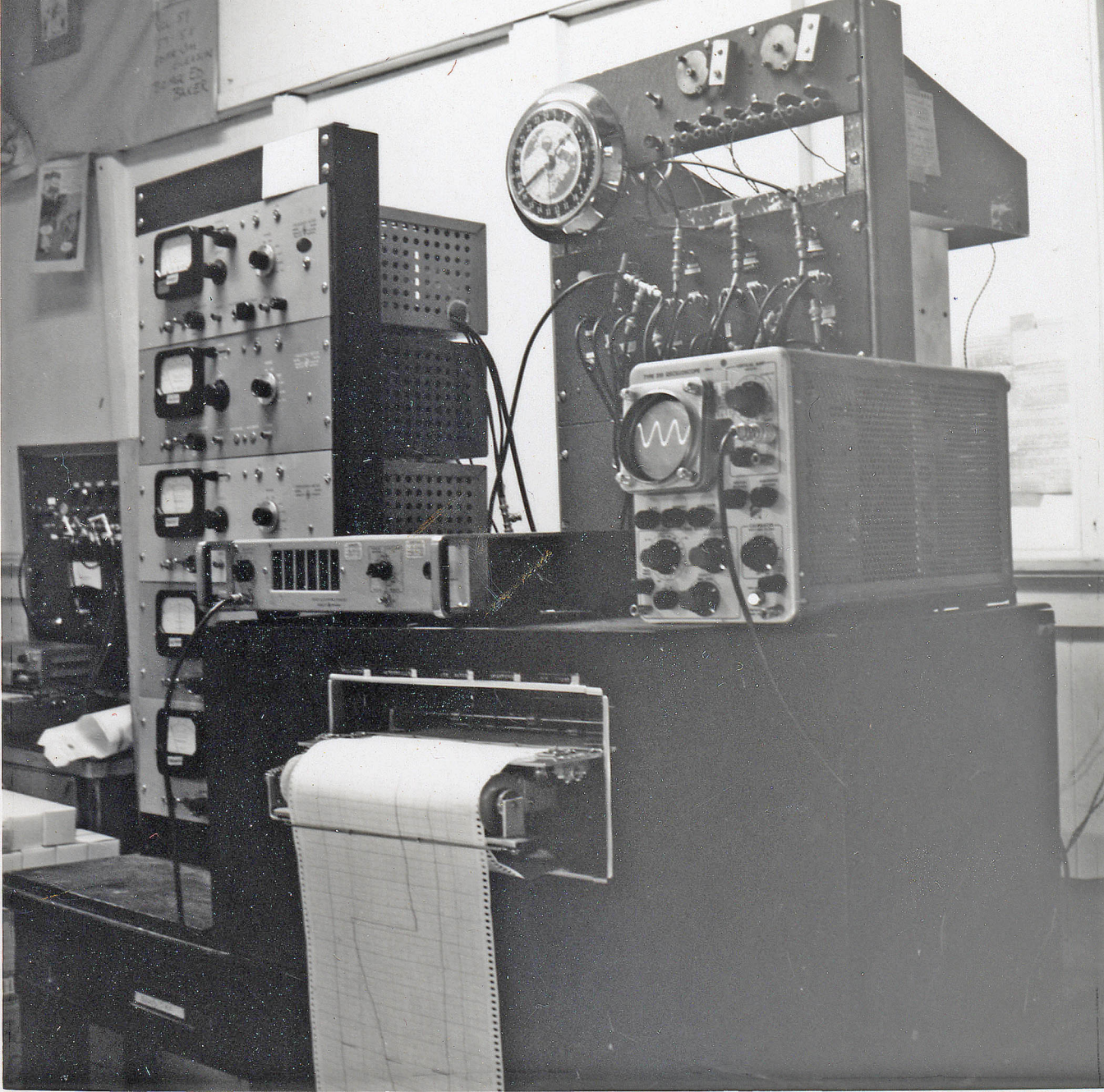

Assume the fault (Figure 8) is infinitely extended along the x axis, and, in addition, that $\vec{M}$ is not a function of x_0 but only of y_0 and z_0 ($\vec{M}$ does not vary along x axis). We have

$$P(r) = dy_0\, dz_0 \int_{-\infty}^{\infty} \frac{M_x(x-x_0) + M_y(y-y_0) + M_z(z-z_0)\, dx_0}{\left[(x-x_0)^2 + (y-y_0)^2 + (z-z_0)^2\right]^{3/2}}$$

The integral

$$\int_{-\infty}^{\infty} \frac{M_x(x-x_0)\, dx_0}{\left[(x-x_0)^2 + (y-y_0)^2 + (z-z_0)^2\right]^{3/2}}$$

= 0 because the integral is an odd function with respect to the variable of integration.

The remaining integrals are

$$P(r) = dy_0\, dz_0 \int_{-\infty}^{\infty} \frac{\left[M_y(y-y_0) + M_z(z-z_0)\right] dx_0}{\left[(x-x_0)^2 + (y-y_0)^2 + (z-z_0)^2\right]^{3/2}}$$

change variables again, letting $x-x_0 = x'$, $dx_0 = -dx'$

$$P(r) = dy_0\, dz_0 \int_{-\infty}^{\infty} \frac{\left[M_y(y-y_0) + M_z(z-z_0)\right] dx'}{\left[x'^2 + (y-y_0)^2 + (z-z_0)^2\right]^{\frac{3}{2}}}$$

Now My can be written as

$$M_y = C_1\beta\left[\frac{d+z_0}{y_0^2+(d+z_0)^2} - \frac{D+z_0}{y_0^2+(D+z_0)^2} + \frac{d-z_0}{y_0^2+(d-z_0)^2} - \frac{D-z_0}{y_0^2+(D-z_0)^2}\right]$$

C_1 = constant

$$M_z = C_1\gamma y_0\left[\frac{1}{y_0^2+(D+z_0)^2} - \frac{1}{y_0^2+(D-z_0)^2} - \frac{1}{y_0^2+(d+z_0)^2} + \frac{1}{y_0^2+(d-z_0)^2}\right]$$

In order to integrate (1) with respect to y_0, two types of integrals must be considered

$$I_1 = C_2 \int_{-\infty}^{\infty} \frac{(y-y_0)\,dy_0}{[y_0^2+a^2][(y-y_0)^2+b^2]} \qquad \text{(for the } M_y \text{ integration)}$$

$$I_2 = C_3 \int_{-\infty}^{\infty} \frac{y_0\,dy_0}{[y_0^2+a'^2][(y-y_0)^2+b'^2]} \qquad \text{(for the } M_z \text{ integration)}$$

Determination of I_1

Let us Fourier transform I_1 with respect to the variable q, thus

$$\text{F.T.}(I_1) = \int_{-\infty}^{\infty} I_1(y)\, e^{-iqy}\,dy$$

so that

$$\text{F.T.}(I_1) = C_2 \int_{-\infty}^{\infty}\int_{-\infty}^{\infty} \frac{e^{-iqy}(y-y_0)\,dy_0\,dy}{[y_0^2+a^2][(y-y_0)^2+b^2]}$$

change variables by letting $y-y_0 = y' \qquad y = y'+y_0$

$$= C_2 \int_{-\infty}^{\infty} \frac{e^{-iqy_0}\,dy_0}{(y_0^2+a^2)} \int_{-\infty}^{\infty} \frac{y' e^{-iqy'}\,dy'}{(y'^2+b^2)}$$

$q > 0$

$$= C_2 \left[\frac{\pi}{a} e^{-qa}\right]\left[-i\pi e^{-qb}\right]$$

$$= \frac{-i C_2 \pi^2 e^{-q(a+b)}}{a}$$

The inverse transform yield I_1

$$= \frac{C_2 \pi}{a} \frac{y}{y^2 + (a+b)^2}$$

Similarly

$$I_2 = \frac{C_3 \pi}{b_1} \frac{y}{(y^2 + (a_1+b_1)^2}$$

$$P(r) = \frac{2 M_y (y-y_0) + M_z (z-z_0)}{\left[(y-y_0)^2 + (z-z_0)^2\right]} dy_0 dz_0$$

Now must specify M_y and M_z and differentiate P(r). Let us write for the magnetization in the y direction

$$M_y = S\sigma_{T_{yx}} \beta k_0$$ (where β is the direction cosine made with the y axis.)

Similarly

$$M_z = S\sigma_{T_{zx}} \gamma k_0$$ (where γ is the direction cosine made with the x axis.)

The direction cosine α yielding M_x is not included since integration of M_x yields zero.

If we let the upper edge of the fault always be at the ground surface, then d = 0. This simplification lets

$$M_y = C_1\beta\left[-\frac{(D+z_0)}{y_0^2+(D+z_0)^2} - \frac{d-z_0}{y_0^2+(D-z_0)^2}\right]$$

and

$$M_z = C_1\gamma y_0\left[\frac{1}{y_0^2+(D+z_0)^2} - \frac{1}{y_0^2+(D-z_0)^2}\right]$$

From the derive c solution for the integration with respect to y_1, we have for the M_y terms,

$$I_1 = \frac{C_2\pi}{a} \quad \frac{y}{[y^2+(a+b)^2]}$$

thus,

$$I_1 = \frac{2C_1\beta\pi}{(D+z_0)} \quad \frac{y}{y_2+(D+z)^2}$$

$$I_3 = \frac{2C_1\beta\pi}{(D-z_0)} \quad \frac{y}{y^2+(D+z-2z_0)^2}$$

and for the M_z terms

$$I_2 = \frac{2C_1\gamma\pi}{z-z_0} \quad \frac{y}{y^2+(D+z)^2}$$

$$I_4 = \frac{2C\gamma\pi}{z-z_0} \quad \frac{y}{y^2+(D+z-2z_0)^2}$$

Thus,

$$P(r) = \int_0^D\int_{-\infty}^{\infty} 2\,\frac{[M_y(y-y_0)+M_z(z-z_0)]}{[(y-y_0)^2+(z-z_0)^2]}\,dy_0\,dz_0$$

$$= -2C_1\beta\pi y\left[\int_0^D \frac{-dz_0}{y^2+(D+z)^2} + \int_0^D \frac{dz_0}{y^2+(D+z-2z_0)^2}\right]$$

$$+ 2C_1\gamma\pi y\left[\int_0^D \frac{dz_0}{y^2+(D+z)^2} - \int_0^D \frac{dz_0}{y^2+(D+z-2z_0)^2}\right]$$

$$P(r) = 2C_1\pi y\left\{(\gamma-\beta)\left[\frac{D}{y^2+(D+z)^2}\right] - (\gamma+\beta)\int_0^D \frac{dz_0}{y^2+(D+z-2z_0)^2}\right\}$$

The integral

$$\int_0^D \frac{dz_1}{y^2+(D+z-2z_1)^2} = \frac{1}{2y}\tan^{-1}\frac{2yD}{y^2-D^2+z^2}$$

Thus

$$P(r) = 2C_1\pi y\,(\gamma-\beta)\frac{D}{y^2+(D+z)^2}\frac{-1}{2y}(\gamma+\beta)\tan^{-1}\frac{2yD}{y^2+z^2-D^2}$$

The component field intensity is obtained from the scalar potential by differentiating P(r) with respect to x, y, and z and noting that terms involving $(\gamma-\beta)$ will be zero.

$$\frac{\partial P(y)_{xz}}{\partial y} = 0$$

$$\frac{\partial P(y)_{xz}}{\partial y} = 2C_1\pi D\left\{\frac{(\gamma-\beta)\left[(D+z)^2-y^2\right]}{\left[y^2+(D+z)^2\right]^2} + \frac{2(\gamma+\beta)\left[4D^2-4z^2+y^2\right]}{(y^2-4D^2+4z^2)^2+(4yD)^2}\right.$$

$$\frac{\partial P(z)_{xy}}{\partial z} = 2C\pi Dy\left\{\frac{(\gamma-\beta)\,2\,(D+z)}{\left[y^2+(D+z)^2\right]^2} \quad \frac{(\gamma+\beta)\,16z}{\left[y^2-4(D^2-z^2)\right]^2+(4yD)^2}\right\}$$

Evaluating the expression at the surface where z = 0, we have for the y component

$$\frac{\partial P(y)}{\partial y} = T_y = 2C_1\pi D\left[\frac{(\gamma-\beta)\,(D^2-y^2)}{(y^2+D^2)^2} + \frac{2(\gamma+\beta)\,(4D^2+y^2)}{(y^2-4D^2)^2+(4yD)^2}\right]$$

Similarly for the z component, we have

$$\frac{\partial P(z)}{\partial z} = T_z = -\frac{4C_1\pi\,D^2y\,(\gamma-\beta)}{(y^2+D^2)^2}$$

The direction cosines are given in the following:

case	$S_c(\times 10^{-4})$	$S_t(\times 10^{-4})$	β	α	$(\alpha-\beta)$	$(\alpha+\beta)$
a)	-2	4	.67	.67	0	1.34
b)	-3	6	.67	.67	0	1.34

Therefore, $T = 0$

Let the projection of the remaining component, T_y in the direction of the total field be ΔF. The total field is inclined 65° to the magnetic north and T_y is horizontal and 38° east of north. Thus the direction consine of 70° is 0.34. The profiles of ΔF for D = 5, 10, and 20 km are presented in Figure 15 for various values of the constants, κ_0, S_c, and S_x.